

Development and evaluation of a 27MHz multi-electrode current-source interstitial hyperthermia system

Robert Kaatee

Druk: Optima, Rotterdam

Cover: Artist impression of an interstitial hyperthermia temperature distribution
by Femke Kaatee.

Copyright:

Taylor & Francis Ltd. (Chapter 2)

IOP Publishing Ltd. (Chapter 3, Chapter 4, and Chapter 5)

Elsevier Sciences Inc. (Chapter 6 and Chapter 7)

Development and evaluation of a 27MHz multi-electrode current-source interstitial hyperthermia system

Ontwikkeling en evaluatie van een
27 MHz multi-elektrode stroombron interstitieel hyperthermiesysteem

PROEFSCHRIFT

ter verkrijging van de graad van doctor aan de
Erasmus Universiteit Rotterdam op gezag van de
Rector Magnificus

Prof.dr. P.W.C. Akkermans M.A.

en volgens besluit van het College voor Promoties

de openbare verdediging zal plaatsvinden op

vrijdag 24 maart 2000 om 16:00 uur

door

Robert Simon Johannes Petrus Kaatee

geboren te Toronto, Canada

Promotiecommissie

Promotor: Prof. Dr. P.C. Levendag

Overige leden: Dr. A.G. Visser (tevens copromotor)

Prof. Dr. Ir. J.J.W. Lagendijk

Prof. Dr. J.W. Oosterhuis

Prof. Dr. C.J. Snijders

Het in dit proefschrift beschreven onderzoek werd uitgevoerd op de subafdeling Klinische Fysica & Instrumentatie en de sectie Hyperthermie van de afdeling Radiotherapie van het Academisch Ziekenhuis Rotterdam/Daniel den Hoed Kliniek. Het onderzoek en dit proefschrift werden mede mogelijk gemaakt door financiële steun van de Nederlandse Kankerbestrijding (Koningin Wilhelmina Fonds).

aan mijn ouders
voor Tjitske, Femke, Lotte en ...

Contents

1. General introduction	1
1. Hyperthermia	
1.1. Biological rationale	
1.2. Clinical rationale	
1.3. Technology of hyperthermia	
2. 27 MHz multi-electrode current-source interstitial hyperthermia.	
2.1 Interstitial hyperthermia	
2.2 History	
3. Study objectives and outline of the thesis	
2. A 27 MHz current source interstitial hyperthermia system for small animals	11
1. Introduction	
2. Materials and methods	
2.1. Tumour model	
2.2. The heating system	
2.3. Thermometry	
2.4. Temperature control	
2.5. Model calculations	
3. Results	
3.1. Model calculations	
3.2. In vivo measurements	
4. Discussion	
3. Design of applicators for a 27 MHz multi-electrode current source interstitial hyperthermia system; impedance matching and effective power	25
1. Introduction	
2. Materials and methods	
2.1. The 27 MHz current source interstitial hyperthermia system	
2.2.1. The electrode impedance	
2.2.2. The afterloading-catheter impedance	
2.2.3. The tissue impedance	

2.2.4. Parasitic pathways to the system ground	
2.2. Applicator impedance	
2.3. Impedance matching	
2.4. Effective power	
2.4.1. Channel input power	
2.4.2. Efficiency of the transmission line	
2.4.3. Applicator efficiency	
2.4.4. Mismatching of the applicator impedance	
2.5. Power requirements	
2.6. Experimental verification	
3. Results	
3.1. Experiments with R and C components	
3.2. Experiments with real applicators	
4. Discussion	
5. Conclusions	
4. Temperature measurement errors with thermocouples inside 27 MHz current source interstitial hyperthermia applicators.	53
1. Introduction	
2. Materials and methods	
2.1. The MECS-IHT system	
2.2. Model calculations	
2.3. Measurements	
3. Results	
3.1. Model calculations	
3.2. Measurements	
4. Discussion	
5. Conclusions	
5. Implications of using thermocouple thermometry in 27 MHz capacitively coupled interstitial hyperthermia; applicator impedance and efficiency	69
1. Introduction	
1.1. Thermometry	
2. Theory	
2.1. Principle of the MECS system	
2.2. Interaction between electrode and thermocouple	
2.3. Simulation of apparent impedance and power loss in the single electrode mode.	
3. Experiment	
3.1. Materials and methods	
3.2. Results	
3.2.1 Interaction between lead and thermocouple	
3.2.2 Reliability thermometry	

Contents

4. Discussion	
5. Conclusion	
6. Spatial temperature control with a 27 MHz current source interstitial hyperthermia system	85
1. Introduction	
2. Materials and methods	
2.1. The 27 MHz current-source hyperthermia system	
2.2. Model calculations	
3. Results; system features affecting temperature homogeneity	
3.1. Current source applicators	
3.2. Longitudinal SAR control	
3.3. Phase configuration SAR control	
3.4. Automatic temperature control	
4. Discussion	
7. Clinical thermometry using a 27 MHz multi-electrode current source interstitial hyperthermia system in brain tumours.	101
1. Introduction	
2. Materials and methods	
2.1. The 27 MHz multi-electrode current-source hyperthermia system	
2.2. Placement of afterloading catheters, applicators and thermometers	
2.3. Treatment schedule and goal	
2.4. Treatment control	
3. Results	
4. Discussion	
Summary and general discussion	117
Samenvatting en discussie	125
Bibliography	135
Dankwoord	137
Curriculum Vitae	141

General introduction

1. Hyperthermia

Hyperthermia is the elevation of tissue temperatures to 40-45°C and is mainly applied as a cancer therapy in combination with other treatment modalities, such as radiotherapy or chemotherapy. A detailed introduction to the biology, physics and clinical application of hyperthermia is given in: *An introduction to the practical aspects of clinical hyperthermia*, edited by Field and Hand and in: *Thermoradiotherapy and Thermochemotherapy* (volumes 1 and 2), edited by Seegenschmiedt, Fessenden and Vernon (Springer-Verlag, Berlin, Heidelberg 1995).

1.1. Biological rationale

At temperatures of 39°C and higher, direct cell kill is possible if this temperature is maintained sufficiently long. Most *in vitro* and *in vivo* studies of the biological effect of a single hyperthermia treatment show similar iso-effect time-temperature curves, for a broad range of different tumour and normal tissues (Field and Morris, 1983). Above a certain transition temperature, between 42 and 43°C, a temperature rise of 1°C allows a reduction of the heating time, of about a factor 2, while maintaining the same level of cell-kill. However, below the transition temperature, decreasing the temperature with 1°C, requires a sixfold longer heating period to maintain the effect.

The basic mechanism behind heat-induced cell kill is considered protein denaturation, which already starts at 39°C. Whether cytotoxicity is the result of damage of plasma membranes, cytoplasm or nucleus is still a point of discussion. The cell kill achieved depends on many factors. For example, the degree of proliferation, phase of the cell cycle (Westra and Dewey, 1971) and the physiological conditions do effect the heat sensitivity. A low pH (Haveman,

1979) and deprivation of oxygen and/or nutrients (Haveman and Hahn, 1981) often the result of a poor blood perfusion, are factors which increase the effect of hyperthermia. Furthermore, cells may become thermo-resistant after a certain period of temperature elevation (Li and Hahn, 1980). On the other hand the effect of heat can be increased through so-called step-down heating, i.e. a short interval at a high temperature followed by a longer period at a lower temperature (Field and Morris, 1984).

With hyperthermia alone, it appears not possible to achieve local tumour control. In vivo experiments with rhabdomyosarcoma's implanted in the flank of Wag/Rij rats show that the surviving fraction of the tumour after 0.5 hours at 44°C was still 0.24, resulting in a grow-delay of only several days (Van Geel *et al.*, 1994).

Hyperthermia as an adjuvant to other therapies has been found to be far more effective. At present, adding hyperthermia to radiotherapy is considered as most effective. The interaction consists of two basic mechanisms. Firstly both therapies are almost complementary. In contrast with hyperthermia, the cytotoxicity of radiotherapy is enhanced in a well oxygenated microenvironment, with sufficient nutrients and a normal pH. In addition, the highest heat sensitivity during a cell cycle is observed in the S-phase while radiation is more toxic during the G1-phase. Secondly, hyperthermia works as a radiosensitizer by inhibiting repair of sub-lethal DNA-damage caused by radiation (Ben-Hur *et al.*, 1974) and, at lower temperatures (<41°C), by reoxygenation of tissue through an increase of bloodflow. Mechanisms of sensitisation of chemotherapy by heat are an increased uptake of the chemotherapeutic drugs, an increased sensitivity of the cells for the drugs, or a combination of both (Meyn *et al.*, 1980). Transport to and into the cells of some drugs can be improved by heat-induced increased blood perfusion and permeability of the membranes. Furthermore hyperthermia can alter the structure of proteins and DNA which in some cases enhances the effect of chemotherapy. The large variety of available drugs and their different working mechanisms makes it very difficult to find the optimum temperature, timing and sequence for thermo-chemotherapy treatments.

1.2. Clinical rationale

Because hyperthermia alone is not effective as cancer therapy, it is generally combined with one or more other treatment modalities. In most clinical applications of hyperthermia the primary treatment goal is improving local tumour control. For those cancers where local control is expected to improve survival, hyperthermia can be used with a curative intent. If cure is not possible, e.g. due to metastatic disease, hyperthermia can still have an important palliative function, enhancing the quality of life. In general, the aim of hyperthermia is to sensitize other treatment modalities with two possible purposes. Firstly, hyperthermia can be added if the response to a certain standard therapy is insufficient and an increase of the standard therapy dose

would lead to unacceptable side effects. For example in case of previously irradiated persistent or recurrent tumours. Secondly, the reason for the addition of heat could be, maintaining the efficacy of the original treatment, while using a lower dose and in this way reducing the side effects.

Since the 1970s many clinical studies demonstrated benefit of hyperthermia (Seegenschmiedt *et al.*, 1995b). More recently, the results of a number of randomized studies showed that hyperthermia can be very effective as an adjuvant to radiotherapy. The outcome of these well controlled, so-called phase III studies are generally considered more valuable than the phase I/II studies.

In a randomized trial by the European Society for Hyperthermic Oncology (ESHO) the value of hyperthermia as an adjuvant to radiotherapy of recurrent or metastatic malignant melanoma was investigated. The results of this study (Overgaard *et al.*, 1996) showed a significantly higher local tumour control after 2 year with hyperthermia (46%) than with radiotherapy alone (28%). A large difference in the 5-years survival rate was found between patients with a locally controlled disease (38%) and those with a still active disease. Another study which showed a benefit of hyperthermia was the multi-centre trial which compared radiotherapy alone with the combined treatment of primary or recurrent breast cancer (Vernon *et al.*, 1996).

The results of a Dutch phase III trial were presented at the Internal Congress on Hyperthermic Oncology in Rome (Van der Zee *et al.*, 1996). The effect of additional hyperthermia for inoperable pelvic tumours, originating from the urinary bladder, the uterine cervix or rectum was investigated. The overall complete response rates were 58% and 37% for respectively thermoradiotherapy and irradiation alone.

Acute heat-related toxicity was limited to 2nd or 3rd grade skin burns and subcutaneous burns. Furthermore no enhancement of radiation-induced complications was found.

So far it has been demonstrated that hyperthermia can improve the response rate and the survival with a acceptably heat-induced toxicity. Possibly, hyperthermia can also be beneficial in those situations where radiotherapy already is effective but it is desirable to reduce normal tissue toxicity, i.e. the addition of heat might decrease the required effective radiotherapy dose and therefore the irradiation-induced toxicity.

1.3. Technology of hyperthermia

It took a long time before the potential of hyperthermia was demonstrated in randomized studies. The main reason for this is that it appears difficult to satisfy the requirements for an good hyperthermia treatment (Oleson *et al.*, 1993, Emami *et al.*, 1996, Hand *et al.*, 1997). Basically, the aim is to achieve an elevated homogeneous temperature distribution within the target volume and no heating of the surrounding tissue. Although, hot spots leading to localized necrotic regions might cause unwanted side-effects, the requirement of homogeneity has rather a practical than a biological ground. In clinical

practice, power deposition is often limited because of temperature-related pain. In a heterogeneous temperature distribution, this may result in insufficient heating in the colder regions.

To reach the heating goal, firstly the hyperthermia equipment must be appropriate for the job. The power which can be deposited in the tissue must be sufficient to reach therapeutic temperatures (40-45°C), the temperature measurements must be accurate ($\pm 0.2^\circ\text{C}$) and the spatial resolution of both power deposition and temperature measurement must correspond with the inhomogeneity of tissue cooling, mainly by blood flow (Lagendijk *et al.*, 1994). For example, it is obvious that in case of a higher blood temperature in the clinical target volume, e.g. due to a systemic temperature rise or because the heated volume is sufficiently larger than the target volume, the necessity of spatial control is reduced. Sometimes, e.g. if many applicators and thermometers are used, automatic temperature control is needed.

Secondly, good treatment planning is required to assure adequate applicator and thermometer placement and a proper use of extra treatment tools such as (absorbing/perfused) waterbols or electric field probes. For treatment planning, various computer models are available to estimate power absorption and temperature distributions for a certain treatment set-up. Both for treatment planning and treatment control, the experience obtained from previous treatments is very important.

In general, the choice for a certain heating method depends on the position, size and shape of the clinical target volume and on the treatment modality with which hyperthermia is combined. Furthermore patient-specific criteria, e.g. the presence of a pacemaker or metal parts, can play a role in this matter.

The heating targets can be divided in four categories: *superficial* (less than about 4 cm from the skin), *loco-regional* or *deep* (at a depth of more than 4 cm), *regional* (organ or extremity, such as an arm or a leg) and *whole body*. The various heating methods differ regarding the physics behind the energy deposition in tissue. Most straightforward is to use *hot sources* and rely on heat conduction. This hot source can be extracorporeal heated blood (regional and whole body hyperthermia), *ferromagnetic* seeds or fluids heated with an external electromagnet, or simply hot water. Other methods for energy deposition in case of superficial or loco-regional hyperthermia are *electromagnetic* or *ultrasound waves*.

Further classification of the heating method is possible using the position of the applicators which can lay outside the body (*external*), in the tissue (*interstitial*) or in cavities of the body (*intracavitary*).

After the heating system is chosen, the decision about the type of thermometer to be used has to be taken. Accuracy, precision and stability must be sufficient in combination with the heating method. The main distinction that can be made is between *invasive* and *non-invasive* thermometry. The most frequently used invasive thermometers are *thermocouples*, *thermistors* and *fiber optic* thermometers, each with its specific advantages and disadvantages (Cetas, 1987). In most situations, temperatures during a hyperthermia

treatment can be measured within $\pm 0.2^\circ\text{C}$, using invasive thermometers. Only in case of ultrasound hyperthermia this accuracy can not always be reached. However because of serious discomfort for the patient the spatial resolution of invasive temperature measurements is generally poor. Therefore, presently great effort is being put in the development of non-invasive techniques, which can be either *passive* or *active*. The passive techniques are based on measurement of electromagnetic or acoustic radiation, spontaneously emitted by a body at a certain temperature. In case of the active method the object of interest is irradiated first, before it sends some temperature-related information back. Examples of passive and the active technique are microwave radiometry (Leroy *et al.*, 1998) and magnetic resonance imaging respectively (Samulski *et al.*, 1992). At present the accuracy, precision and spatial/temporal resolution of these and other non-invasive thermometry systems are still insufficient for most clinical situations. Despite all the sophisticated thermometry systems available at the moment, the patient remains an important thermometer in clinical practice.

Detailed information about physics and technology of various heating techniques, thermometry systems, and methods to calculate power absorption or temperature distributions can be found in above mentioned handbooks. For an optimal choice and use of hyperthermia equipment there are a number of quality assurance guidelines available, e.g. Hand *et al.* (1989) for external hyperthermia and Emami *et al.* (1991) or Visser *et al.* (1993b) for interstitial hyperthermia, based on the experience of specialists of the different fields of hyperthermia.

2. 27 MHz multi-electrode current-source interstitial hyperthermia.

2.1 Interstitial hyperthermia

Interstitial hyperthermia systems were primarily developed to be used in combination with interstitial radiotherapy (IRT) and so far IHT is usually not performed without IRT. Generally, interstitial treatment is chosen, when sparing of normal tissue is very important, e.g. when the clinical target is located near critical organ or in a previously irradiated area. Furthermore interstitial applicators might be advantageous if a target is difficult to access with external applicators, e.g. because of an irregular patient contour or body cavities close to the target volume. Because of patient tolerance, the number of brachytherapy needles or plastic catheters that can be used is limited and therefore the target has to be relatively small, i.e. with diameters in the range 1-10 cm. Regions which are often treated interstitially are head & neck, pelvis and brain.

An important advantage of interstitial hyperthermia is a high spatial density of applicators and thermometers which makes compensation for local cooling by bloodflow possible. In theory, this should make it possible to deliver a high heat dose to the tumour without overheating the surrounding tissue. However

in practice this appears to be rather difficult. Despite the large number of applicators, temperature distributions obtained with IHT are often quite inhomogeneous and hot-spot-induced pain causes insufficient heating at other places. Two reasons for this problem are firstly, that power absorption decreases rapidly with increasing distance from the applicators and secondly, cooling by blood perfusion is large because only small volumes are heated and incoming blood is not pre-heated.

This inhomogeneous heating is one of the reasons for the disappointing results of some interstitial clinical trials (Emami *et al.*, 1996). An exception to this are treatments of brain tumours which do not have the problem of high-temperature-induced pain (Sneed *et al.*, 1998). A general introduction to interstitial hyperthermia can be found in: Interstitial and intracavitary thermoradiotherapy, edited by Seegenschmiedt and Sauer (Springer-Verlag, Berlin, Heidelberg 1993) and in the handbooks mentioned above. One of the, relatively large number of different IHT systems is the 27 MHz multi-electrode current-source (MECS) IHT-system, which has been developed during the past 15 years.

2.2. History

In the middle eighties Marchal demonstrated to Visser and Van Rhoon that electrodes operating at 27 MHz, inserted in plastic catheters (as frequently used in brachytherapy) could be used for hyperthermia. After that, both in Centre Alexis Vautrin in Nancy and in the Daniel den Hoed Cancer Centre in Rotterdam research was started to test this heating method (Marchal *et al.* 1989, Visser *et al.*, 1989). In Rotterdam, the early investigation was supported by the Dutch Cancer Society (grant RRTI 87-3). Deurloo *et al.* (1991) demonstrated the advantage of the capacitive coupling between electrodes and tissue over galvanic coupling via metallic needles in case of the older local-current radio-frequency method. A more extensive comparison between various RF-IHT systems has been given by Visser *et al.* (1993a). The 27 MHz capacitively-coupled method was applied in a rat-tumour model to investigate the effect of the combination of IHT and low-dose-rate IRT (Ruifrok *et al.*, 1991) and photo dynamic therapy (Levendag *et al.*, 1989). Furthermore, the research resulted in a 12-channel prototype of a clinical capacitive-coupled IHT-system. In a feasibility study 11 patients with advanced and/or recurrent cancers in head and neck were treated. (Levendag *et al.*, 1993). However the temperature distributions obtained were rather inhomogeneous and the minimum tumour temperatures were low. Reasons for this were the relatively large spacing between the afterloading catheters (1.5 to more than 2 cm) and absorption of electromagnetic energy in the catheter wall. Furthermore, cross-coupling between electrodes made adequate control of applicator power, which had to be performed manually, very difficult.

In a collaboration between the University Hospital Utrecht and the Daniel den Hoed Cancer Centre, the IHT-system was improved on several points. Firstly the number of heating channels was increased to 2 groups of each 32

channels with opposite phase. This made the use of multi-electrode applicators and thus a better spatial control of the power deposition possible. Furthermore, the inconvenient external ground at the patient skin could now be omitted and a more localized current pattern was obtained. In the new system both power steering and temperature measurement were computer controlled, which made automatic temperature control possible. At this point the name of the system changed from capacitive-coupled IHT-system to multi-electrode current-source (abbreviated as MECS) IHT-system. Furthermore, the development of IHT-treatment planning software and a search for catheter materials with lower dielectric loss were started. A general description about the technical features of the MECS-IHT system has been given by Lagendijk *et al.* (1995).

3. Study objectives and outline of this thesis

The work presented in this thesis was part of a project which was supported by the Dutch Cancer Society (grant DDHK 91-13). Two main sub-projects could be distinguished: 1) investigation of the effectiveness of IHT in combination with brachytherapy in a rat tumour model, 2) physical development of IHT equipment. The main objective of the technical part, the subject of this thesis, was to prepare the MECS-system for clinical introduction and to investigate the performance in clinical practice. Furthermore, the available IHT-system for small animals had to be improved.

With this latter system, the effect of high-dose-rate and low-dose-rate IRT in combination with IHT was investigated in solid tumours transplanted in the flank of rats. The design and the performance of a 4-channel IHT-system for small animals are described in chapter 2.

Regarding the clinical IHT-system the main concerns were the efficiency of the power deposition in the tissue and the optimization of the homogeneity of the temperature distributions.

The part of the generator power which is actually absorbed by the tissue is called the effective power (P_{eff}). P_{eff} depends on the method used to match the impedance of the applicator and afterloading catheter in the tissue with the generator impedance. Chapter 3, gives a detailed description of electrical aspects of impedance matching, applicator design, afterloading catheter choice and tissue to heat. Furthermore, a model is presented with which the required power absorption density can be estimated for a certain tumour size, applicator density and effective heat conductivity of the tissue. Calculations and measurements of P_{eff} are compared with each other and evaluated in respect of the power requirements.

Several aspects of thermocouple thermometry in combination with the 27 MHz current source IHT are discussed in the chapters 4 and 5. If a thermocouple probe is inserted in a afterloading catheter, the thermal conductivity along the thermocouple wires is considerably larger than this in radial direction. This, in combination with large temperature gradients in the tissue, 1-2°C/mm are

typical for IHT, is a potential source of measurement errors. Furthermore, the fact that thermometers are used inside applicators and are not directly in the tissue in combination with power dissipation in the afterloading catheter wall and/or in the applicator itself causes a difference in the measured temperature and the tissue temperature to be known. These two facets are illuminated in chapter 4. Implications of thermocouple probes inside applicators for P_{eff} and for the applicator impedance, and thus the impedance matching, are discussed in chapter 5.

Features of the MECS-IHT system which affect the temperature homogeneity have been evaluated in chapter 6.

Finally in chapter 7, the feasibility of heating brain tumours, using the MECS-IHT system and methods of thermometry use are discussed.

References

Ben-Hur E, Elkind MM and Bronk BV, 1974, thermally enhanced radioresponse of cultured chinese hamster cells: inhibition of repair of sublethal damage and enhancement of lethal damage, *Radiation Research* **58**: 38-51.

Cetas TC, 1987, *Physics and Technology of Hyperthermia*, edited by S.B. Field and C. Franconi (M.Nijhof, Amsterdam), pp 470-508.

Deurloo IKK, Visser AG, Morawska-Kaczynska M, Van Geel CAJF, Van Rhoon GC and Levendag PC, 1991, Application of a capacitive coupling interstitial hyperthermia system at 27 MHz; study of different applicator configurations. *Physics in Medicine and Biology* **36**: 119-132.

Emami B, Scott C, Perez CA, Asbell S, Swift P, Grigsby P, Montesano A, Rubin P, Curran W, Delrowe J, Arastu H, Fu K and Moros E, 1996, Phase III study of interstitial thermoradiotherapy compared with interstitial radiotherapy alone in the treatment of recurrent or persistent human tumours: a prospectively controlled randomized study by the radiation therapy oncology group. *International Journal of Radiation Oncology, Biology, Physics* **34**: 1097-1104.

Field SB and Morris CC, 1983, The relationship between heating time and temperature: its relevance to clinical hyperthermia. *Radiotherapy and Oncology*, **1**: 179-186

Field SB and Morris CC, 1984, Application of the relationship between heating time and temperature for use as measure for thermal dose., *Hyperthermic Oncology*, edited by J. Overgaard, (Taylor and Francis, London, Philadelphia), Vol I: 183-186

Field CC and Hand JW (eds), 1990, *An Introduction to the Practical Aspects of Clinical Hyperthermia*. (London, New York, Philadelphia: Taylor & Francis).

Hand JW, Legendijk JJW, Bach Andersen J, Bolomey JC, 1989, Quality assurance guidelines for ESHO protocols. *International Journal of Hyperthermia* **5**: 421-428.

Hand JW, Machin D, Vernon CC, Whaley JB, 1997, Analysis of thermal parameters obtained during phase III trials of hyperthermia as an adjunct to radiotherapy in the treatment of breast carcinoma. *International Journal of Hyperthermia* **13**: 343-364.

Haveman J, 1979, The pH of the cytoplasm as an important factor in the survival of in vitro cultured malignant cells after hyperthermia. effects of carbonylcyanide 3 chlorophenyl hydrazone. *European Journal of Cancer* **15**: 1281-1288.

Haveman J and Hahn GM 1981, The role of energy in hyperthermia induced mammalian cell inactivation: a study of the effect of glucose starvation and an uncoupler of oxidative phosphorylation. *Journal of Cellular Physiology* **107**: 237-241.

Lagendijk JJ, Crezee J, Hand JW, 1994, Dose uniformity in scanned focused ultrasound hyperthermia. *International Journal of Hyperthermia*, **10**: 775-784

Lagendijk JJW, Visser AG, Kaatee RSJP, Crezee J, Van der Koijk JF, De Bree J, Kotte ANTJ, Kanis AP, Levendag PC and Battermann JJ, 1995, The 27 MHz current source multi-electrode interstitial hyperthermia method. *Nucletron-Oldelft Activity Report* **6**: 83-90.

Leroy Y, Bocquet B and Mamouni A, 1998, Non-invasive microwave radiometry thermometry. *Physiology Measurements* **19**: 127-148.

Levendag PC, Ruifrok ACC, Marijnissen JPA, Van Putten WLJ and Visser AG, 1989, Preliminary experience with interstitial radiation, interstitial hyperthermia and interstitial photodynamic therapy in a simple animal model. *Strahlentherapie und Onkologie* **165**: 56-60.

Levendag PC, Kaatee RSJP, Visser AG, Kolkman-Deurloo IKK, Van Rhoon GC, Meeuwis CA, Van Geel CAJF and Van Hooije CMC, 1993, Interstitial radiation and/or interstitial hyperthermia for advanced and/or recurrent cancers in the head and neck: a pilot study. In: *Interstitial and Intracavitary Thermoradiotherapy*. MH Seegenschmiedt and R Sauer (Berlin, Heidelberg: Springer-Verlag), pp 233-239.

Li GC and Hahn GM, 1980, A proposed operational model of thermotolerance based on effects of nutrients and initial treatment temperature. *Cancer Research*, **40**: 4501-4508

Marchal C, Nadi M, Hoffstetter S, Bey P, Pernot M and Prieur G, 1989, Practical interstitial method of heating at 27.12 MHz. *International Journal of Hyperthermia* **4**: 451-466.

Meyn RE, Corry PN, Fletcher SE and Demetriades M, 1980, Thermal enhancement of DNA damage in mammalian cells treated with *cis*-diaminechloroplatinum (II) *Cancer Research* **40**: 1136-1139.

Oleson JR, Samulski TV, Leopold KA, Clegg ST, Dewhirst MW, Dodge RK, George SL, 1993, Sensitivity of hyperthermia trial outcomes to temperature and time: implications for thermal goals of treatment. *International Journal of Radiation Oncology, Biology, Physics* **25**: 289-297.

Overgaard J, Gonzales D, Hulshof MCCM, Arcangeli G, Dahl O, Mella O and Bentzen SM, 1996, Randomized trial of hyperthermia as adjuvant to radiotherapy for recurrent or metastatic malignant melanoma. *The Lancet*, **345**, 540-543

Ruifrok ACC, Levendag PC, Lakeman RF, Deurloo IKK and Visser AG, 1991, Combined treatment with interstitial hyperthermia and interstitial radiotherapy in an animal tumour model. *International Journal of Radiation Oncology, Biology, Physics* **20**: 1281-1286.

Samulski TV, MacFall J, Zhang Y, Grant W and Charles C, 1992, Non-invasive thermometry using magnetic resonance diffusion imaging: potential for application in hyperthermic oncology. *International Journal of Hyperthermia* **8**: 819-29

Seegenschmiedt MH, Fessenden P and Vernon CC (eds), 1995a, *Thermoradiotherapy and Thermochemotherapy, Volume 1, Biology, physiology and physics*. (Berlin, Heidelberg: Springer-Verlag).

Seegenschmiedt MH, Fessenden P and Vernon CC (eds), 1995b, *Thermoradiotherapy and Thermochemotherapy, Volume 2, Clinical applications*. (Berlin, Heidelberg: Springer-Verlag).

Sneed PK, Stauffer PR, McDermott MW, Diedrich CJ, Lamborn KR, Prados MD, Chang S, Weaver KA, Spry L, Malec MK, Lamb SA, Voss B, Davis RL, Wara WM, Larson DA, Phillips TL and Gutin PH, 1998, Survival Benefit of hyperthermia in a prospective randomized trial of brachytherapy boost \pm hyperthermia for glioblastoma multiforme. *International Journal of Radiation Oncology, Biology, Physics* 40: 287-295.

Van der Zee J, Gonzalez Gonzalez DG, Van Rhoon GC, Van Dijk JDP, Van Putten WLJ, Hart AAM, Koper PCM, De Wit GA and De Charro FT, 1996, Results of additional hyperthermia in inoperable pelvic tumours. In: *Hyperthermic Oncology 1996, Volume II. Proceedings of the 7th International Congress on Hyperthermic Oncology. Roma, Italy, April 9-13, 1996*. CFG Arcangeli and R Cavaliere (Rome: Tor Vergata University of Rome, Italy), pp 215-217.

Van Geel CAJF, Visser AG, Van Hooije CMC, Van den Aardweg GJM, Kolkman-Deurloo IKK, Kaatee RSJP and Levendag PC, 1994, Interstitial hyperthermia and interstitial radiotherapy of a rat rhabdomyosarcoma; effects of sequential treatment and consequences for clonogenic repopulation. *International Journal of Hyperthermia* 10: 835-844.

Vernon CC, Hand JW, Field SB, Machin D, Whaley JB, Van der Zee J, Van Putten WLJ, Van Rhoon GC, Van Dijk JDP, Gonzalez Gonzalez DG, Liu F-F, Goodman P and Sherar M, 1996, Radiotherapy with or without hyperthermia in the treatment of superficial localized breast cancer: results from five randomized controlled trials. *International Journal of Radiation Oncology, Biology, Physics* 35: 731-744.

Visser AG, Deurloo IKK, Levendag PC, Ruifrok ACC, Cornet B and Van Rhoon GC, 1989, An interstitial hyperthermia system at 27 MHz. *International Journal of Hyperthermia* 5: 265-276.

Visser AG and Kaatee RSJP, 1993a, Technical quality assurance for interstitial hyperthermia. In: *Interstitial and Intracavitary Thermoradiotherapy*. MH Seegenschmiedt and R Sauer (Berlin, Heidelberg: Springer-Verlag), pp 341-345.

Visser AG, Kaatee RSJP and Levendag PC, 1993b, Radiofrequency techniques for interstitial hyperthermia. In: *Interstitial and Intracavitary Thermoradiotherapy*. MH Seegenschmiedt and R Sauer (Berlin, Heidelberg: Springer-Verlag), pp 35-41.

Westra A and Dewey WC, 1971, Variation in sensitivity to heat shock during the cell cycle of chinese hamster cells in vitro, *International Journal of Radiation Biology* 19: 467-477.

Chapter 2

A 27 MHz current-source interstitial hyperthermia system for small animals

This chapter was published as:

Kaatee RSJP, Kampmeijer AG, Van Hooije CMC, Van Rhoon GC, Kanis AP, Levendag PC and Visser AG, 1995, A 27 MHz current source interstitial hyperthermia system for small animals. *International Journal of Hyperthermia* 11: 785-796.

Abstract

Temperature distribution is an important factor in thermo-radiotherapy and it is greatly dependent on the applied heating technique. Consistency of the heating method is therefore important in translating in vivo experimental data to the clinical situation.

To further evaluate the combination of interstitial hyperthermia and interstitial radiotherapy, an experimental interstitial hyperthermia system has been developed for small (500-2000 mm³) tumours growing in the flank of a rat. The system used reproduces the properties of our clinical current source interstitial hyperthermia system. The heating system consists of four applicators, each with independent tuning and power control. The applicators are situated inside plastic afterloading catheters and are capacitively coupled with the surrounding tissue. The tumour is heated through dissipation of a 27 MHz current flowing to an external ground plane.

An effective RF-filter allows reliable thermocouple temperature measurements when the power is switched on. The tumour temperature is easily controlled by means of a continuous temperature read-out and a clear temperature display. A minimum temperature up to 46°C can be reached within 4-10 minutes and maintained ($\pm 0.5^\circ\text{C}$) throughout the treatment period.

Modelling calculations performed for this heating system indicate that the applicator temperatures should be kept equal in order to minimize the

difference between maximum and minimum tumour temperature. Significantly higher applicator currents are needed at larger distances from the ground plane. In addition, the homogeneity of the temperature distribution is improved when either the tumour is isolated or when the environmental temperature is increased. The calculations also show that temperature distribution is strongly dependant on effective heat conductivity.

A description of the system and its performance is presented.

1. Introduction

The experiments of Ben-Hur *et al.* (1974), and numerous other subsequent *in vitro* and *in vivo* studies have demonstrated the radiosensitizing effect of hyperthermia (HT). However, specific research is needed to determine optimal *clinical conditions* for combined treatment. Detailed *clinical* study of the most optimal clinical set up has often not been possible because of the limited number of patients in clinical studies. Despite the differences between animal tumours and human tumours (Hahn *et al.*, 1989), an *in vivo* tumour model is more likely to approximate the clinical situation than an *in vitro* experiment, even if cell lines of human origin are studied in the latter. As dose distribution, and ultimately, the outcome of treatment, is dependent on the applied heating and irradiation techniques, *in vivo* experiments should be carried out, using the same techniques as during a *clinical* treatment. An animal model is, therefore, invaluable for investigating the effects of dose and sequencing of multiple radiotherapy (RT) and HT treatment sessions.

Whilst available clinical data on the combination of *interstitial* or *intracavitary* radiotherapy (IRT), i.e. brachytherapy and *interstitial* hyperthermia (IHT), were recently summarized by Seegenschmiedt and Sauer (1992), limited experimental *in vivo* studies (Miller *et al.*, 1978; Papadopoulos *et al.*, 1989; Mieler *et al.*, 1989; Ruifrok *et al.*, 1991; Van Geel *et al.*, 1994) have been published to date. To gain an insight in the combined treatment, e.g. regarding the effect of treatment sequence when IHT is combined with either low-dose-rate (LDR), pulsed-dose-rate (PDR) or high-dose-rate (HDR) brachytherapy or regarding the relation between thermal dose (temperature, treatment time) and tumour response, a 27 MHz current source IHT-system for small animals has been developed. It is able to heat adequately small (1500-2000 mm³) solid tumours, growing in the flank of a rat. This paper describes the heating system, the thermometry and their performance.

2. Materials and methods

2.1. Tumour model

Small experimental tumours (1500-2000 mm³), growing in the flank of a rat, are implanted with four parallel nylon catheters (inner diameter (d_i) = 1.1 mm,

outer diameter (d_o) = 1.6 mm) in a square geometry (7x7 mm) using a stainless steel template (Levendag *et al.*, 1989). Several different tumours in different rats (R1m in female WagRij, L27 in female Brown Norwegian and CC531 in male WagRij) have been studied.

2.2. The heating system

The heating system is based on the 27 MHz current source heating method (Marchal *et al.*, 1985; Visser *et al.*, 1989). A schematic design is shown in Figure 1. Applicators, which are constructed of flexible nylon catheters ($d_i=0.75$ mm, $d_o=0.96$ mm) covered over 15 mm from the tip with a conducting paint (Electrodag 1415, Acheson Industries), are inserted inside the afterloading catheters. The painted segment serves as an electrode. A thin (0.1 mm) copper wire inside the applicator catheter is attached to the paint. Each applicator is connected to its own 27 MHz generator (0-10 Watt, SSB Electronic). Due to the high frequency, an electrode is capacitively coupled with the surrounding tissue, through the wall of the implanted catheter. An electrical current can flow to an external ground return below the rat (Figure 1).

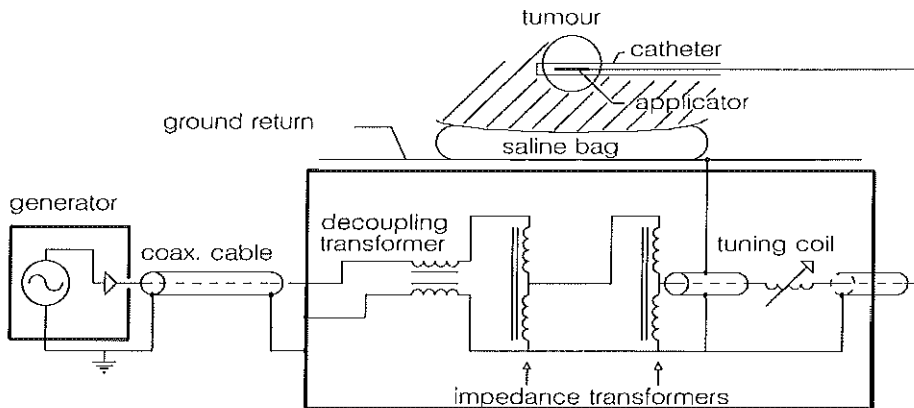


Figure 1. Schematic design of the IHT-system. Each applicator is connected to its own generator via a matching network, containing a tuning coil and two 4:1 impedance transformers, and a decoupling transformer. A saline bag is used for an optimal contact between tissue and ground return.

A saline bag is used to avoid hot spots on the surface between rat and ground return. The tumour is heated through ohmic losses. About 35% of the generator output is actually dissipated in the tissue. The capacitive coupling between the copper feeder wire inside the applicator and the tissue is negligible, so that the heated region is limited to the painted segment. Due to the high impedance associated with the capacitive coupling between applicator

and tissue, the current density along the heated region is hardly dependent on tissue impedance. This current source character of the applicator leads to a homogeneous heating along the catheter, even if the implanted catheters are not strictly parallel. These features were described in detail by Deurloo *et al.* (1991).

The small (25x19x9 cm³) box below the rat contains a matching network and a decoupling transformer for each applicator (Figure 1) to minimize reflected power and cross-coupling between applicators. The mainly capacitive impedance ($Z \approx 50\text{-}650j$ ohm) of the applicator inside the tissue is transformed to 50 ohms, through a variable air coil (15 turns, $d_o = 3\text{cm}$) and two 4:1 impedance transformers. The decoupling transformers prevent current from flowing from one applicator to another. This so called cross-coupling has to be avoided to allow a reliable power steering of individual applicators.

2.3. Thermometry

The thermometry is based on copper-constantan thermocouples. Temperature monitoring is performed with a 40-channel data-acquisition-system (Helios I, Fluke). The maximum measurement frequency is 15 times per minute and the accuracy is 0.05 °C. Inside each applicator the temperature is measured with a single point probe. Furthermore, temperatures are measured every 5 mm with a seven point probe inside an extra thermometry catheter ($d_i = 1.1$ mm, $d_o = 1.6$ mm) implanted, through the tumour centre, perpendicular to the applicator catheters (Figure 2). This is the long axis of the ellipsoidal tumours.

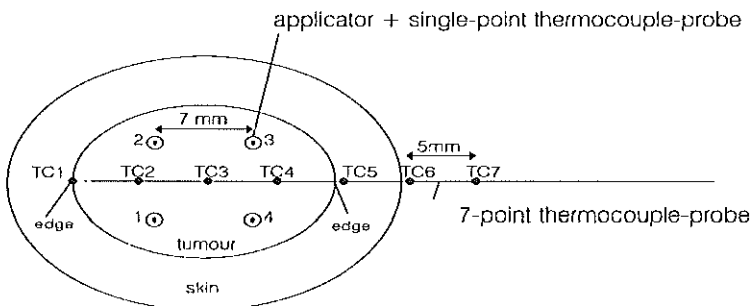


Figure 2. Position of applicators and thermocouples in the tumour. The applicators are positioned in a square geometry with 7 mm sides. Inside each applicator a single thermocouple thermometer is inserted. Furthermore, perpendicular on the applicators a 7-point thermocouple probe is placed.

The data acquisition system is connected to a PC which provides clear display and automatic storage on disk of the temperature data and also a thermocouple calibration procedure.

An RF-filter system (-60dB), constructed with ferrite toroids, allows continuous, undisturbed temperature measurements in a 27 MHz environment. A schematic design is given in Figure 3. The filter system can be distinguished in two identical units, both surrounded by a Faraday cage, one including the connectors for the 2 m long thermocouple probes and the other attached to the data acquisition system. The copper and constantan extension wires between the two filter units are shielded by a stainless steel braid. Each single thermocouple wire is wound around two ferrite toroids ($\mu = 100$, 14x9x5 mm, ferrox-cube 4C6, Philips) to create a large impedance. Furthermore, each pair of wires is coiled around two other toroids to equalize the difference in RF-current which is due to the different electric resistances of copper and constantan. In this way, the junction current error as described by Chakraborty and Brezovich (1982) is minimized.

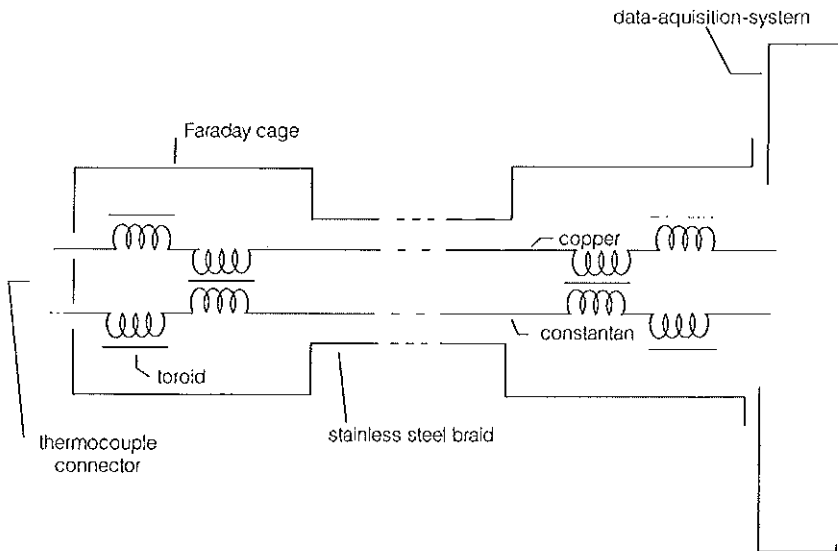


Figure 3. Diagram of the RF-filter system. The filter has two identical units, both surrounded by a Faraday cage. The copper and constantan extension wires in between are shielded by a stainless steel braid. Each thermocouple wire is separately wound around two ferrite toroids. Furthermore, each pair of wires is coiled around two other toroids.

2.4. Temperature control

Generally, the aim of a hyperthermia treatment is to achieve a homogeneous temperature distribution inside the tumour, at a chosen elevated temperature, without over-heating the surrounding normal tissue. In practice this means: aim at temperatures above a chosen minimum temperature (T_{\min}) and keep the maximum temperature (T_{\max}) as low as possible.

If the applicators have been implanted in the centre of the tumour, than the

lowest temperature is expected to be at the edge of the tumour. For power steering the temperatures measured along the longest axis at the edges of the tumour are used as *minimum* temperatures. One edge temperature can be measured directly if the measure point at the tip of the probe is positioned at the boundary of the tumour. If there is no measure point at the opposite tumour edge, the edge temperature is calculated through interpolation from three temperature measurements, two in the tumour and one in the skin, around this edge. The "applicator temperatures" are seen as the, power limiting, *maximum* temperatures.

Due to a continuous read-out and a clear display of minimum and maximum temperatures, the tumour temperature is controlled easily by manual power steering of the four generators.

2.5. Model calculations

The modelling software used for the computations was developed by the group of Lagendijk (De Bree *et al.*, 1994; Kotte *et al.*, 1994). Using a quasi-static approximation of the Maxwell equations, potential and power absorption distributions can be computed for a certain volume if the electrical properties (electrical conductivity (σ), relative permittivity (ϵ_r)) and the position of current and/or voltage sources are known (SAR model). From the SAR distribution and the thermal properties (density (ρ), specific heat capacity (c_p), thermal conductivity (k)), the temperature distribution at a certain time can be calculated (thermal model). In Figure 4 the volume used for the computations is shown. Electric and thermal properties are given in Table 1. The temperature at the edges of the rat (T_r) was held at 30°C.

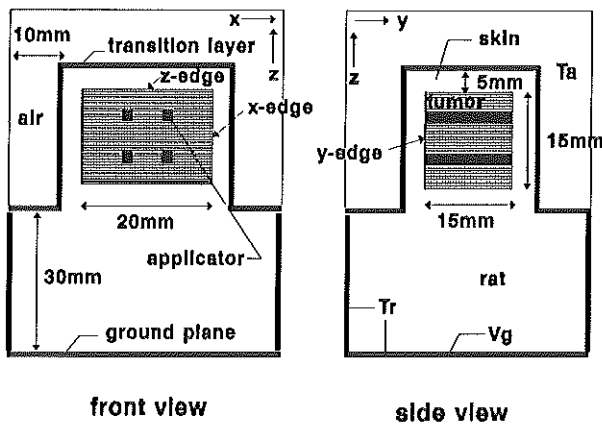


Figure 4. The volume as it was used for the model calculations. It consists of a block shaped tumour on a rectangular rat. In the centre of the tumour, four current sources were positioned in a 7 mm square geometry. The tissue is separated from the surrounding air by a transition layer. Both air and the edges of the rat were held at a constant temperature (T_a , T_r). The ground potential was fixed at 0 Volt.

The tumour is surrounded by an air layer with a fixed temperature (T_a). To bring into account the heat transfer from skin to air, a transition layer with a thickness of one voxel (1 mm^3) was defined. This layer is composed of half air, half tissue and the total heat transfer coefficient (h_{tl}) is given by the formula

$$\frac{1}{h_{tl}} = \frac{1}{h_{air}} + \frac{1}{h_A} + \frac{1}{h_{tissue}} = \frac{d_{air}}{k_{air}} + \frac{1}{h_A} + \frac{d_{tissue}}{k_{tissue}} \quad (1)$$

where h_{air} and h_{tissue} are the heat transfer coefficients of air and tissue respectively and h_A represents the heat transfer coefficient of the actual transition. The latter can be determined experimentally and is, in case of a solid wall and a gas (free convection), in the range of $5\text{-}15 \text{ Wm}^{-2} \text{ K}^{-1}$ (forced convection: $10\text{-}100 \text{ Wm}^{-2} \text{ K}^{-1}$). From equation 1, the effective thermal conductivity can be determined with

$$k_{tl} = (d_{air} + d_{tissue}) h_{tl} \quad (2)$$

For the model calculations the default value of h_A was set at $10 \text{ Wm}^{-2} \text{ K}^{-1}$ and of d_{air} and d_{tissue} at 0.5 mm . With these values, the thermal conductivity of the transition layer is $0.0083 \text{ Wm}^{-1} \text{ K}^{-1}$. The density and the heat capacity are chosen equal to the average of these values of air and tissue (Table 1). The temperature of the surrounding air (T_a) was set at 25°C .

Table 1. Electric and thermal properties used for the model calculations.

Medium	σ [$\Omega^{-1} \text{ m}^{-1}$]	ϵ_r [..]	ρ [kgm^{-3}]	c_p [$\text{Jkg}^{-1} \text{ K}^{-1}$]	k [$\text{Wm}^{-1} \text{ K}^{-1}$]
air	0	1	1.29	1000	0.024
tissue	0.6	80	1020	3500	0.6
transition layer	0	1	500	2250	0.0083
applicator/ground	0	1	1020	3500	0.6

3. Results

3.1. Model calculations

The main aim of model calculations was to establish if the temperature at the edge of the x-axis ($T_{x\text{-edge}}$) and the temperature measured inside the applicators T_{appl} were representative for respectively the minimum and the maximum tumour temperature (T_{min} and T_{max}) and thus useful as appropriate input

parameters for temperature control.

If the temperature distribution is calculated starting from a tissue temperature of 30°C and with a realistic fixed current per applicator (135 mA) it takes 330 s to reach a temperature of 46°C at the x-edge of the tumour.

The temperature distribution along the x-axis as a function of heat exchange between the tumour and the surrounding air, is shown in Figure 5a. The effect of isolating the tumour ($h_A = 0 \text{ W m}^{-2} \text{ K}^{-1}$) is small. A relatively cold (20°C) air flow around the tumour, i.e. large heat exchange, lowers the tumour temperature with about 2°C and increases the difference between the temperature at the edge and the temperature in the centre with 0.8°C.

The temperature distribution is effected more by heat transport through blood flow than by heat exchange with the surrounding air. Blood flow through small vessels (diameter smaller than 0.5mm) is best described with an enhanced effective heat conductivity (Crezee *et al.*, 1991). The effective heat conductivity was varied between 0.6, corresponding with no blood flow, and $3 \text{ W m}^{-1} \text{ K}^{-1}$, which is typical for well perfused tissues like the tongue. A lower effective heat conductivity gives a less homogeneous temperature distribution (Figure 5b). Because of the poor blood flow in most rat tumours, steep temperature gradients outside the square implant are often seen. This results, especially for larger tumours, in a large difference between T_{edge} and T_{centre} (Figure 6).

To find out if $T_{\text{x-edge}}$ is representative for the minimum tumour temperature the x-edge temperature was elevated to 46°C. If the *current* is kept the same (135 mA/applicator) for each applicator, the temperature distribution along the z-axis will be substantially asymmetric around the centre of the implant (Figure 5c) which is due to the position of the ground plane. So, in this case, the upper side of the tumour ($T_{\text{z-edge}}$) would be seriously under-dosed if $T_{\text{x-edge}}$ were seen as T_{min} . This error is smaller if the applicator *temperatures* are maintained equal (upper applicators 180 mA, lower applicators 50 mA) as can be seen in Figure 5d. However, to get $T_{\text{z-edge}}$ equal to $T_{\text{x-edge}}$, so that $T_{\text{x-edge}}$ becomes really the *minimum* tumour temperature, it is still necessary to position the centre of the implant at least 1 mm above the centre of the tumour.

In the equal applicator temperature situation, T_{max} is located in the centre of the implant and is a little higher (56°C) than the temperature inside the applicators (54°C). However, in *in vivo* experiments, the applicator temperatures are always higher than the central temperature. This is mainly due to the dielectric loss in the nylon catheter wall which is not included in the model. Therefore, the highest applicator temperature can be seen as T_{max} .

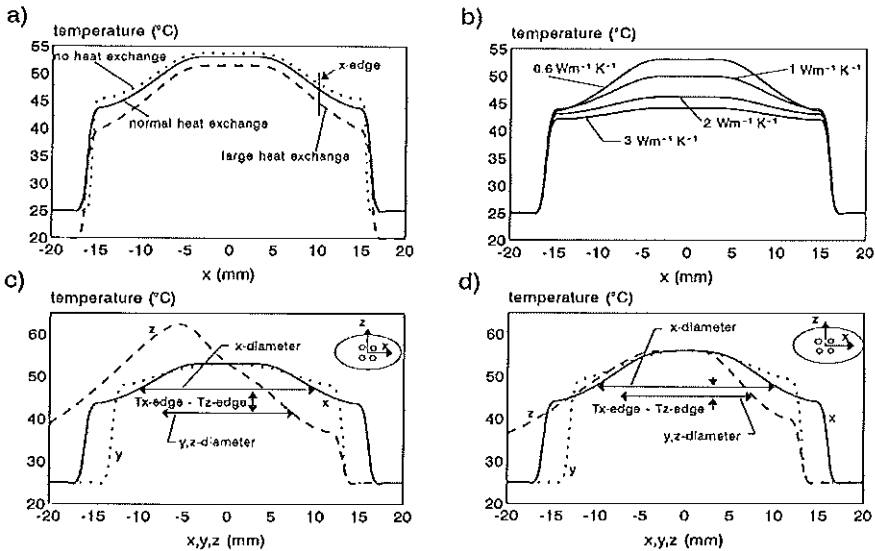


Figure 5. Model calculations of the temperature distribution along three orthogonal axes through the centre of the implant after 330 s of heating.

a) Effect of heat exchange between the tumour and the surrounding air on the temperature distribution along the x-axis, for three combinations of air temperature and heat transfer coefficient. solid line: $T_a = 25^\circ\text{C}$, $h_A = 10\text{Wm}^{-1}\text{K}^{-1}$ (normal exchange, dotted line: $T_a = 25^\circ\text{C}$, $h_A = 0\text{Wm}^{-1}\text{K}^{-1}$ (isolation), dashed line: $T_a = 20^\circ\text{C}$, $h_A = 100\text{Wm}^{-1}\text{K}^{-1}$ (large exchange).

b) The temperature distribution along the x-axis as a function of the effective heat conductivity. thick solid line: $k_{\text{eff}} = 0.6$, dotted line: $k_{\text{eff}} = 1$, dashed line: $k_{\text{eff}} = 2$, thin solid line: $k_{\text{eff}} = 3$.

c) Temperature distribution along the x(solid), y(dotted) and z(dashed) axes. The *current* per applicator was held the same for each applicator.

d) As in c) but now the applicator *temperatures* are equal.

3.2. In vivo measurements

Several different tumours (rhabdomyosarcoma (R1m, $n = 14$), lung carcinoma (L27, $n = 4$), colon carcinoma (CC531, $n = 15$)) have been treated. All of them were solid tumours growing in the flank of a rat (R1m in female WagRij, L27 in female Brown Norwegian, CC531 in male WagRij) with tumour volumes in the range of $1500\text{-}2000\text{ mm}^3$.

In Figure 6 two typical examples of an IHT-treatment are given. In a colon carcinoma the minimum tumour temperature was held at 44°C for 30 minutes (upper panels). The second example is a treatment of a rhabdomyosarcoma where the aim was $T_{\text{min}} = 46^\circ\text{C}$ for 15 minutes (lower panels). Although the tumour volume was the same (1750 mm^3) for both tumours, the maximum tumour dimension of the R1-tumour was larger (17 mm) than that of the CC531-tumour (12 mm), which had a more spherical shape. The left panels of Figure 6 display the minimum and maximum temperatures during the treatment. The charts on the right show the temperature distributions through the

tumour, measured with the 7-point thermometer probe just before power off at the end of the treatment time. In both treatments T_{x-edge} was easily elevated to the target temperature and maintained stable ($\pm 0.5^\circ\text{C}$) during the whole treatment time. During the heating-up period about 2-3W was used. If the tissue resistance is about 50Ω and the efficiency is 35% the current per applicator was in the range of (120-150 mA). To maintain T_{min} , about 0.6 W per applicator (nett generator output) was sufficient for the 44°C treatment and about 1W to keep T_{min} at 46°C . Further differences are that the target temperature was reached more rapidly in the CC531-tumour than in the R1 and that the temperature distribution in the lower panels of Figure 6 is considerably less homogeneous.

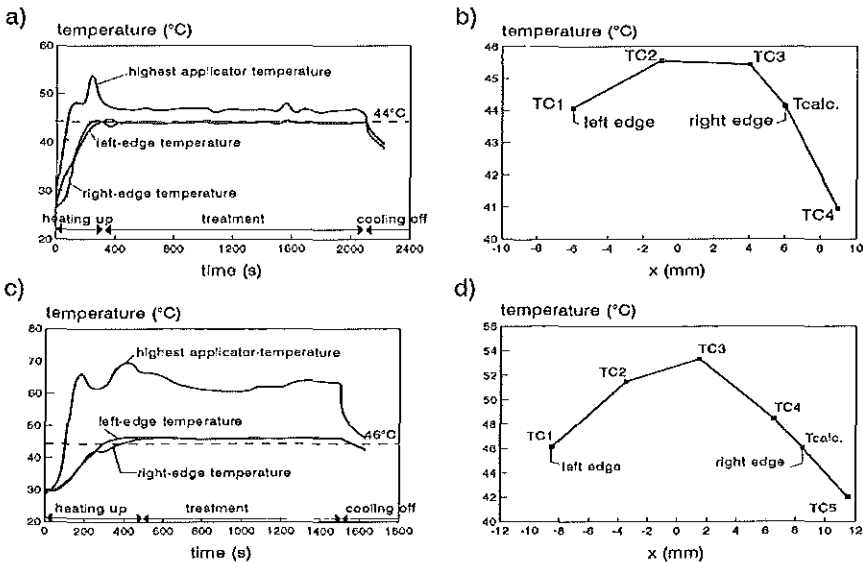


Figure 6. Typical IHT treatments; The minimum temperature was held at 44°C for 30 minutes inside a colon carcinoma (upper panels), and at 46°C for 15 minutes inside a rhabdomyosarcoma (lower panels). The temperatures measured at the edges of the tumour and inside the warmest applicator, during the treatment (left panels). The figures on the right show the temperature distribution through the tumour at the end of the treatment time.

In general, it was found that treatment characteristics as temperature uniformity, applicator power and time before the target temperature was reached depend on T_{min} and the tumour diameter. The reason for this is that the absorption of the electromagnetic energy falls steeply with increasing distance from the applicator, resulting in a large temperature gradient ($10\text{-}15^\circ\text{C}/\text{cm}$) outside the 7 mm square implant. The results are summarized in Table 2, where the difference between T_{min} and T_{appl} is a measure for inhomogeneity. For a given implant, T_{min} and heating rate are limited by the maximum tissue temperature allowed (in our case 70°C inside the applicators during heating) and by the size of the tumour.

Tumour type (R1m, L27, CC531) and mean start temperature (28.8°C, SD=1.2°C, range:26.4°C-31.9°C) did not have a noticeable effect on the heating process. The rectal temperature was measured during a number of treatments and this revealed a slow (about 0.1°C/min) decrease of core temperature, probably due to anaesthesia with pentobarbital. No correlation with the tumour temperature has been seen. To minimize the cooling of the rat the saline bag below is warmed up to about 30°C before treatment. During the treatment a lamp keeps the environment of the rat warm.

Table 2. Characteristics of the IHT-treatments (n=33): mean \pm SD (range)

small tumours ($\varnothing \leq 14$ mm)				large tumour ($\varnothing > 14$ mm)		
T_{\min} [°C]	$T_{\text{appl}} - T_{\min}$ [°C]	$t_{\text{heat-up}}$ [s]	$P_{\text{steady state}}$ [W]	$T_{\text{appl}} - T_{\min}$ [°C]	$t_{\text{heat-up}}$ [s]	$P_{\text{steady state}}$ [W]
44	3.6 \pm 1.4 (n=12)	5.3 \pm 1.7	0.68 \pm 0.13	9.4 \pm 1.5 (n=7)	7.3 \pm 4.4	0.87 \pm 0.15
46	4.5 \pm 1.6 (n=6)	5.2 \pm 1.6	0.90 \pm 0.00	10.4 \pm 2.4 (n=8)	8.4 \pm 1.3	1.00 \pm 0.11

4. Discussion

The IHT-system described in this report can reliably heat small tumours in the flank of a rat in an uniform manner. In tumours measuring less than 2 cm, a minimum tumour temperature of 46°C can be reached and maintained. In larger tumours the minimum temperature is limited by the maximum temperature, measured inside the applicators.

However, these observations do not necessarily imply that the system is not suitable for heating larger tumours and at other locations. For the R1m tumours the maximum spacing between the catheters was about 7 mm. It was chosen to keep the implant geometry constant. However, in somewhat larger tumours a larger spacing between the applicators would improve the homogeneity of the temperature distribution. Furthermore, it is possible to use longer applicators. The maximum generator power is sufficiently high (10 W) to heat the tissue over a length of about 4 cm and the matching network is capable to match the impedance of longer applicators. For much larger tumours it would be necessary to increase the number of channels.

If the system is used to investigate the effect of thermal dose on tumour response, specially when the treatment time is short (15 min), the 3-10 minutes heating up time should not be neglected. To minimize the variation in thermal dose given before the actual treatment starts, the range in tumour diameter (x-axis) must be small.

In vivo studies indicate that the most efficient treatment involves the

simultaneous application of heat and radiation (Overgaard, 1980). A limitation of the current source system is that IHT and IRT can not be delivered simultaneously. However, the time gap between radiotherapy and hyperthermia can be short (≤ 5 min). This makes it feasible to study the effects of (quasi) simultaneous treatments through alternating (PDR) IRT and IHT sessions.

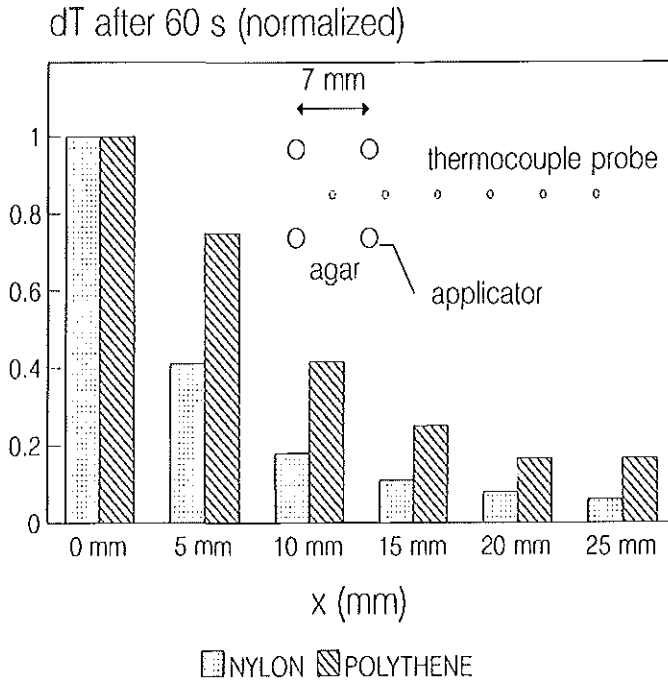


Figure 7. Temperature inhomogeneity due to dissipation in nylon (crosshatched bars) and polythene (hatched bars) afterloading catheters. The normalized temperature rise after 1 minute heating along the central implant axis, measured in an agar phantom.

A few points are pertinent when comparing animal experiments and clinical treatments. The maximum temperature of almost 70°C (Figure 6c) would not be acceptable in human tissue. Furthermore, a 7 mm spacing between the afterloading catheters is relatively small, compared with clinical practice. Dielectric loss in the nylon catheter material is the main reason for the high applicator temperatures. Due to the high dielectric loss factor of nylon ($\text{tg}\delta=0.04$) 20 to 50% of the electromagnetic energy is absorbed inside the catheter wall. A more homogeneous power distribution can be obtained if teflon or polythene catheters, with a negligible loss ($\text{tg}\delta=0.0002$), are used (Figure 7). However, these catheters have not been used for the treatments described in this paper, because of the relatively large energy loss in the impe-

dance matching circuit which leads to a power shortage. In addition, the diameter of the present brachytherapy catheters used with afterloading systems (microSelectron HDR/PDR/LDR) is 2.0 mm instead of 1.6 mm used for the animal treatments. This improves the homogeneity of the power distribution. A pilot study with head/neck tumours (Levendag *et al.*, 1993) showed that, using 2 mm nylon catheters and a mean spacing of 15 mm, minimum temperatures of about 40°C and mean applicator temperatures of 45°C are feasible. Present *in vivo* experiments are done with 2 mm polyoxymethylene (POM, $\text{tg}\delta=0.005$) brachytherapy catheters.

Acknowledgements

We would like to thank Dr. Senan for his comments on the English. This study is supported by a grant of the Dutch Cancer Society, grant DDHK 91-13. A contribution of the Maurits and Anna the Kock Foundation is gratefully acknowledged.

References

- Crezee J, Mooibroek J, Bos CK and Lagendijk JJW, 1991, Interstitial heating: experiments in artificially perfused bovine tongues. *Physics in Medicine and Biology* **36**: 823-833.
- De Bree J, Van der Koijk JF and Lagendijk JJW, 1994, A fast calculation method of SAR for interstitial hyperthermia. *Programme and Abstract book ESRB/ESHO* (abstract 44).
- Hahn GM, Ning SC, Elizaga M, Kapp DS and Anderson RI, 1989, A comparison of thermal responses of human and rodent cells. *International Journal of Radiation Biology* **56**: 817-825.
- Kotte ANTJ, De Bree J, Crezee J, Van der Koijk JF, Van Leeuwen GMJ and Lagendijk JJW, 1994, A thermal model featuring a semi-analytical discrete vessel description. *Abstract book ESRB/ESHO* (abstract 154).
- Levendag PC, Ruifrok ACC, Marijnissen JPA, Van Putten WLJ and Visser AG, 1989, Preliminary experience with interstitial radiation, interstitial hyperthermia and interstitial photodynamic therapy in a simple animal model. *Strahlentherapie und Onkologie* **165**: 56-60.
- Levendag PC, Kaatee RSJP, Visser AG, Kolkman-Deurloo IKK, Van Rhoon GC, Meeuwis CA, Van Geel CAJF and Van Hooije CMC, 1993, Interstitial radiation and/or interstitial hyperthermia for advanced and/or recurrent cancers in the head and neck: a pilot study. In: *Interstitial and Intracavitary Thermoradiotherapy*. MH Seegenschmiedt and R Sauer, eds. (Berlin, Heidelberg: Springer-Verlag), pp 233-239.
- Marchal C, Hoffstetter S, Bey P, Pernot M and Gaulard ML, 1985, Development of a new interstitial method of heating which can be used with conventional afterloading brachytherapy using Ir-192. *Strahlentherapie* **161**: 543-544.
- Mieler WF, Jaffe GJ and Steeves RA, 1989, Ferromagnetic hyperthermia and iodine 125 brachytherapy in treatment of choroidal melanoma in a rabbit model. *Archives of Ophthalmology* **107**: 1524-1528.

Miller RC, Leith JT, Veomett RC and Gerner EW, 1978, Effects of interstitial irradiation alone, or in combination with localized hyperthermia on the response of a mouse mammary tumor. *Journal of Radiation Research* 19: 175-180.

Overgaard J, 1980, Simultaneous and sequential hyperthermia and radiation treatment of an experimental tumour and its surrounding normal tissue *in vivo*. *International Journal of Radiation Oncology, Biology, Physics* 6: 1507-1517.

Papadopoulos D, Kimler BF, Estes NC and Durham FJ, 1989, Growth delay effect of combined interstitial hyperthermia and brachytherapy in a rat solid tumor model. *Anticancer Research* 9: 45-48.

Ruifrok ACC, Levendag PC, Lakeman RF, Deurloo IKK and Visser AG, 1991, Combined treatment with interstitial hyperthermia and interstitial radiotherapy in an animal tumor model. *International Journal of Radiation Oncology, Biology, Physics* 20: 1281-1286.

Van Geel CAJF, Visser AG, Van Hooije CMC, Van den Aardweg GJM, Kolkman-Deurloo IKK, Kaatee RSJP and Levendag PC, 1994, Interstitial hyperthermia and interstitial radiotherapy of a rat rhabdomyosarcoma; effects of sequential treatment and consequences for clonogenic repopulation. *International Journal of Hyperthermia* 10: 835-844.

Visser AG, Deurloo IKK, Levendag PC, Ruifrok ACC, Cornet B and Van Rhooon GC, 1989, An interstitial hyperthermia system at 27 MHz. *International Journal of Hyperthermia* 5: 265-276.

Chapter 3

Design of applicators for a 27 MHz multi electrode current source interstitial hyperthermia system; impedance matching and effective power

This chapter was published as:

Kaatee RSJP, Crezee J, Kanis AP, Lagendijk JJW, Levendag PC and Visser AG, 1997b, Design of applicators for a 27 MHz multi electrode current source interstitial hyperthermia system: impedance matching and effective power. *Physics in Medicine and Biology* 42: 1087-1108.

Abstract

In interstitial heating one of the main requirements to achieve a certain elevated temperature in a tumour, is that the effective power per applicator (P_{eff}), i.e. the power which is actually deposited in the tissue, is sufficiently high. In this paper this requirement is discussed for the applicators of the 27 MHz multi-electrode current-source (MECS) interstitial hyperthermia (IHT) system.

To minimize power reflection, the applicator impedance was matched with the generator impedance by adjusting the length of the coaxial cable in between. Transmission line losses, applicator efficiency and subsequently P_{eff} were computed for several applicator types. The actual P_{eff} per electrode was obtained from calorimetric measurements. Experiments with RC-loads, which can be seen as perfect applicators, were performed to investigate the effect of mismatching on P_{eff} . Applicator losses were measured for clinically used applicators, both single- and dual-electrode, utilizing saline phantoms. A simple spherical tumour model, using the effective heat conductivity (k_{eff}) to account for heat transport, was used to estimate P_{eff} for a given tumour size, implant size, and applicator density.

Computations of P_{eff} of various MECS-IHT electrodes were in close agreement with the phantom measurements. Most of the initial generator power

was absorbed in the transmission line (60-65%). The efficiency of the applicators was about 65%. Both for single-electrode and dual-electrode applicators the effective electrode power was found to be about 1 W.

Model calculations show that P_{eff} of 1 W is sufficient to reach a minimum tumour temperature of 43°C in well perfused tumours ($k_{\text{eff}} = 3 \text{ W m}^{-1} \text{ }^\circ\text{C}^{-1}$), using a typical implant with 2 cm electrodes and 1.5 cm spacing. Mismatching can considerably affect P_{eff} . Both a reduction to almost zero and a two-fold increase are possible. However, because the matching theory is well understood, mismatching is not a serious problem in clinical practice and can even be used to increase P_{eff} , if necessary.

The applicator design and the impedance matching method chosen in the MECS-system allow heating to temperatures in the therapeutic range, with implants used in clinical practice.

1. Introduction

The multi-electrode current-source (MECS) interstitial hyperthermia (IHT) system has been developed in a collaboration between the University Hospital Utrecht and the Dr Daniel den Hoed Cancer Center Rotterdam. Flexible multi-electrode applicators can be inserted in standard afterloading catheters, which can also be used for brachytherapy. The 27 MHz current-source heating method is based on the capacitive coupling of electrodes, through the plastic catheter wall, with the surrounding tissue. Electrical current, which flows either to an external ground plane or to electrodes with opposite phase, is dissipated in the tissue. Because the impedance of the catheter wall, typically 5-10 pF, is high compared to the tissue impedance (generally less than 100 Ω), the current injection into the tissue is independent of the implant geometry and quite homogeneous along the electrodes (Marchal *et al.*, 1989; Visser *et al.*, 1989a; Deurloo *et al.*, 1991).

The subject of this paper is the heating efficiency of the MECS-system, i.e. the ratio between power effectively deposited in the tissue and the generator power. The power per channel is about 5 W and the system was designed to have an efficiency of about 0.2-0.3. The remaining effective power of 1-1.5 W per channel was considered to be enough to reach therapeutic tumour temperatures. However, in practice a large variation in heating rates was observed. A study has been performed to investigate which parameters influence the effective power per channel and to what extent. Energy loss between generator and tissue can be divided in a part which is related to the method used to match the electrical impedance of the applicators with the generator impedance and a part, associated with the applicator design.

After a short description of the MECS-system in section 2.1, the theoretical models used to calculate the heating efficiency for a certain applicator-catheter-tissue combination are described in section 2.2. Furthermore, it is shown in this section how the power absorption density needed to reach a certain temperature rise can be estimated, using a simple spherical homogene-

ous tumour model with an effective heat conductivity to account for heat transport.

The heating efficiency theory has been verified in the section 3.

In section 4, the predicted efficiency of the MECS-IHT system will be discussed in relation to the estimated power absorption density requirements and conclusions will be drawn in section 5.

2. Materials and methods

2.1. The 27 MHz current source interstitial hyperthermia system

In Figure 1a a diagram of the 27 MHz current source hyperthermia system is shown. Three units can be distinguished, i.e. a 27 MHz power unit, a thermometry system, and a workstation for treatment planning and treatment control.

The power system has 64 coherent channels, divided into two groups with a phase difference of 180° . Duty cycle power steering is used to maintain the strict phase relation between the channels. The duty cycle switches of four channels are grouped in one module. In Figure 1b a schematic of a switch module is shown. The channel power is proportional with the ratio between the time that the corresponding switch is closed and the total cycle time (200 ms). Each of the 16 switch modules has its own power amplifier. The output of the power amplifiers contains higher harmonics of 27 MHz (≈ -10 dB). A purer 27 MHz signal of about 20 W is obtained, using low pass absorption filters (transmission of higher harmonics: ≈ -15 dB).

Temperature measurements are performed with 7-point constantan-manganin thermocouple probes (ELLA-CS, Czech Republic). Fast data acquisition (all 196 channels read within 320 ms) is feasible with a high resolution (0.005°C) thermometry system (De Leeuw *et al.*, 1993).

A UNIX-workstation provides the connection between thermometry, power supply and operator. Features of the treatment control software are: pre-treatment functionality check of applicators and thermometry, automatic or manual temperature control per electrode, clear display and automatic storage of treatment data and a user-friendly graphical user interface.

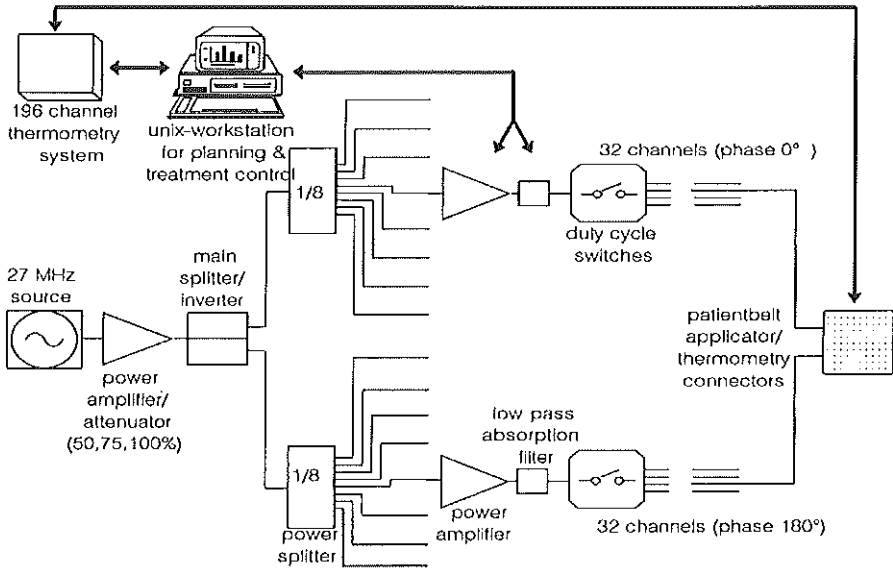
Furthermore, the workstation is used for treatment planning. Three-dimensional models are available for calculation of the distributions of power absorption and temperature for heterogeneous tissues.

A more extensive description of the MECS-system has been given by Legendijk *et al.* (1995).

Both single-electrode applicators and multi-electrode applicators of various lengths can be used. In Figure 2a a diagram of a dual-electrode applicator is shown. An applicator consists of the applicator catheter, one or more electrodes and a multi-point thermometer. An electrode comprises a tubular conducting segment which is connected to a thin feeder wire. The segments

of the standard applicators are constructed from a layer of silver paint (Electrodag 1415, Acheson Industries). For thermometry a multi-point thermocouple probe is inserted into the applicator catheter.

a)



b)

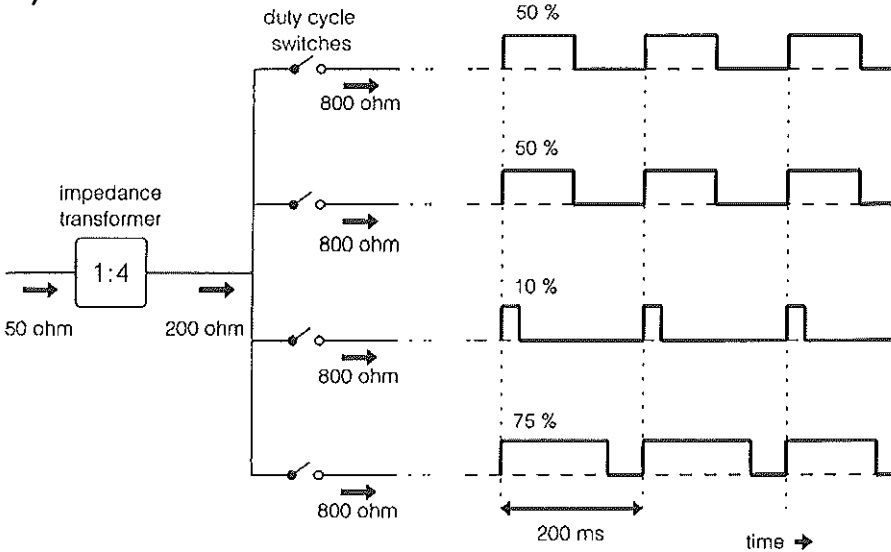


Figure 1. a) Diagram of the 27 MHz MECS-IHT system. b) Schematic of a switch module. The channel power can be adjusted by changing the duty time of the corresponding switch. Furthermore is shown how the channel input impedances (800 Ω) are transformed to the amplifier impedance (50Ω)

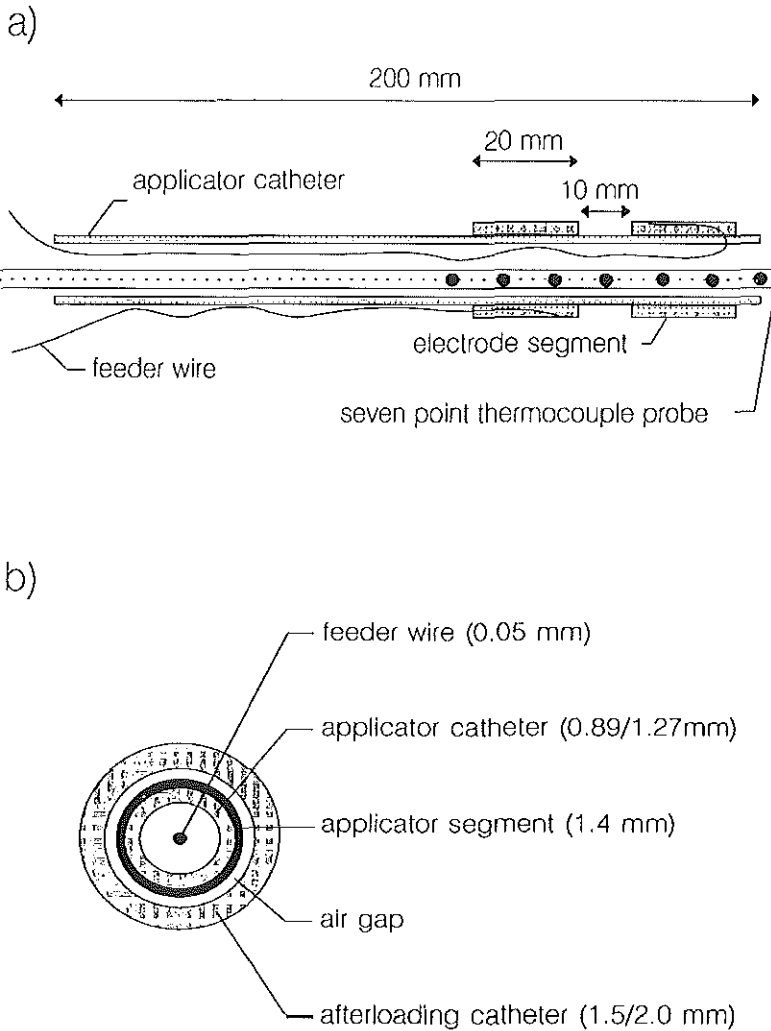


Figure 2. Diagram of a dual-electrode applicator. a) cross section parallel with applicator. b) cross section perpendicular to the applicator.

2.2. Applicator impedance

The applicator impedance (Z_a) is the electrical equivalent of one applicator electrode inserted in an afterloading catheter surrounded by tissue. For a single electrode applicator Z_a can be divided into three serial components, the electrode impedance (Z_e), the afterloading-catheter impedance (Z_c) and the tissue impedance (Z_t).

2.2.1. The electrode impedance

The electrode consists of a cylindrical feeder wire which is connected to a conducting tubular segment. The resistance of a tubular or cylindrical ($d_i = 0$ m) conductor is

$$R_e = \frac{4l}{\sigma\pi(d_o^2 - d_i^2)} \quad [\Omega] \quad (1)$$

With l [m] the length, d_i [m] the inner diameter, d_o [m] the outer diameter and σ [$S\ m^{-1}$] the electrical conductivity. Using this equation the electrode impedance can be computed. The resistance of a 20 cm long (typical applicator length), 50 μ m thick copper feeder wire ($\sigma = 0.6 \times 10^8\ S\ m^{-1}$) is about 1.7 Ω . The resistance of an applicator segment, constructed from a thin (5 μ m) layer of moderately conducting ($\sigma = 0.04 \times 10^8\ S\ m^{-1}$) silver paint (Electrodag 1415, Acheson Industries) on a catheter ($d_i = 1.3$ mm) is only 0.12 Ω/cm . The feeder wire resistance is thus relatively large, compared with the segment resistance.

2.2.2. The afterloading-catheter impedance

The afterloading-catheter impedance (Z_c) includes both the capacitive coupling between the segment and the surrounding tissue, and the coupling between feeder wire and tissue.

The coupling is predominantly capacitive. Nevertheless, the dielectric losses in the catheter materials have to be taken into account. These can be described by defining the complex dielectric constant:

$$\bar{\epsilon}_r = \epsilon_r' - j\epsilon_r'' \quad (2)$$

The impedance between two, in one dimension infinitely long, conductors, separated by a dielectricum, is given by:

$$Z = \frac{\epsilon_r'' - j\epsilon_r'}{\omega\epsilon_0(\epsilon_r'^2 + \epsilon_r''^2)} F_g \quad [\Omega m] \quad (3)$$

with ϵ_0 the permittivity of free space ($8.85 \times 10^{-12}\ F\ m^{-1}$) and ϵ_r the dielectric constant of the dielectricum between the conductors. F_g is the geometry factor which is, for two concentric cylinders:

$$F_g = \frac{1}{2\pi} \ln \frac{d_o}{d_i} \quad (4)$$

with d_o and d_i the diameters of the outer and the inner cylinder, respectively. Usually, dielectric materials are characterized by the dielectric constant (ϵ_r) and the dielectric loss factor

$$\tan(\delta) = \frac{\epsilon_r''}{\epsilon_r'} \quad (5)$$

Using this expression, equation (3) becomes

$$Z = \frac{\tan(\delta) - j}{\omega \epsilon_o \epsilon_r (1 + \tan^2(\delta))} F_g \quad [\Omega m] \quad (6)$$

Because the electrode segment and feeder wire lengths are relatively large, compared with the diameter of the afterloading catheter, Z_o can be approximated using equation (6). As an example a typical single-electrode applicator is chosen with a 2 cm long electrode segment ($d = 1.4$ mm). The applicator catheter ($d_o = 1.27$ mm, $d_i = 0.86$) is made of polythene (PE: $\epsilon_r = 2.4$, $\tan(\delta) = 0.0002$). Inserted 12 cm deep in a standard polyoxymethylene (POM: $\epsilon_r = 3.7$, $\tan(\delta) = 0.005$) afterloading catheter ($d_o = 2$ mm, $d_i = 1.5$ mm), the afterloading catheter impedance is about $1.4 - 625j \Omega$. The wire-tissue coupling ($C_{w,t} = 0.18$ pF cm^{-1}) is small compared with the coupling between the electrode segment and tissue ($C = 3.82$ pF cm^{-1}). Consequently, heating along the leads will be insignificant.

2.2.3. The tissue impedance

The tissue impedance depends on the electrical conductivity and the dielectric constant of the tissue. Measurements of these properties on some mammalian tissues have been summarized by Gabriel *et al.* (1996). The complex dielectric constant of biological tissues is often written as:

$$\bar{\epsilon}_r = \epsilon_r' - j \frac{\sigma}{\epsilon_o \omega} \quad (7)$$

with σ the electrical conductivity and ϵ_r the dielectric constant of the tissue. The tissue impedance can be computed with:

$$Z_t = \frac{\sigma - j\omega\epsilon_0\epsilon_r'}{(\omega\epsilon_0\epsilon_r')^2 + (\sigma)^2} F_g \quad [\Omega\text{m}] \quad (8)$$

F_g is a geometry factor, which depends on the geometry of applicators and ground plane. For two parallel cylindrical conductors with diameter d and spacing D the geometry factor is:

$$F_g = \frac{1}{\pi} \ln \frac{2D-d}{d} \quad (9)$$

To calculate the tissue impedance in the situation of two parallel electrode segments with opposite phase, i.e. the impedance between one of the segments and the virtual ground plane in between, F_g has to be divided by a factor 2.

In Table 1 this impedance (Ω cm) is given for the situation: $d=2$ mm and $D=15$ mm in fat, muscle and agar, respectively. This is an approximation of Z_t of 1 cm long electrodes which are separated 1.5 cm from each other. It should be noticed that the electrode length is not small compared with the spacing and therefore, the actual Z_t is somewhat smaller. The tissue impedance has a significant capacitive part, especially in case of fatty tissue, but it is small compared with the imaginary component of the catheter impedance.

Table 1. Tissue impedance between a conducting cylinder (diameter: 2 mm) and a 7.5 mm distant parallel conducting plane, calculated for several tissues.

Tissue	σ [S m ⁻¹]	ϵ_r []	Z_t	
			Real [Ω cm]	Imaginary [Ω cm]
Fat	0.2	20	206	-31
Muscle	0.7	50	60	-7
Agar	0.6	80	68	-14

2.2.4. Parasitic pathways to the system ground

Besides the coupling between feeder wire and tissue ($C_{w,t}$), already mentioned in section 2.2.2., other unwanted routes for the 27 MHz current to flow to the system ground may be present. An overview of possible pathways in case of a dual-electrode applicator is shown in Figure 3. The coupling between an electrode and the thermocouple probe ($C_{w,tc}$ and $C_{s,tc}$) causes two extra pathways to the system ground. One through the tissue ($C_{t,t}$) which might induce, like $C_{w,t}$, extra unwanted tissue heating along the applicator, and one

through the thermocouple wires which might result in a decrease of the effective power and causes extra disturbance of the thermometry system. The direct coupling, not through tissue, between the electrodes of a multi-electrode applicator ($C_{w,w}$ and $C_{w,s}$) could lead to energy absorption in the isolation material in between, and cause heating away from the electrode segments. Therefore, only applicator catheters with negligible dielectric loss factors should be used.

The parasitic impedances between electrode(s), thermocouple probe and tissue, computed with equation 6 and the geometry factors (4) and (9), are in good agreement with measurements. Typical measured values for the different types of parasitic coupling are given in Table 2. An overall parasitic capacitive coupling between the electrodes of an applicator as shown in Figure 2 of several pico-Farads is inevitable. This is of the same order as the coupling between the electrode segments through the tissue. Therefore, it is important to construct the applicator from low loss materials to minimize self-heating of the applicator.

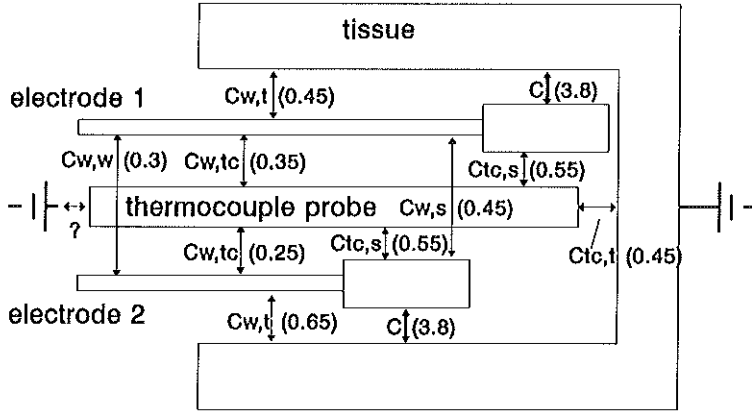


Figure 3. Schematic drawing of a dual-electrode applicator with the various capacitive pathways between the electrodes, the thermocouple probe and the tissue. The value between brackets gives the magnitude of the coupling in pF cm^{-1} .

Table 2. Parasitic capacitive coupling [pF cm^{-1}] between the components of a dual-electrode applicator and the tissue (measured).

$C_{w,t}$	$C_{w,w}$	$C_{w,tc}$	$C_{w,s}$	$C_{tc,s}$	$C_{tc,t}$
0.45 ¹	0.30	0.35 ¹	0.45	0.55	0.45
0.65 ²				0.25 ²	

¹: feeder wire inside the applicator catheter
²: feeder wire outside the applicator catheter

2.3. Impedance matching

To minimize power reflection, the applicator impedance must be matched with the output impedance of the generator (50 Ω). The procedure is as follows. As was demonstrated in section 2.2., the impedance of an applicator in a tumour is mainly capacitive. Using a coaxial cable, about 3.5 meter long, to connect the electrode(s) to the power system, the applicator impedance is transformed to a real impedance of about 800 Ω . For four parallel channels, the impedance becomes 200 Ω , which is transformed into 50 Ω using a 4:1 transmission line impedance transformer (Figure 1b). The higher harmonics filter is a 50 Ω device.

Transformation of a given load impedance (Z_{out}) through a coaxial cable to an input impedance (Z_{in}) can be calculated using the transmission line formula:

$$Z_{in} = \frac{Z_{out} \cosh(Q) + Z_0 \sinh(Q)}{Z_0 \cosh(Q) + Z_{out} \sinh(Q)} Z_0 \quad [\Omega] \quad (10)$$

with $Q = (\alpha + j\beta)l$, in which α [nepers m^{-1}] is the cable attenuation, β ($= 2\pi/\lambda = \omega^2 \mu_0 \mu_r \epsilon_0 \epsilon_r)^{1/2}$) [m^{-1}] the wave number and l [m] the cable length. Furthermore, Z_0 is the cable impedance and $\mu_0 \mu_r$ and $\epsilon_0 \epsilon_r$, the permeability and permittivity of the cable, respectively ($\mu_0 = 1.3 \times 10^{-6}$ H m^{-1}).

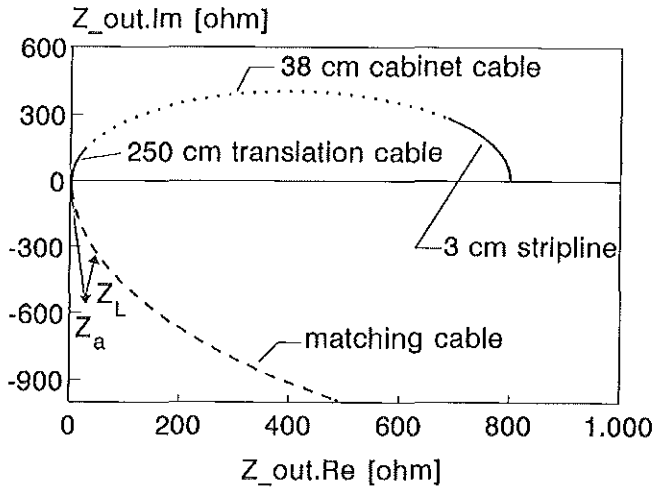
The procedure used to transform the applicator impedance (Z_a) to 800 Ω (Z_{in}) has been visualized in Figure 4a. The transmission line between switch and applicator includes 0.03 m stripline on the switch module ($\epsilon_r = 2.2$, $\alpha = 0.011$), 0.38 m coaxial cable in the 19-inch-cabinet (cabinet cable, $\epsilon_r = 2.03$, $\alpha = 0.017$), 2.5 m low loss coaxial cable from cabinet to patient (translation cable, $\epsilon_r = 1.79$, $\alpha = 0.007$) and the coaxial cable with a length meeting the matching conditions (matching cable, $\epsilon_r = 2.03$, $\alpha = 0.017$). The relative permeability (μ_r) is 1 for all cables. If Z_a is on the dashed matching-cable-curve, it is transformed to exactly 800 Ω , using a transmission line only and the appropriate length of the matching cable can be calculated using equation (10). If not, fine tuning, i.e. modification of Z_a by addition of either a serial inductance (Z_L) or a capacitor parallel to the applicator (Z_C) is needed.

For example, to match the impedance of a 2 cm electrode inserted in a polyoxymethylene (POM) afterloading catheter in muscle tissue ($Z_a \approx 30 - j630 \Omega$), an inductance of 2.1 μH ($Z_L \approx 5 + j360 \Omega$) and a matching cable length of about 0.90 m are required.

Normally, each electrode is connected to one channel of the power system. However, two to four channels can be combined if a high power is needed, e.g. in situations with large blood flow or with long applicators. Figure 4b shows the impedances which transform, without fine tuning, to 800 Ω , if Z_{out} is connected to one or more power channels. In general, a longer matching cable and a larger modification of Z_a are needed for impedance matching, if an applicator is connected to more than one parallel transmission line ($n = 2, 3$ or

4). This means that part of the extra power gained is lost again in the extra Z_L . For a small applicator impedance, e.g. in case of a long applicator, it might be more advantageous to take only the permanent parts of the transmission lines (striplines, cabinet cables and translation cables) parallel and connect them to one matching cable ($n = 2, 3, 4$). It should be noticed that the loss in this single matching cable increases due to the higher current (see section 2.4.2., Figure 6).

a)



b)

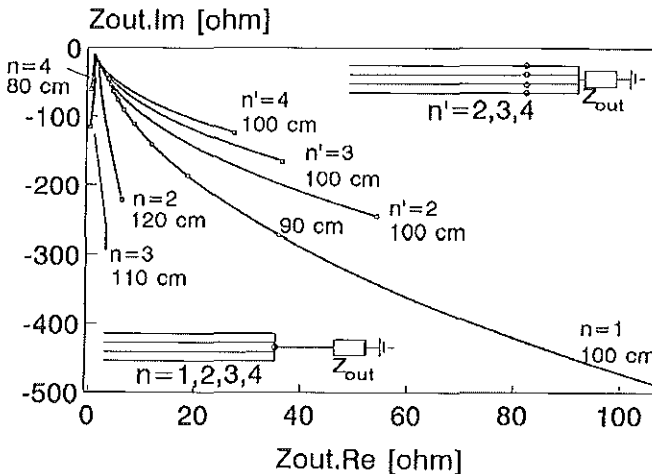


Figure 4. Impedance matching. a) If an applicator impedance (Z_a) cannot be transformed to 800 Ω , using a transmission line only, a small inductance (Z_L) or capacitor (not shown) is added. b) The cable-only matching curves for an applicator segment connected to one, two, three or four power channels with a single matching cable ($n = 1, 2, 3$ or 4) and with parallel matching cables ($n' = 2, 3$ or 4). Only the matching cable part of the transmission line is shown. The distance between subsequent square symbols on the "n = 1" curve is 10 cm.

2.4. Effective power

The effective power is defined as the power which contributes to the heating of the tissue, in the neighbourhood of the conducting segment. Using this definition means that absorption of electromagnetic energy in the afterloading-catheter wall, followed by heat conduction into the tissue, is included. However, heating along the leads is excluded by this definition.

The effective power per electrode depends on the input power of the channel(s) to which it is connected and furthermore on different kinds of energy loss between the duty cycle switches and the tissue, such as transmission line loss, dissipation in the matching inductance, self-heating of the applicator along the leads and energy leakage into the thermocouple probe. Figure 5 is a schematic drawing of an electrode connected to one channel of a switch module. The power effectively dissipated in the tissue around an electrode, i.e. dissipated in R, is:

$$P_{eff} = \eta_a \sum_{i=1}^n (\eta_{t,i} P_{in,i}) \quad [W] \quad (11)$$

$P_{in,i}$ is the input power of channel i and n is the number of channels to which the electrode is connected. Furthermore, $\eta_{t,i}$ is the efficiency of the transmission line i and η_a is the applicator efficiency.

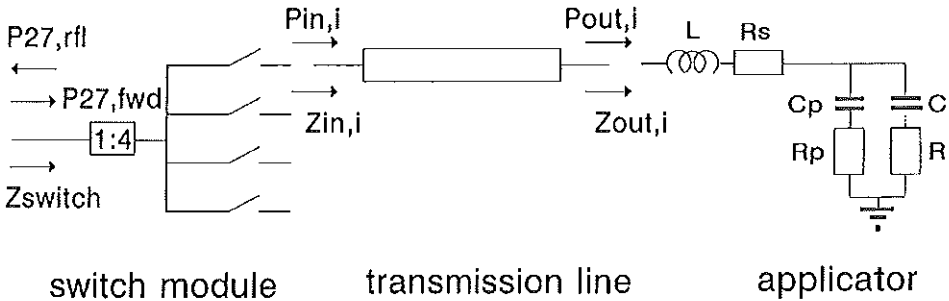


Figure 5. Schematic drawing of an electrode connected to one channel of a switch module.

2.4.1. Channel input power

In case of a perfect impedance matching ($Z_{in,i} = 800 \Omega$ for $i=1,2,3,4$) and neglecting the losses on the switch module, each of the four channels receives $\frac{1}{4}P_{gen}$. However, this channel input power ($P_{in,i}$, $i=1,2,3,4$) alters if one or more channels are mismatched. First, since the input impedance of the switch module is not 50Ω , P_{gen} is partially reflected (P_{rfl}) and secondly, the remaining forward power (P_{fwd}) does not necessarily split into four equal portions if the channel impedances ($Z_{in,i}$) are not the same.

The power dissipated beyond a higher harmonics filter is:

$$P_{fwd} = (1 - |\rho|^2) P_{gen} \quad [\text{W}] \quad (12)$$

with ρ the complex reflection coefficient, defined as:

$$\rho = \frac{50 - Z_{switch}}{50 + Z_{switch}} \quad (13)$$

and Z_{switch} the equivalent impedance of four parallel channels transformed, with the 1:4 impedance transformer

$$Z_{switch} = \frac{1}{4} \left[\sum_{i=1}^4 \frac{1}{Z_{n,i}} \right]^{-1} \quad [\Omega] \quad (14)$$

The fraction of P_{fwd} which goes into channel i is:

$$f_i = \frac{\text{Re} \{ 4Z_{switch} \}}{\text{Re} \{ Z_{in,i} \}} \quad (15)$$

Now the input power flowing into channel i can be calculated, using the equations (12) and (15):

$$P_{in,i} = \eta_s f_i P_{fwd} \quad [\text{W}] \quad (16)$$

with η_s the efficiency of the switch module, representing the losses in the impedance transformer and in the switches.

2.4.2. Efficiency of the transmission line

The efficiency of a transmission line i is defined as

$$\eta_{tl,i} = \frac{P_{out,i}}{P_{in,i}} \quad (17)$$

The power dissipated in an impedance Z is

$$P = \operatorname{Re} \left\{ U \left[\frac{U}{Z} \right]^* \right\} \quad (18)$$

with U the electrical potential over Z . The complex conjugated is denoted with an asterisk.

Knowing that $Z_{in,i}$ can be written as a function of $Z_{out,i}$, Z_0 and Q (eq. 10), and, furthermore, using the relationship between the electrical potentials at both sides of the transmission line

$$\frac{U_{in}}{U_{out}} = \frac{Z_0 \sinh(Q) + Z_{out} \cosh(Q)}{Z_{out}} \quad (19)$$

the ratio between $P_{in,i}$ and $P_{out,i}$ can be computed as a function of $Z_{out,i}$ and the properties of the transmission line (Z_0 , Q).

The efficiency of the transmission line, as a function of the length of the matching cable, is shown in Figure 6. The efficiencies were calculated for a situation of perfect matching, i.e. for each length of the matching cable a Z_{out} was taken which transforms to $Z_{in} = 800 \Omega$. If parallel transmission lines are used, generally longer matching cables and/or a larger "dissipating" matching inductance are needed. Therefore, the effective power is not fully proportional to the number of channels. Especially in case of parallel channels plus a single matching cable ($n = 2, 3, 4$) the efficiency might be disappointing because of the larger current and thus an increased loss in the matching cable.

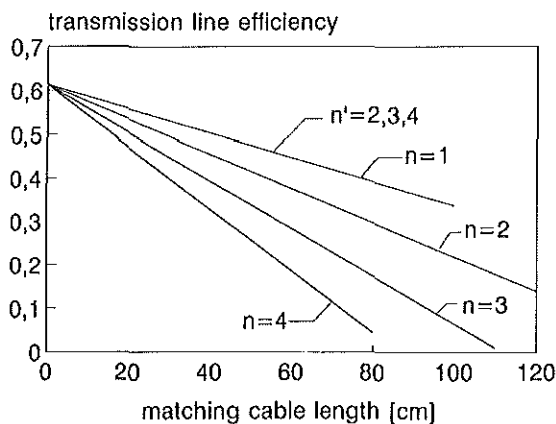


Figure 6. The efficiency of the transmission line as function of the length of the matching cable which is needed for matching Z_{out} with 800Ω . For an applicator segment connected to one, two, three or four power channels with a single matching cable ($n = 1, 2, 3, 4$) and with parallel matching cables ($n' = 2, 3, 4$).

2.4.3. Applicator efficiency

Not all output power of the transmission line is effective power. In Figure 5 the electrical equivalent of an applicator plus matching inductance is drawn. The effective part of $P_{out,i}$ is the power which is absorbed in R (P_{eff}). As mentioned above, extra ways to the system ground (C_p) might result in energy loss, indicated by R_p . Also dissipation in the matching inductance (L) and in the feeder wire do not contribute to tissue heating near the electrode segment. These losses are represented by R_s . The applicator efficiency (η_a) is defined as the ratio of the power dissipated in R and the sum of the output powers of the channels to which the applicator electrode is connected:

$$\eta_a = \frac{P_{eff}}{\sum_{i=1}^n P_{out,i}} \quad (20)$$

The loss in R_s depends on the ratio between R_s and R , as can be seen in Figure 7a in which $R_p=0$. Further decrease of η_a due to dissipation in R_s will occur if the ratio between C_p and C increases. This is also demonstrated in Figure 7a. In Figure 7b, η_a is shown as a function of R_p/R , if $R_s=0$. As long as the impedances associated with C_p and C are large compared with R_p and R , respectively, η_a is mainly dependent on the ratios between C_p/C , R_p/R and R_s/R and not on the actual values of C_p , C , R_p and R_s (in these calculations $C=10$ pF, $R=40$ Ω , $L=1$ μ H). Furthermore, losses in R_s or R_p are independent of L . However, the part of R_s which is due to dissipation in the inductance is proportional to L .

The overall efficiency (η_{calc}), which is defined as the ratio between P_{eff} and $\frac{1}{4}P_{gen}$, can be obtained by substitution of equation (16) by equation (11). In case of an appropriate impedance matching η_{calc} is the product of η_s , η_{tl} and η_a . In practice, a power loss of 30-40% in the applicator is not extreme. Typical transmission line efficiencies are in the range 35-45%. Hence, assuming negligible switch losses, the overall efficiency is about 20-30%. This means that if an electrode is connected to one power channel (5 W), the effective power is about 1-1.5 W.

2.4.4. Mismatching of the applicator impedance

In theory, an applicator impedance can always be transformed to exactly 800 Ω . In practice, however, mismatching to some extent is unavoidable. The most important reason for this is that, for practical reasons, the impedance matching is performed in an agar-phantom at room temperature. As the electrical properties and/or the applicator geometry in the clinical situation are not exactly the same as in the matching set-up, the applicator impedance will differ, too. Even if applicators are matched in a patient just before treatment, mismatching will occur as Z_a changes during treatment due to the temperature rise, changes

in blood flow or because of a change in the impedance of the afterloading catheter due to water absorption in the catheter wall. Other practical reasons for a, generally small, mismatch are that the matching inductances are only available at distinct values and that the transmission line used, often does not have exactly the right length.

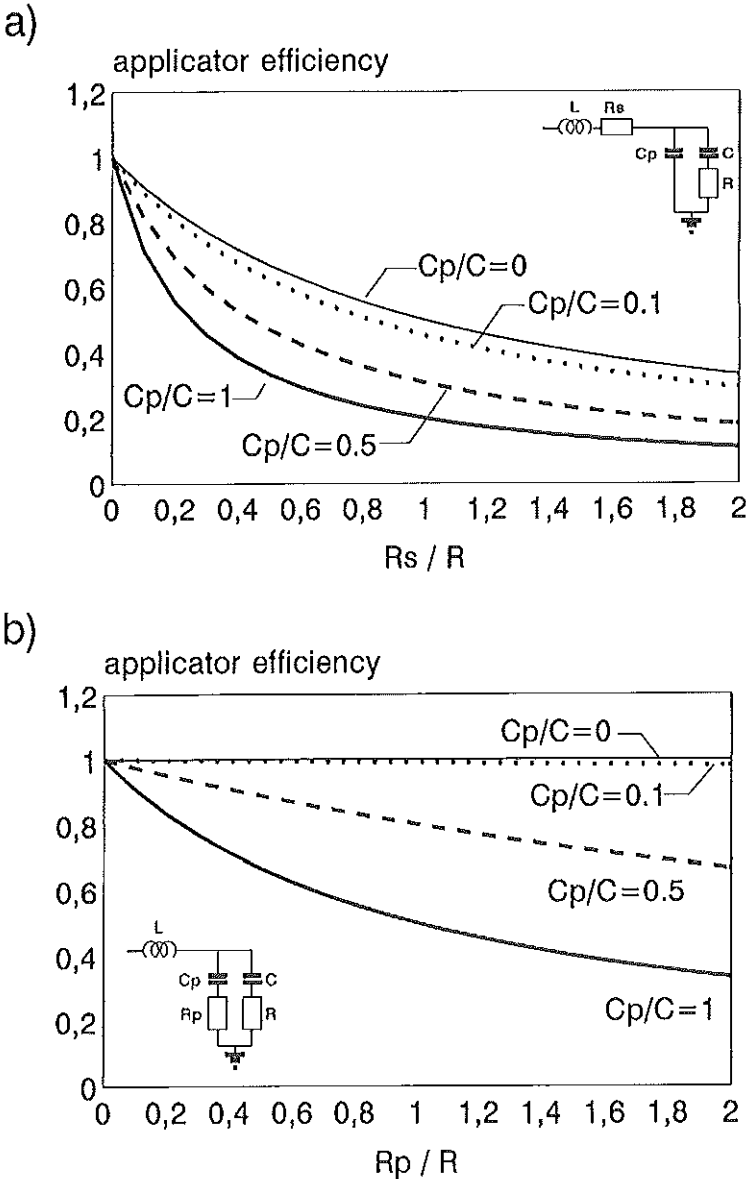


Figure 7. The applicator efficiency, a) as function of R_s/R ($R_p=0$), b) as function of R_p/R ($R_s=0$). C_p/C is varied (0, 0.1, 0.5 and 1).

The problems that may arise if applicator impedances are not matched accurately ($Z_{in} \neq 800\Omega$) are insufficient effective power and, if Z_{in} varies per channel, a cross-coupling between the four channels of one switch-module. In case of mismatching, part of the generator power is reflected, which decreases P_{eff} . In the worst case situation, i.e. if more than 20% of the power is reflected, the generators are switched off automatically to protect both patient and heating system. Mismatching does not always result in a lower efficiency. The transmission line efficiency can be lower as well as higher than under perfect matching conditions. Furthermore, if Z_{in} is different per channel, some channels will get more and some will get less than $\frac{1}{4}$ of the generator power. This latter effect makes the power control of one channel dependent of another. Using the theory described above, the heating efficiency can be predicted for a certain Z_{out} and transmission line length (see Figure 8).

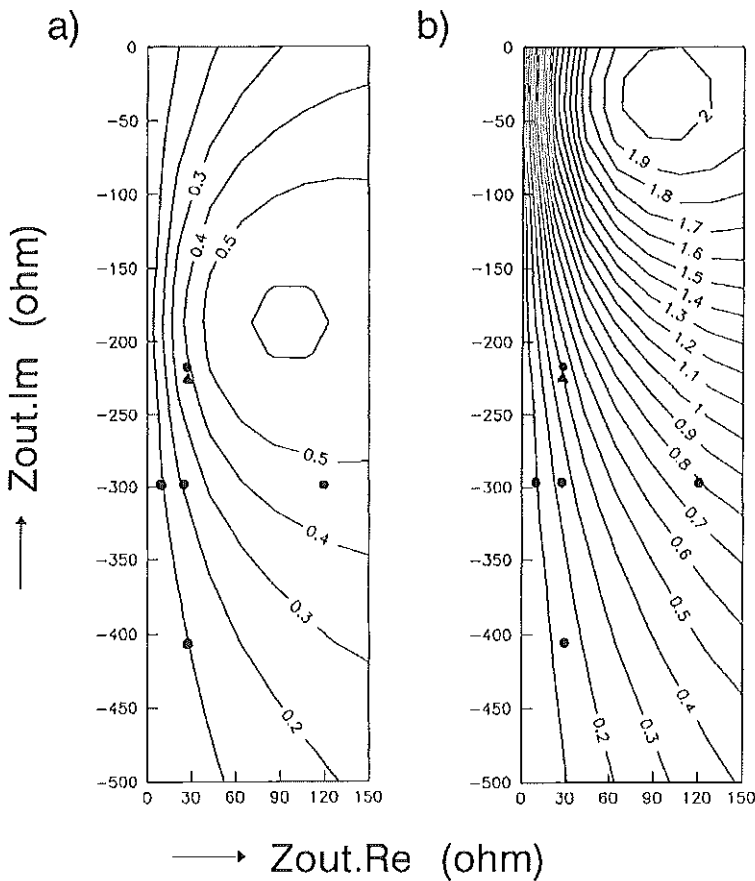


Figure 8. Computed channel-efficiency as a function of Z_{out} . Applicator losses are omitted. a) Same Z_{out} for all four channels of the switch module. b) Z_{out} of only one channel is varied. Z_{in} for the other channels is kept at 800Ω . The length of the matching cables is 85.5 cm. The triangle indicates the perfect match point and the dots correspond with the five experiments of Table 3.

2.5. Power requirements

To estimate the power absorption density, required to reach a certain minimum tumour temperature rise in the steady state, a simple spherical homogeneous tumour model was used. An effective heat conductivity was used to account for increased heat transport due to blood flow. The tumour and the implant volume are two concentric spheres. If the implant consists of "n" electrodes each with a length "l" (including the longitudinal spacing) and they are inserted in parallel afterloading catheters with a spacing "d", then the radius of the implant volume can be defined as $r_{\text{implant}} = (\frac{3}{4}nld^2/\pi)^{1/3}$. The effective power of electrodes is assumed to be homogeneously spread over the implant volume, resulting in a power absorption rate:

$$P = P_{\text{eff}} D_e \quad [\text{Wm}^{-3}] \quad (21)$$

with P_{eff} the power deposited in the tissue by each electrode and $D_e = (ld^2)^{-1}$ the electrode density [m^{-3}].

The stationary radial temperature distribution can be obtained by solving the heat equation for a sphere-symmetric medium:

$$\frac{1}{r^2} \frac{\partial}{\partial r} \left(k r^2 \frac{\partial T(r)}{\partial r} \right) = -P(r) \quad [\text{Wm}^{-3}] \quad (22)$$

with $T(r)$ the temperature [$^{\circ}\text{C}$], k the effective heat conductivity [$\text{W m}^{-1} \text{ } ^{\circ}\text{C}^{-1}$] and $P(r)$ the power absorption rate [W m^{-3}]. The solution of equation 22 is:

$$T(r) = T_{\infty} + \frac{Pr_{\text{implant}}^2}{2k} - \frac{Pr^2}{6k} \quad [^{\circ}\text{C}] \quad (23)$$

and

$$T(r) = T_{\infty} + \frac{Pr_{\text{implant}}^3}{3k} \frac{1}{r} \quad [^{\circ}\text{C}] \quad (24)$$

for $r < r_{\text{implant}}$ and $r \geq r_{\text{implant}}$, respectively. T_{∞} [$^{\circ}\text{C}$] is the temperature at large distance from the implant centre. The minimum tumour temperature (T_{min}) is found at the edge of the tumour, i.e. at $r = r_{\text{tumour}}$. With $r = r_{\text{tumour}}$ and $T = T_{\text{min}}$ in equations 23 and 24, expressions for the required power absorption rate are obtained:

$$P = \frac{2k(T_{\min}-37)}{r_{\text{implant}}^2 - \frac{1}{3}r_{\text{tumour}}^2} \quad [\text{W}] \quad (25)$$

and

$$P = \frac{3r_{\text{tumour}}k(T_{\min}-37)}{r_{\text{implant}}^3} \quad [\text{W}] \quad (26)$$

for $r_{\text{tumour}} < r_{\text{implant}}$ and for $r_{\text{tumour}} \geq r_{\text{implant}}$, respectively, with $T_{\infty} = 37^{\circ}\text{C}$.

2.6. Experimental verification

The aim of the experiments was to test the effective power theory of section 2.4. First, a series of calorimetric effective power measurements were performed, using load impedances (Z_{out}), consisting of a resistor (R) and a capacitor (C) only. The resistors were placed in a known quantity of demineralized water and the temperature rise was measured after a certain time of heating, using a thermocouple probe. From these data and the specific heat coefficient of water ($4180 \text{ J kg}^{-1}\text{ }^{\circ}\text{C}^{-1}$) the effective power per load was computed.

Because most of P_{out} is dissipated in the resistors, the loads can be seen as perfect applicators, i.e. with $\eta_a \approx 1$.

The experiments were performed with four equal loads, connected to the four channels of one switch module. The magnitudes of both R and C were varied to study the effect of mismatching on P_{eff} . Equal Z_{in} and different Z_{in} mismatching were investigated with all four channels switched on or only one channel switched on, respectively.

Furthermore, P_{eff} was measured for two types of clinically used applicators to study the applicator losses. A thermally isolated box ($5 \times 5.5 \times 8 \text{ cm}^3$) was filled with 200 ml saline solution with a muscle-equivalent NaCl concentration of 3.8 g/l (at 20°C : $\epsilon_r = 79$, $\sigma = 0.6 \text{ } \Omega^{-1}\text{ m}^{-1}$). Four parallel POM catheters ($d_i = 1.5 \text{ mm}$, $d_o = 2 \text{ mm}$) were positioned in a square geometry, with 1.5 cm spacing. In each catheter either a dual-electrode applicator (electrode-segment length: 2 cm, longitudinal spacing: 1 cm) was inserted or it was loaded with two single-electrode applicators (electrode-segment length: 2 cm), inserted from opposite sides and also with a longitudinal spacing of 1 cm. In each catheter, one electrode was connected to a 0° -channel and one to a 180° -channel of the power system. All 0° -electrodes were at one side of the central plane perpendicular to the catheters and the 180° -electrodes were at the other side. The measurements were performed with or without a 7-point thermocouple probe. Each P_{eff} -value is the average of five measurements.

The applicators were matched in the saline solution at environmental temperature. First, the applicator impedance Z_a was established. The impedance between the two electrodes, of one dual-electrode applicator or of two single-electrode applicators, in one afterloading catheter ($2Z_a$) was measured using a network-analyzer (HP8751A). A balanced-to-unbalanced 1:1 impedance transformer was inserted between applicators and network-analyzer to assure that the measurement was symmetric around the system ground. Subsequently, the inductance (L) and the length of the matching cable (l_{match}), needed for a perfect matching, were computed.

The components of Z_{out} , i.e. the applicator impedance plus the impedance of the matching inductance (Z_L) (Figure 5), were obtained to compute the applicator efficiency (η_a). First, the electrode impedance (R_e , about 1.7 Ω) and the impedance of the matching coil (Z_L) were measured. From these measurements R_s , which is the sum of R_e and the real part of Z_L , was obtained. In order to estimate C_p and R_p the impedance between two electrodes was measured in air instead of the saline solution and R_e was subtracted. The measurements in air and in the NaCl-solution together give C and R .

Simultaneously with all P_{eff} -measurements P_{fwd} and P_{rfl} were measured between filter and switch module, using a Bird-power-meter.

3. Results

3.1. Experiments with R and C components

The aim was to investigate the effect of impedance matching on P_{eff} . The experiments with the simulated applicators, described in section 2.6., were performed with a matching cable of 85.5 cm. P_{eff} has been measured for five load impedances, one giving a negligible power reflection ($Z_{\text{out}} = 27\text{-}295j \Omega$) and four values around this optimum. Furthermore, the measurements were compared with the theory. The results are summarized in Table 3. The generator power, with all channels switched off, i.e. switched to 800 Ω -loads, was 20.4 W. The overall efficiency (η_{meas}) which is defined as the ratio between P_{eff} and $\frac{1}{4}P_{\text{gen}}$ was found to be rather dependent on Z_{out} . More power was absorbed in the water for increasing C and for increasing R . This is in qualitative agreement with efficiency calculations. Figure 8 shows the computed efficiency as a function of Z_{out} for the situation in which $\eta_a = \eta_s = 1$. The triangle denotes the load impedance which transforms to exactly 800 Ω if l_{match} is 85.5 cm. The circles mark the five loads used in the experiments. Looking at Table 3, load no. 2 seems to give the best impedance matching, i.e. the lowest reflected power, while the theory predicts the best match for load no. 5.

On the other hand, in case of mismatching the sum of P_{fwd} and P_{rfl} is expected to remain equal to P_{gen} . This is only seen with load no. 5. Apparently, the 1/8 power splitting (Figure 1a) does not function perfectly for larger

mismatching, resulting in a lower P_{rfl} with load no. 2 than with load no. 5.

A more quantitative comparison of the efficiencies obtained from the measurements and the calculated efficiencies (Table 3) shows a difference which cannot be explained in terms of measurement errors. The ratio between η_{meas} and η_{calc} is a measure for losses which were not included in the calculations. These were found to be in the range of 36 to 64%. The losses in Z_{out} and in the switch module are the ones that were omitted in the computations. However, since R is the main dissipating component of Z_{out} and energy leakage out of the water can be neglected, P_{out} can be calculated from the temperature rise of the water and η_a is expected to be close to 1. Furthermore, no significant temperature rise was observed in the switch module when all four channels were switched on. Therefore, it is unlikely that the η_a multiplied by η_s could have been so low that this could explain the differences between η_{meas} and η_{calc} .

Table 3. Effective power measurements with Z_{out} consisting of a resistor and a capacitor.

(i) Four channels switched on.

No	Z_{out}		P_{eff}	P_{fwd}	P_{rfl}	η_{meas}	η_{calc}^1
	[Ω]	[Ω]					
1	10	-295j	0.29 (0.02)	21.5	0.8	0.06	0.10
2	27	-295j	0.87 (0.04)	22.0	0.3	0.17	0.24
3	119	-295j	1.56 (0.06)	20.5	1.8	0.31	0.48
4	27	-405j	0.33 (0.01)	21.7	3.5	0.06	0.13
5	27	-220j	1.14 (0.04)	17.6	2.1	0.22	0.40

(ii) One channel switched on.

No	Z_{out}		P_{eff}	P_{fwd}	P_{rfl}	η_{meas}	η_{calc}^1
	[Ω]	[Ω]					
1	10	-295j	0.17 (0.04)	20.7	0.3	0.03	0.08
2	27	-295j	0.75 (0.03)	21.3	0.3	0.15	0.25
3	119	-295j	1.91 (0.12)	20.0	0.3	0.37	0.79
4	27	-405j	0.24 (0.02)	20.6	0.3	0.05	0.13
5	27	-220j	1.25 (0.03)	19.7	0.7	0.25	0.41

values between brackets are the standard deviations after five measurements.

¹ With $\eta_s = \eta_a = 1$

The exact cause for this missing power is still unknown at the moment. Probably, the load impedances also act as antennas, as a result of which part of the energy is not dissipated in the resistances and therefore not absorbed in the water.

3.2. Experiments with real applicators

If real applicators are used, applicator losses are unavoidable. We will show how the applicator design can affect the composition of Z_{out} and thus η_a . The components of Z_{out} were measured for both a single-electrode and a dual-electrode applicator, with or without thermo-couple probe. From the measurements of Z_a in the saline solution the appropriate I_{match} and L were chosen. For the single-electrode and the dual-electrode applicators the lengths of the matching cables were 85.5 cm and 72.5 cm, respectively. To transform Z_{out} roughly to $Z_{out,ideal}$ corresponding with these lengths, i.e. 26-227j Ω and 13-150j Ω , respectively, a matching inductance was added. For the dual-electrode applicators, with or without thermometer inside, 1.6 μH was taken. Because the single-electrode impedance is rather dependent on whether or not a thermometer is inserted, two different matching inductances were used, i.e. 2.6 μH with and 1.3 μH without thermocouple probe. The actual impedance of Z_L was measured separately. The components of Z_{out} and the resulting applicator efficiency are shown in Table 4. Because the matching cable is shorter when the dual-electrodes are used, the transmission line efficiency is somewhat larger than for the single-electrode applicators, i.e. 0.41 versus 0.38 (Figure 6).

The measured and calculated effective powers are given in Table 5. As with the RC-loads the measured heating efficiency is somewhat lower than predicted, but the qualitative agreement between measurements and computations is good. If no thermocouple probe is inserted, the single-electrode applicator is, as expected, more effective than the dual-electrode applicator, in which extra losses are induced by the cross-coupling between the leads. However, if a thermometer is added, the single-electrode applicator efficiency decreases considerably, while P_{eff} of the dual-electrode applicator is only slightly lower with than without thermocouple probe. The reason for this difference is that in the latter case the thermocouple probe is inside the applicator at about zero potential and therefore energy leakage through the thermocouple leads towards the thermometry system can be neglected. A thermometer in a single-electrode applicator enlarges the antenna behaviour of the applicator which causes a high-resistive parasitic pathway to the system ground.

Although the impedance matching was performed with a set of two electrodes, the matching with eight electrodes remained good, except for the eight single-electrode applicators with thermometer. In this situation, the thermocouple leads are radiating antennas. Therefore, the applicator impedance strongly depends on the experimental set-up. For example, Z_a with

eight applicators in the phantom is different from Z_a with two applicators. Another example is that Z_a changes if the thermometers are disconnected from the thermometry system. These effects are not seen if dual-electrode applicators are used. To obtain a good matching, using the single-electrode applicators with thermometer, these measurements of P_{eff} have been performed in the matching situation, i.e. using two applicators.

Table 4. Components of Z_{out} and the calculated applicator efficiency.

		Single-electrode applicator		Dual-electrode applicator	
		(-)	(+)	(-)	(+)
Z_{out}	[Ω]	34-228j	36-228j	19-202j	16-155j
C	[pF]	6.2	6.0	6.3	6.3
R	[Ω]	49.7	55.4	49.6	50.1
C_p	[pF]	2.5	6.9	6.2	7.6
R_p	[Ω]	34.2	68.7	6.7	4.7
L	[μ H]	2.6	1.3	1.6	1.6
R_s	[Ω]	6.2	4.3	4.7	4.7
$\eta_{a,\text{calc}}$	[]	0.74	0.33	0.67	0.63

(-): Without thermocouple probe inside the applicator.

(+): With thermocouple probe connected to thermometry system.

Table 5. P_{eff} , computed and measured values.

		Single-electrode applicator		Dual-electrode applicator	
		(-)	(+)	(-)	(+)
$P_{\text{eff,calc}}$	[W]	1.41	0.63	1.37	1.29
$P_{\text{eff,meas}}$	[W]	1.25 (0.03)	0.59 (0.02)	1.04 (0.04)	0.92 (0.04)

Values between brackets is the standard deviation after five measurements.

(-): Without thermocouple probe inside the applicator.

(+): With thermocouple probe connected to thermometry system.

4. Discussion

In the previous section it was found that, using typically clinical applicators with well matched electrodes, P_{eff} is about 1 W. To investigate under which conditions this value is high enough, the model described in section 2.5. can be used. With a P_{eff} of about 0.5 W some unwanted power loss due to mismatching is taken into account. As an example a well perfused tumour is taken which can be described with an effective heat conductivity of $k = 3 \text{ Wm}^{-1} \text{ } ^\circ\text{C}^{-1}$ (Crezee *et al.*, 1991), which is about five times the intrinsic value of muscle tissue. Furthermore, a target temperature at the edge of the tumour of 43°C and an electrode density of about 0.2×10^6 electrodes per m^3 were chosen. The latter, for example, corresponds with electrodes with an effective length (l), i.e. including the longitudinal spacing between the electrodes, of 2.5 cm and a distance between the afterloading catheters (d) of 1.5 cm. Here, D_e was defined as $(ld^2)^{-1}$. The power absorption rate follows from either equation 25 or equation 26 and P_{eff} can be computed using equation 21. In Figure 9 P_{eff} is shown as a function of the tumour radius. The radius of the implanted volume was varied. It can be seen that small tumours can be heated sufficiently with a P_{eff} of 0.5 W, but only if the implanted volume exceeds the tumour volume. For larger tumours lower P_{eff} is sufficient. It is obvious that with increasing tumour size more electrodes are needed to cover the whole tumour. Therefore, there is an upper limit for the tumour radius which depends on the available number of electrodes (n_{max}). If $r_{\text{tumour}} = r_{\text{implant}}$ this radius follows from the equations 21 and 26:

$$r_{\text{tumour,max}} = \frac{n_{\text{max}} P_{\text{eff}}}{4 \pi k (T_{\text{min}} - 37)} \quad [\text{m}] \quad (27)$$

The maximum number of electrodes that can be used is 64. If $k = 3 \text{ Wm}^{-1} \text{ } ^\circ\text{C}^{-1}$, $T_{\text{min}} = 43^\circ\text{C}$ and $P_{\text{eff}} = 0.5 \text{ W}$, $r_{\text{tumour,max}} = 7 \text{ cm}$. The electrode density ($3n/4\pi r^3$) in this situation is $0.04 \times 10^6 \text{ m}^{-3}$, e.g. 5.5 cm long electrodes and 2 cm catheter spacing.

It should be noticed that, in contrast with the model assumption that the power absorption is homogeneous in the implant volume, in reality it is rather inhomogeneous. It is an intrinsic property of interstitial hyperthermia that the highest absorption rate is found near the applicators. If the distance between the electrodes would be too large, T_{min} may no longer be located at the edge of the tumour, but somewhere in between the electrodes. In these situations T_{min} is often limited by pain caused by high temperatures near the electrodes and not by the available P_{eff} . Therefore, large catheter spacing should be avoided, especially in sensible regions as the head and neck. With the 27 MHz current source IHT-system a reasonably homogeneous temperature distribution can be reached through heat conduction, as long as the distances between the afterloading catheters do not exceed 1.5 cm, which is also an upper limit in brachytherapy.

Furthermore, in order to minimize inhomogeneous heating due to larger blood vessels or spatial variation of electrical and thermal tissue properties, one should always choose the shortest possible electrodes. Sometimes a compromise has to be found between l and d . For example, if $D_e = 0.04 \times 10^6 \text{ m}^3$ and the tissue is quite homogeneous, it might be better to take l longer and d smaller than the above-mentioned $l = 5.5 \text{ cm}$ and $d = 2 \text{ cm}$.

In practice, a high-density implant with 1 cm distance between the afterloading catheters and electrodes with an effective length of 1.5 cm ($D_e \approx 0.7 \times 10^6$ electrodes per m^3) is feasible. This decreases the required effective power with a factor of almost 4 in comparison with the example shown in Figure 9.

There may be situations in which sufficient power is not available, for example, in case of a small, highly perfused tumour. Especially if it is preferred to keep the afterloading catheters within the tumour volume, e.g. because of the risk of normal tissue damage in brain tumours. To achieve more effective power in these situations, there are several possibilities. First, it is possible to connect each electrode to two, three or four channels. This reduces the number of electrodes which can be used and thus limits the maximum treatable tumour size. However, shortage of effective power mainly occurs for smaller tumours.

Secondly, one could deliberately allow some mismatching to improve η_{it} . In Figure 8 it can be seen that if Z_{out} is less capacitive or more resistive than $Z_{out,ideal}$ for a certain l_{match} , the overall efficiency increases. Furthermore, one can search for ways to optimize η_a . This applicator efficiency depends on R_s/R , R_p/R and C_p/C (Figure 7) and can be improved by decreasing one or more of these ratios. Applicator design, size and material of afterloading catheter, and the losses in the matching inductances are the main factors to be improved.

To reach an optimal coupling with the tissue the electrode segments must fit tightly in the afterloading catheters. This requires either straight catheters or flexible segments and the catheters must not be narrowed by e.g. buttons, screws or sharp curves.

The applicator efficiency also depends on the afterloading catheter. C_p/C can be lowered by decreasing the ratio between the outer and inner diameter or by increasing the dielectric constant of the catheter material. A higher dielectric loss factor would increase R and thus decrease R_s/R and R_p/R . However, this would make the applicators acting like hot sources which results in a less homogeneous temperature distribution.

The losses represented by R_s are mainly due to dissipation in the serial matching inductance. Impedance matching with a parallel low loss capacitor instead of L might lower R_s . In case of a dual-electrode applicator this can be achieved by a design with a larger coupling between the electrodes.

Factors which do have effect on η_a but cannot be manipulated are the electrical properties of the tissue. Hot spots are often seen in high-resistive fatty tissue. Although σ and ϵ_r cannot be changed, some manipulation of R is possible by choosing a more or a less resistive phase configuration of the electrodes.

In the present design of the heating system the maximum P_{eff} is limited by the choice to transform the applicator impedance to 800 Ω . Therefore, the maximum efficiency will be in the range 0.35-0.45, which is the efficiency of the transmission line (Figure 6). Together with an additional loss factor of about 0.5 this means that maximally about 1 W of the 5 W channel input power will be dissipated effectively in the tissue if the electrode is properly matched. Using the theory of section 2.4.2., it can be easily shown that transforming the impedance to a lower value results in a higher transmission line efficiency. For example, with $Z_{\text{in}} = 200 \Omega$ instead of 800 Ω η_{tl} will be more than 0.8. For the moment, the above mentioned solutions of more channels per electrode or deliberate mismatching are adequate in situations in which sufficient power is not available.

Uncontrolled mismatching should be avoided. If for some reason the impedance is not matched correctly, three problems may occur. First, a system error makes it impossible to continue the treatment. Secondly, power steering problems may arise due to cross coupling between electrodes connected to the same switch module. This means that P_{eff} of each electrode depends on the duty cycle of the other three electrodes. Last, but probably most important, adequate heating is not possible due to a decreased P_{eff} .

A system error due to mismatching is in most cases induced by too much reflected power. It arises when an applicator is defective, connected to the wrong channel or when the electrode segments are shifted out of the tissue. In practice, the solution to this problem can be found in checking each applicator separately and replacing them if necessary.

Mismatching occurs when the tissue impedance is different from the match phantom and does affect P_{eff} . If different electrodes are surrounded by different tissues, P_{eff} may vary per electrode. These variations have proved to be small in clinical applications and can be controlled by the automatic temperature control algorithm of the system. However, if four electrodes connected to the same switching module are mismatched, their power cannot be controlled independently. In Table 3 it can be seen that P_{eff} changes if three out of four channels are switched off. To avoid toxicity in the patient, abrupt large changes of duty cycles, such as 100% to 0%, should be carried out in several steps. Safety procedures have been incorporated in the temperature control algorithm to avoid overheating.

If P_{eff} decreases due to mismatching, the target temperature may not be reached. This happens mostly when R *in vivo* is lower than in the agar phantom used for impedance matching. Because a muscle-equivalent phantom is used, patient tissue resistance is in most cases equal or higher. Furthermore, the phase configuration used in the patient could be less resistive than in the phantom. For example, in section 3.2. it was shown that P_{eff} of the dual-electrode applicators with thermometer was 0.92 W. Changing the phases of the electrodes in two of the four catheters reduces R with about 10 Ω . $P_{\text{eff, meas}}$ in this situation decreases to 0.55 W. A third reason for a lower R during treatment is the higher temperature. In Figure 10 the ratio between the tissue impedances at a certain temperature T and at 24°C is shown as function of

the temperature. The ratio was calculated using equation 8 and σ and ϵ_r were computed with the equations of Stogryn (1971) for a saline solution with 3.8 g NaCl per litre and a frequency of 27 MHz. If e.g. the matching took place at 24°C with $Z_t = 60-7j \Omega$, the tissue impedance is $42-3j \Omega$ at 44°C. This certainly results in a lower P_{eff} but is on the other hand a protection mechanism at higher temperatures.

In general, pre-matching in a muscle-equivalent phantom in a one- dual-electrode applicator configuration gives clinically applicable applicators.

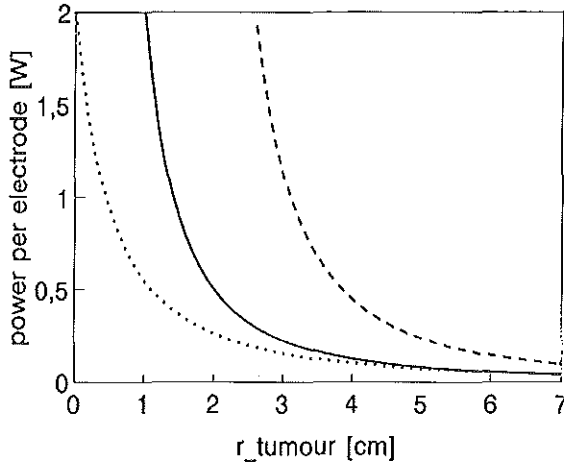


Figure 9. P_{eff} as a function of the tumour radius, for r_{implant} 1 cm smaller than r_{tumour} (dashed line), for r_{implant} equal to r_{tumour} (solid line) and for r_{implant} 1 cm larger than r_{tumour} (dotted line).

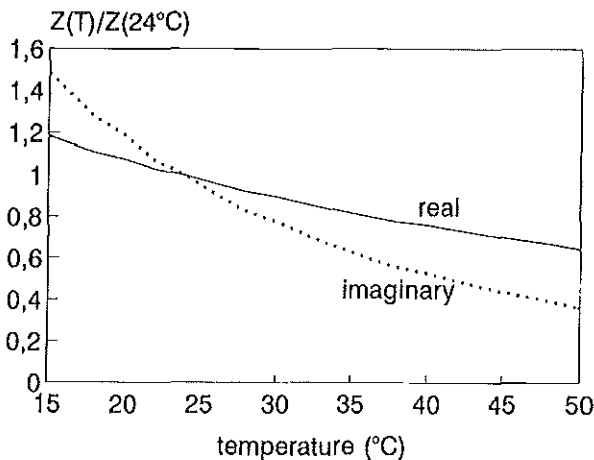


Figure 10. Ratio between the tissue impedance, calculated for a saline solution (3.8 g/l), at a certain temperature and the impedance at 24°C, as a function of the temperature.

5. Conclusions

The effective power per electrode which is matched correctly is about 1 W. Mismatching can affect P_{eff} considerably. However, because the matching theory is well understood, mismatching is not a serious problem in clinical practice and can even be used to increase P_{eff} if necessary. Impedance matching of applicators in a muscle-equivalent phantom is feasible. No serious mismatching is expected during treatment. The main conclusion is that with the MECS-IHT system sufficient power can be deposited in the tissue to obtain an adequate heating treatment of well perfused tumours.

Acknowledgements

The authors wish to thank Ms. Inge Dijkstra for her help in preparing the manuscript. This study is supported by the Dutch Cancer Society and by Nucletron Corporation Veenendaal

References

- Crezee J, Mooibroek J, Bos CK and Lagendijk JJW, 1991, Interstitial heating: experiments in artificially perfused bovine tongues. *Physics in Medicine and Biology* **36**: 823-833.
- De Leeuw AAC, Crezee J and Lagendijk JJW, 1993, Temperature and SAR measurements in deep-body hyperthermia with thermocouple thermometry. *International Journal of Hyperthermia* **5**: 685-697.
- Deurloo IKK, Visser AG, Morawska-Kaczynska M, Van Geel CAJF, Van Rhoon GC and Levendag PC, 1991, Application of a capacitive coupling interstitial hyperthermia system at 27 MHz; study of different applicator configurations. *Physics in Medicine and Biology* **36**: 119-132.
- Gabriel C, Gabriel S and Corthout E, 1996, The dielectric properties of biological tissues: I. Literature survey. *Physics in Medicine and Biology* **41**: 2231-2249.
- Lagendijk JJW, Visser AG, Kaatee RSJP, Crezee J, Van der Koijk JF, De Bree J, Kotte ANTJ, Kanis AP, Levendag PC and Battermann JJ, 1995, The 27 MHz current source multi-electrode interstitial hyperthermia method. *Activity, International Nucletron-Oldelft Radiotherapy* **6**: 83-90.
- Marchal C, Nadi M, Hoffstetter S, Bey P, Pernot M and Prieur G, 1989, Practical interstitial method of heating at 27.12 MHz. *International Journal of Hyperthermia* **4**: 451-466.
- Stogryn A, 1971, Equations for calculating the dielectric constant of saline water. *IEEE Transactions on Microwave Theory and Techniques* **19**: 733-736.
- Visser AG, Deurloo IKK, Levendag PC, Ruijrok ACC, Cornet B and Van Rhoon GC, 1989a, An interstitial hyperthermia system at 27 MHz. *International Journal of Hyperthermia* **5**: 265-276.
-

Chapter 4

Temperature measurement errors with thermocouples inside 27 MHz multi electrode current source interstitial hyperthermia applicators

This chapter was published as:

Kaatee RSJP, Crezee J and Visser AG, 1999, Temperature measurement errors with thermocouples inside 27 MHz multi electrode current source interstitial hyperthermia applicator . *Physics in Medicine and Biology* **44**: 1499-1511.

Abstract

The multi-electrode current source (MECS) interstitial hyperthermia (IHT) system uses thermocouple thermometry. To obtain inhomogeneous temperature distribution and to limit the number of traumas due to implanted catheters, most catheters are use for both heating and thermometry. Implications of temperature measurement inside applicators are discussed. Particularly, the impact of selfheating of both the applicator and the afterloading catheter were investigated.

A one-dimensional cylindrical model was used to compute the difference between the temperature inside the applicators (ΔT_{in}) and the tissue just outside the afterloading catheter (ΔT_{out}) as a function of power absorption in the afterloading catheter, selfheating of the applicator and the effective thermal conductivity of the surrounding tissue. Furthermore, the relative artefact (ERR), i.e. $(\Delta T_{in} - \Delta T_{out}) / \Delta T_{in}$, was measured in a muscle equivalent agar phantom at different positions in a dual-electrode applicator and for different catheter materials. A method to estimate the tissue temperature by power-off temperature decay measurement inside the applicator was investigated.

Using clinical dual-electrode applicators in standard brachytherapy catheters in a muscle-equivalent phantom, ΔT_{in} is typically twice as high as ΔT_{out} . The main reason for this difference is selfheating of the thin feeder wires in the

centre of the applicator. The measurement error caused by energy absorption in the afterloading catheter is small, i.e. even for materials with a high dielectric loss factor less than 5%. About 5 s after power has been switched off, T_{in} in the electrodes represents the maximum tissue temperature just before power-off. This delay time (t_{delay}) and ERR are independent of T_{in} . However, they do depend on the thermal properties of the tissue. Therefore, ERR and t_{delay} and their stability in perfused tissues have to be investigated to enable a reliable estimation of the tissue temperatures around electrodes in clinical practice.

1. Introduction

In hyperthermia, accurate measurement of tissue temperatures is essential. During a treatment, temperature information is needed as an input for power steering in order to optimize the temperature distribution. Furthermore, the temperature as a function of location and time is crucial in the discussion about the relation between thermal dose and clinical outcome, i.e. tumour response and normal tissue toxicity.

A temperature measurement error can be defined as the difference between the temperature reading and the tissue temperature at the position of interest which is not necessarily the sensor position.

The 27 MHz multi electrode current source (MECS) interstitial hyperthermia (IHT) system (Visser *et al* 1989, Lagendijk *et al* 1995) uses manganin-constantan thermocouple thermometry. Clinical use of thermocouples has been discussed thoroughly by Carnochan *et al* (1986). Using thermocouples in combination with 27 MHz IHT, the two important potential sources of measurement errors are: firstly, the presence of large temperature gradients and secondly, the applied 27 MHz electromagnetic field.

Temperature gradients of $1-2^{\circ}\text{C mm}^{-1}$ at the edge of the tumour and near the applicators during the heating-up period are typical for interstitial hyperthermia. Measurement errors, due to thermal conduction along the thermocouple leads (Dickinson 1985) or along the applicator plus thermometer (Ryan *et al* 1989), or due to a temperature gradient across the junctions of multi-point thermocouple probes (Bach Anderson *et al* 1984, Dickinson 1985, Lagendijk and De Leeuw 1993), can be reduced considerably if manganin-constantan instead of copper-constantan thermocouples are used.

In practice, measurement errors with manganin-constantan thermocouples due to high longitudinal temperature gradients are equivalent to a shift of the thermocouple probe of less than 1 mm. This is considered to be acceptable, particularly because the uncertainty about the exact sensor position relative to the target volume is generally more than 1 mm.

With respect to the measurement errors related to the 27 MHz heating method, it should be noticed that, due to the high operating frequency and the fact that, generally, thermocouple probes are inserted in the applicators, the capacitive coupling between thermocouple probe and heating applicator is not

negligible (1-5 pF) compared with the electrode-tissue coupling (5-10 pF). This coupling may induce a so-called common mode current if the impedance towards the thermometry instrumentation is low, resulting in disturbance of the thermocouple-voltage reading and in selfheating of the thermocouple leads and/or the cold junction connector. This problem has been discussed in detail by Crezee *et al* (1997). In addition, the surrounding tissue may be heated due to either capacitive or inductive coupling between tissue and leads. Furthermore, a difference between the electrical resistances of the thermocouple metals may give rise to a junction current, increasing the junction temperature (Chakraborty and Brezovich 1982). This can be minimized by choosing balanced thermocouples made of, for example, manganin-constantan instead of copper-constantan. In general, the so-called pick-up errors due to the 27 MHz electromagnetic field can be reduced by low-pass filtering of the thermocouple signals.

The most important measurement error in interstitial hyperthermia is caused by the fact that sensors are often placed inside the heating applicator and are not in direct contact with the tissue. Although the distance between the sensor and the actual position of interest in the tissue, just outside the afterloading catheter, is small (about 1 mm), a radial temperature gradient may occur. The temperature measured in the applicator will be higher than the tissue temperature if electromagnetic energy is absorbed in between tissue and thermometer, e.g. in the catheter wall due to dielectric losses or because of selfheating in the applicator and/or the thermocouple probes.

The difference between the temperature in the applicator and the tissue temperature distribution just outside the afterloading catheter, as a function of thermal properties of the tissue and of selfheating in the applicator and the afterloading catheter, was examined through model calculations and phantom measurements. Furthermore, a method was explored to minimize this artifact, by applying a certain delay time between power switch-off and temperature measurement.

2. Materials and methods

2.1. The MECS-IHT system

The 27 MHz MECS-IHT system has been developed in a collaboration between the University Hospital Utrecht and the Daniel den Hoed Cancer Center Rotterdam (Lagendijk *et al* 1995). Three units can be distinguished, i.e. a power supply system, a thermometry system and a UNIX workstation to provide the connection between the first two units and the operator. The power unit consists of has two groups of 32 coherent channels each. The two groups are 180° out of phase.

Multi-electrode applicators can be inserted in standard brachytherapy afterloading catheters. The current source heating method has been described earlier (Marchal *et al* 1989, Visser *et al* 1989, Deurloo *et al* 1991).

Temperature measurements are performed with 7-point constantan-manganin thermocouple probes (ELLA-CS, Czech Republic). Fast data acquisition (all 196 channels within 320 ms) is feasible with a high resolution thermometry system (De Leeuw *et al* 1993).

Undisturbed temperature measurement is possible with 7-channel RF-filters, specially designed for the 7-point thermocouple probes. They consist of a ferrite toroid ($14 \times 9 \times 5$ mm, $\mu=100$, ferroxcube 4C6, Philips) and eight ceramic capacitors (220 nF). All eight thermocouple wires were wound 10 times around half a single toroid and were connected to the shielding, via a capacitor. The coil impedance at 27 MHz is about $870 + 1310j \Omega$ ($7.7 \mu\text{H}$). Measurements using a network analyzer (HP8751A) show that an attenuation of more than 90 dB can be achieved. A diagram is shown in Figure 1.

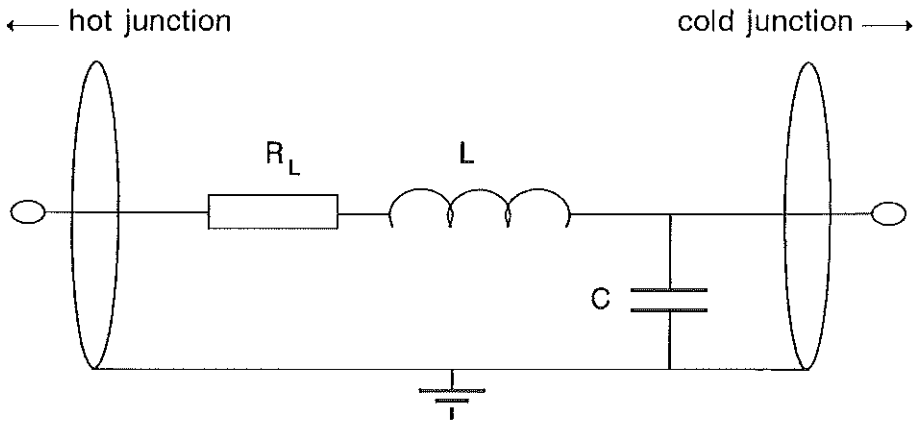


Figure 1. Design for one of the leads of a 7-channel RF-filter.

2.2. Model calculations

A simple steady state model was used to estimate the difference between the temperature in the centre of the applicator and the tissue temperature at the outside of the afterloading catheter. The applicator, afterloading catheter and tissue were approximated by infinitely long cylinders. A cross section is shown in Figure 2. The effective heat conductivity model was used to take blood flow into account. For a homogeneous, cylinder-symmetric medium, the heat equation is

$$\frac{1}{r} \frac{\partial}{\partial r} r k_{\text{eff}}(r) \frac{\partial T(r)}{\partial r} + P(r) = 0 \quad (1)$$

With $k_{\text{eff}}(r)$ the effective heat conductivity ($\text{Wm}^{-1} \text{C}^{-1}$) of the medium and $P(r)$ the cylinder symmetric-volumetric heat production (Wm^{-3}).

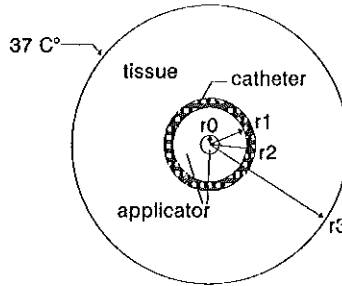


Figure 2. Cross section of the model for the applicator ($r \leq r_1$), the afterloading catheter ($r_1 < r \leq r_2$) and the part of surrounding tissue in which a temperature gradient exists ($r_2 < r \leq r_3$). The applicator is divided in an absorbing part ($r \leq r_0$) and a non-absorbing part ($r_0 < r \leq r_1$). Typical values for r_0 , r_1 , r_2 and r_3 are 0.1, 0.75, 1 and 10 mm, respectively.

The selfheating in the electrodes and in the thermocouple probe was modelled using a power-absorption-per-meter factor Q (Wm^{-1}). Q is assumed to be absorbed homogeneously within a cylinder with radius r_0 . The heat absorption density in this cylinder is

$$P_o(r) = \frac{Q}{\pi r_0^2} \quad (Wm^{-3}) \quad (2)$$

The remaining part of the applicator (a low-loss polythene catheter) and the afterloading catheter lumen, i.e. between r_0 and r_1 , is assumed to be without loss. If the afterloading catheter material and the tissue are assumed to be homogeneous, the absorption density is proportional to $1/r^2$. The densities of electromagnetic energy absorption in the afterloading catheter wall (between r_1 and r_2) and in the surrounding tissue (between r_2 and r_3) are

$$P_c(r) = \left[\frac{I}{2\pi} \right]^2 \frac{\tan\delta}{\omega\epsilon_0\epsilon_{r,c}(1+\tan^2\delta)} \frac{1}{r^2} = \frac{\alpha_c}{r^2} \quad (Wm^{-3}) \quad (3)$$

and

$$P_t(r) = \left[\frac{I}{2\pi} \right]^2 \frac{\sigma}{(\omega\epsilon_0\epsilon_{r,t})^2 + (\sigma)^2} \frac{1}{r^2} = \frac{\alpha_t}{r^2} \quad [W m^{-3}] \quad (4)$$

respectively, with I the current flowing from the applicator ($A m^{-1}$), ϵ_0 the permittivity of free space and ω the radial frequency of the heating system. Furthermore, $\tan(\delta)$ and $\epsilon_{r,c}$ are the dielectric loss factor and the relative permittivity of the catheter material, respectively; σ and $\epsilon_{r,t}$ are the electric conductivity and the relative permittivity of the tissue. The metabolic heat production in the tissue was neglected. α_c and α_t are constants.

The following boundary conditions were used to solve equation 1 for each

of the media. Firstly, the heat flow through a certain cylinder surface is equal to the heat absorbed within that cylinder, which means that the applicator is thermally isolated at $r=0$. Secondly, the temperature distribution is continuous at the transition of two media and is assumed to be 37°C at $r=r_3$. The resulting temperature distributions in the tissue (T_t), the afterloading catheter wall (T_c), the non-absorbing part of the applicator and catheter (T_a), and the central absorbing part of the applicator (T_o) are given by the equations 5, 6, 7 and 8, respectively

$$T_t(r) = 37 + \left[-\frac{Q}{2\pi k_t} - \frac{\alpha_c \ln \frac{r_2}{r_3} + \alpha_t \ln r_2}{k_t} \right] \ln \frac{r}{r_3} + \frac{\alpha_t}{2k_t} ((\ln r_3)^2 - (\ln r)^2) \quad [^\circ\text{C}] \quad (5)$$

$$T_c(r) = T_t(r_2) + \left[-\frac{Q}{2\pi k_c} - \frac{\alpha_c \ln r_1}{k_c} \right] \ln \frac{r}{r_2} + \frac{\alpha_c}{2k_c} ((\ln r_2)^2 - (\ln r)^2) \quad [^\circ\text{C}] \quad (6)$$

$$T_a(r) = T_c(r_1) + \left[-\frac{Q}{2\pi k_a} \right] \ln \frac{r}{r_1} \quad [^\circ\text{C}] \quad (7)$$

$$T_o(r) = T_a(r_0) + \frac{Q}{4\pi k_o} \left[1 - \left(\frac{r}{r_0} \right)^2 \right] \quad [^\circ\text{C}] \quad (8)$$

The radial temperature artefact is defined as the difference between the temperature rise inside the applicator at $r=0$ (ΔT_{in}) and just outside the afterloading catheter at $r=r_2$ (ΔT_{out}). Because this artefact is proportional to the absolute temperature rise, the artefact was divided by (ΔT_{in}) to obtain a dimensionless relative artefact

$$ERR = \frac{\Delta T_{in} - \Delta T_{out}}{\Delta T_{in}} \quad (9)$$

2.3. Measurements

The difference between the temperature inside the applicator (T_{in}) and outside the afterloading catheter (T_{out}) has been studied in situations similar to clinical practice, with respect to the afterloading catheter, the applicator and the thermocouple probe. A dual-electrode applicator (outer diameter ≈ 1.4 mm) was inserted in a standard brachytherapy catheter (inner diameter = 1.5 mm, outer diameter = 2.0 mm), in a muscle-equivalent agar phantom (Ishida and Kato 1980). Both T_{in} and T_{out} were measured with a 7-point manganin-constantan thermocouple probe (outer diameter = 0.5 mm). One probe was inserted inside the applicator, the other was placed outside the afterloading catheter.

Two parameters were used to evaluate the relative measurement error (ERR), as was defined in equation 9, and the so-called delay time (t_{delay}). The latter

is the time after power has been switched off, at which T_{in} has become equal to T_{out} at the moment of switching power off. If t_{delay} is known, it can be used to approximate T_{out} by measuring T_{in} .

ERR was determined for four different brachytherapy afterloading catheters. One catheter was made of high-loss PA11-nylon (NY1, $\tan(\delta) \approx 0.04$) and one of polyoxymethylene (POM) with a ten-fold lower dielectric loss factor ($\tan(\delta) \approx 0.005$). The other two were made of PA6-nylon (NY2 (brown), NY3 (white)) catheters with lower dielectric losses than NY1 but comparable with POM. In the experiments a dual-electrode applicator with 20 mm long electrodes at 10 mm separation was used and T_{in} and T_{out} were measured with two 7-point manganin-constantan thermocouple probes with a distance of 10 mm between the points (Figure 3a).

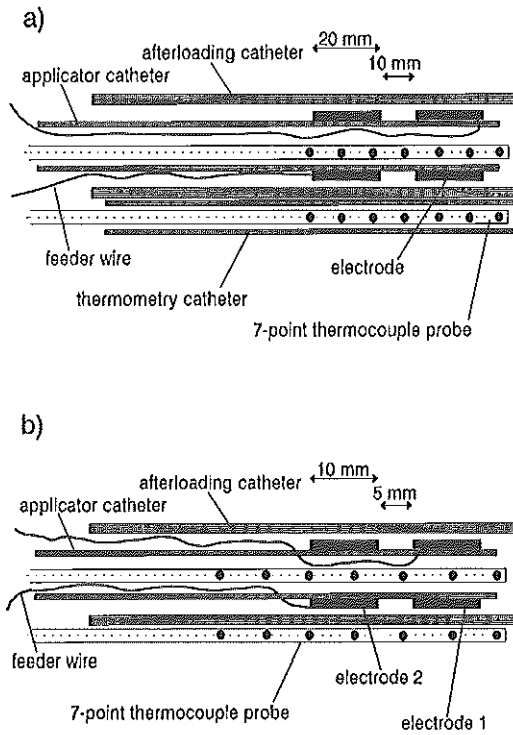


Figure 3. Diagrams of the two applicator-thermometer geometries used for the T_{in} - T_{out} measurements. The applicators consist of two tubular electrodes, constructed from layers of silver paint on an applicator ($\varnothing:0.9/1.3$ mm) and connected to thin feeder wires ($\varnothing:0.05$ mm). Inside the applicator and outside the afterloading catheter ($\varnothing:1.5/2.0$ mm) 7-point thermocouple probes ($\varnothing:0.5$ mm) are placed.

Nowadays, IHT treatments of brain tumours are performed using dual-electrode applicators with 10 mm long electrodes, inserted in low-loss ($\epsilon_r = 3.6$, $\tan(\delta) \approx 0.005$) afterloading catheters (NY3). For this combination ERR and t_{delay} were studied. Firstly, during and after a short 60 s power pulse, using an RF filter and secondly, for a longer period, during which the electrode temperatures were controlled automatically (Kaatee *et al* 1997), thereby

mimicking clinical practice. Both T_{in} and T_{out} were measured with a 7-point manganin-constantan thermocouple probe with a distance of 7.5 mm between the points. A diagram is shown in Figure 3b. During an IHT-treatment the temperatures measured inside in each electrode are controlled automatically. The power of each electrode can be adjusted independently with steps of 5%, whereby 100% corresponds with an effective power of about 1 W. A control cycle consists of a power-on period and a power-off period for temperature measurement. The power-off period is divided into a "recovery period", to allow the electronic disturbance of the data acquisition equipment to disappear, and the actual "measuring period", during which temperatures are measured with a frequency of one measurement per second and starting from about 0.5 s after the beginning of the measuring period. The length of these periods can be chosen freely. Temperature rises inside and outside the two electrodes were measured with power-on, recovery and measuring times of 20, 2 and 8 s, respectively. The relative measurement error as a function of time was examined. Furthermore, T_{in} was compared with T_{out} at the moment the power was actually switched off ($T_{out,max}$). The latter was obtained by linear extrapolation using the first two T_{out} -measurements of each control cycle. This $T_{out,max}$ can be seen as the maximum tissue temperature and therefore the value which should be controlled.

3. Results

3.1. Model calculations

If not explicitly stated otherwise, the following parameters were used: $I = 5$ A/m, $\tan\delta = 0.04$, $\epsilon_r = 3.6$, $r_0 = 0.1$ mm, $r_1 = 0.75$ mm, $r_2 = 1$ mm and $r_3 = 10$ mm. Furthermore, the effective heat conductivities for the dissipating and the non-absorbing parts of the applicator, the afterloading catheter and the tissue were taken 390, 0.1, 0.3 and 0.6 W m⁻¹°C⁻¹, respectively.

In Figure 4a the dependency of the relative artefact on the electrical properties of the afterloading catheter material, i.e. the dielectric loss factor ($\tan(\delta)$) and the electrical permittivity (ϵ_r), is shown. Selfheating of the applicator was omitted in this case, i.e. Q was taken 0 W/m. The ranges over which $\tan(\delta)$ and ϵ_r were varied comprise the properties of most afterloading catheter materials. It can be seen that the contribution of power dissipation in the afterloading catheter to the artefact is relatively small. Even for high-loss nylon the difference between T_{in} and T_{out} is only about 6% of the temperature rise inside the applicator.

A more serious effect can be expected from absorption in the applicator itself. This is demonstrated in Figure 4b. The relative artefact is shown as a function of the relative absorption in the applicator (Q_{rel}), i.e. the ratio between Q and the total power absorption per meter. $\tan(\delta)$ was set at 0, so there was no absorption in the afterloading catheter. If only 5% of the electromagnetic energy is absorbed in the applicator and it is assumed that

power absorption is limited to a small cylinder in the centre of the applicator, e.g. the thermocouple probe and/or the feeder wires ($r_0 = 0.1$ mm), then the difference between T_{in} and T_{out} is about 40% of the temperature rise inside the applicator.

Finally, the radial heat flow was varied by varying k_{eff} . A dissipating catheter material ($\tan\delta = 0.04$, $\epsilon_r = 3.6$) was used and Q was kept constant at 0.23 W/m, which is 1% of the total absorbed power if $k_{eff} = 0.6$ W m⁻¹°C⁻¹ and $r_3 = 10$ mm. Figure 4c shows that the difference between T_{in} and T_{out} increases considerably with increasing heat flow in the tissue.

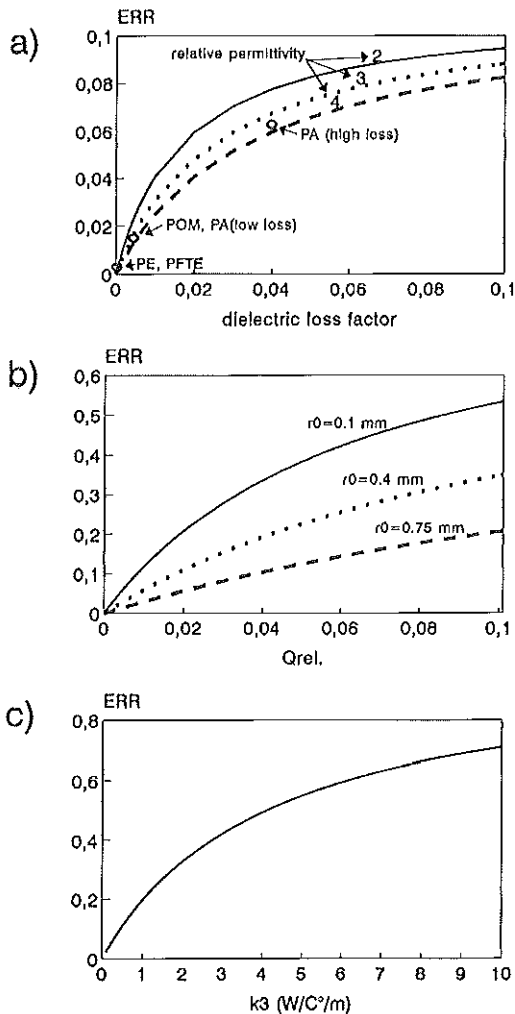


Figure 4. The relative artefact, i.e. $\Delta T_{in} - \Delta T_{out} / \Delta T_{in}$, as a function of a) the dielectric properties of the afterloading catheter ($\tan\delta$, ϵ_r) without selfheating of the applicator; b) selfheating of the applicator (Q_{rel} , r_0) without absorption in the afterloading catheter; c) effective heat conductivity of the tissue (k_3) with absorption in both afterloading catheter ($\tan\delta = 0.04$, $\epsilon_r = 3.6$) and applicator ($Q = 0.23$ W/m).

3.2. Measurements

Figure 5a shows the temperature rise after 60 s of heating along a dual electrode applicator with 2 cm long electrodes (Figure 3a), for various catheter materials. As expected, the highest temperatures were measured using the strongly absorbing nylon (NY1). However, no higher relative error was seen (Figure 5b). The mean values of ERR in the electrodes for the different catheter materials were $0.31 (\pm 0.05)$, $0.30 (\pm 0.03)$, $0.34 (\pm 0.10)$ and $0.36 (\pm 0.04)$ for POM, NY1, NY2 and NY3 respectively. The values between brackets are the standard deviations. Furthermore, note that ERR is higher at those positions where the agar is not heated directly by the electrodes.

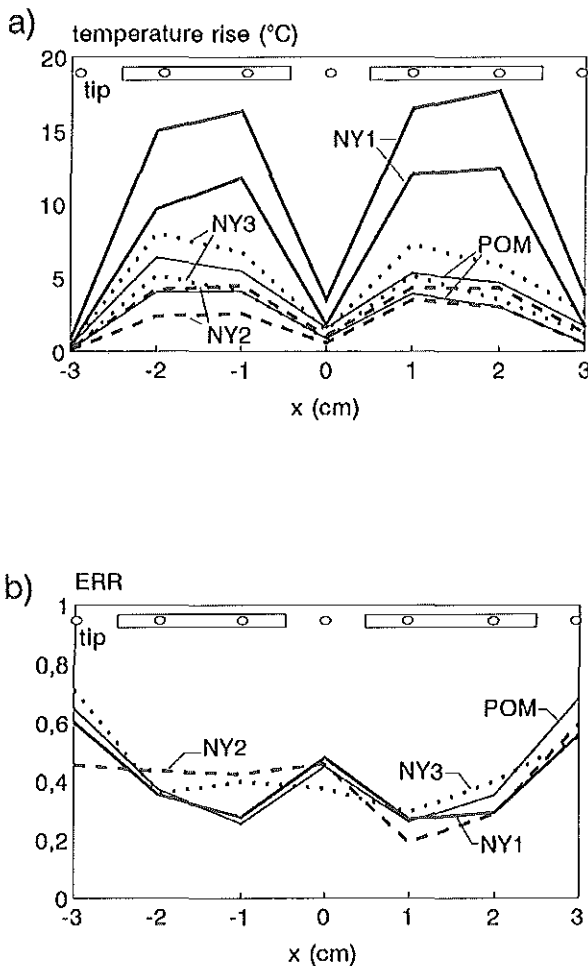


Figure 5. a) ΔT_{in} and ΔT_{out} after a power pulse of 60 s and b) the corresponding relative error (ERR) along a dual-electrode applicator (see Figure 3a) in four afterloading catheters of different materials.

In Figure 6a, the temperature rises inside (ΔT_{in}) and outside (ΔT_{out}) both electrodes of a dual-electrode applicator (Figure 3b) are shown as a function of time, using an RF-filter. The temperature rise in electrode 1 (tip) is higher than in electrode 2, which is due to a higher efficiency of the tip-electrode in this applicator design. The corresponding ERRs, according to equation 1 are displayed in Figure 6b. After about 10 s, ERR has reached its maximum and decreases slowly until the power is switched off, after which a steep decay is observed.

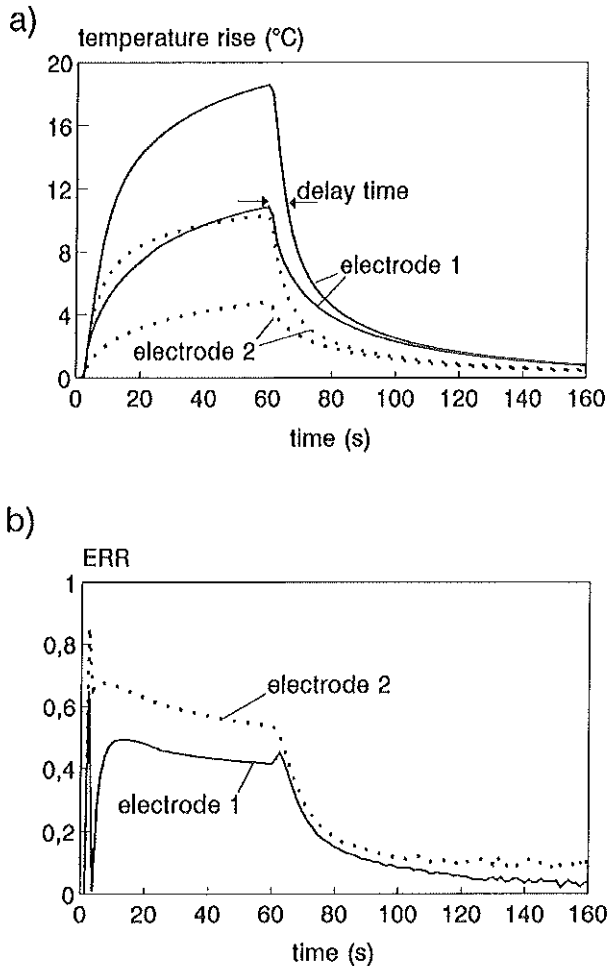


Figure 6. a) ΔT_{in} and ΔT_{out} for both electrodes of a dual-electrode applicator (see Figure 3b), during and after a 60 s power pulse, b) the corresponding relative errors (ERR).

The results of the automatic temperature control measurements are shown in Figure 7. A control cycle of 20 s power on and 10 s power off (Figure 7a) appears ideal to control the maximum agar temperature ($\Delta T_{out,max}$), i.e. the last measured ΔT_{in} is the same as the estimated value of ΔT_{out} just after the

electrodes have been switched off. In Figure 7b it can be seen that ERR rapidly decreases during each power-off period. However, ERR at a certain time in the control cycle stabilizes after a number of cycles.

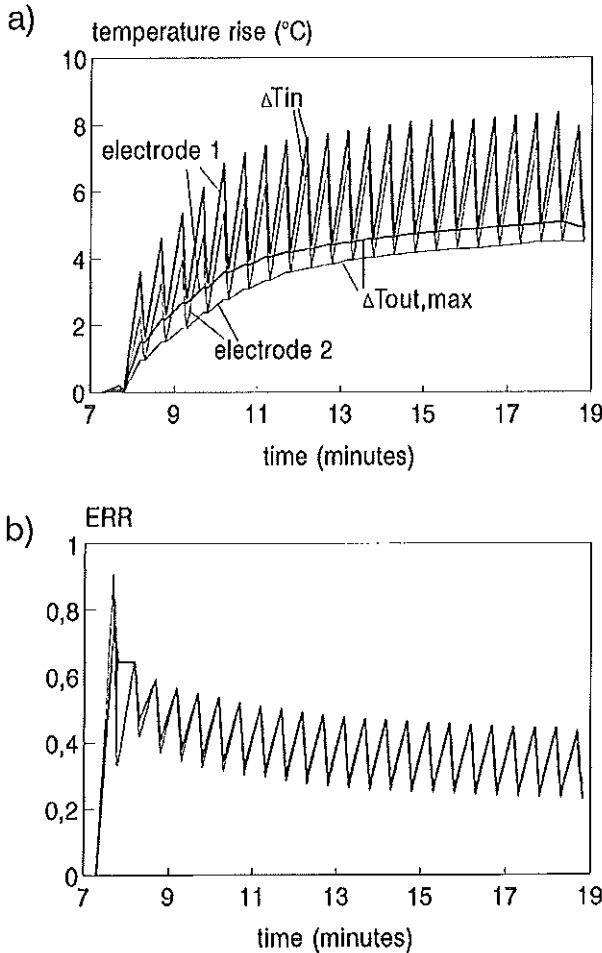


Figure 7. a) ΔT_{in} (thin lines) and $\Delta T_{out,max}$ (thick lines) and b) ERR for both electrodes of a dual-electrode applicator (see Figure 3b), during a period of automatic temperature control using a control cycle: 20 s power on, 2 s recovery time and 8 s temperature measurements. $\Delta T_{out,max}$ is the estimated maximum tissue temperature at the time of switching off the power, which was obtained by extrapolation of the temperatures measured outside the afterloading catheter.

4. Discussion

In clinical IHT, the number of catheters, which can be implanted, is limited by patient tolerance. In general, most catheters should be used for heating to reach a reasonable homogeneous temperature distribution. Therefore, temperature information is mainly obtained from measurements inside

applicator (T_{in}). However, it is important to know and control the temperature just outside the afterloading catheter (T_{out}), which, in general, is lower than T_{in} . Firstly, to avoid overestimation of the tissue temperatures, resulting in insufficient thermal dose. Secondly, to avoid hot spots, which are usually found near the electrodes and which can cause pain. If those hot spots are not detected they will limit the tolerated power levels for all electrodes and lead to cold regions in other parts of the treatment target volume.

As stated before, the radial measurement error is induced by dissipation of electromagnetic energy between the measuring position and the site of interest, in combination with a thermal resistance in between. For the electrodes of a dual-electrode applicator (as was shown in Figure 3b) inserted in an agar phantom, ERR and t_{delay} are typically 0.5 and 5 s, respectively. This means that with power switched on, the temperature rise just outside the afterloading catheter is only 50% of the temperature rise measured inside the electrodes and that T_{in} , measured 5 s after power is switched off, gives a good estimation of the maximum T_{out} . It was found that ERR and t_{delay} were the same, with or without an RF-filter (data not shown). Furthermore, by varying the electrode power, it was confirmed that both ERR and t_{delay} are independent of the absolute temperature rise (data not shown). On the other hand, ERR and t_{delay} do depend on the applicator design and are not constant along an applicator. In general, both ERR and t_{delay} are higher at those regions where the tissue is not heated directly by an electrode. This means that the above-mentioned values for ERR and t_{delay} are appropriate to predict the maximum T_{out} near switched on electrodes, which makes it possible to control the maximum tissue temperature. However, this method is less suitable to obtain more detailed information about the temperature distribution along the afterloading catheter, e.g. to study dose-response relationships.

Selfheating of the applicator, i.e. particularly of the thin (50 μm) leads to the tip-electrodes in the centre of the applicator, is probably a more important cause for the difference between T_{in} and T_{out} than the dielectric losses in the afterloading catheter. This was demonstrated in the model calculations (Figures 4a and 4b) and by the experiments with the different catheter materials, in which no significant difference was found between the measurements of ERR for high-loss nylon and the other catheter materials with a lower dielectric loss factor (Figure 5b). However, this does not mean there is no need to avoid using afterloading catheter material with a high dielectric loss factor. The effect on ERR may be limited but high-loss catheters still considerably increase the inhomogeneity of the temperature distribution in the surrounding tissue (Kaatee *et al* 1995) because less electromagnetic energy is absorbed directly in the tissue.

ERR and t_{delay} are not only a function of applicator design and afterloading catheter properties but also of the time-dependent temperature distribution in the tissue. In the Figures 6b and 7b it can be seen that the relative error decreases until a steady state is reached. The actual steady state temperature distribution and thus ERR will depend on the thermal properties of the tissue (Figure 4c), but also on the power absorption distribution and thus on the

presence of neighbouring electrodes and on the electrical tissue properties.

The simplified cylindrical steady state model seems not appropriate to predict ERR accurately. The main reason for this is that the concentric cylinder geometry in the model is not suitable to describe a real applicator with feeder wires and a thermocouple probe each at different distances from the central axis, which may vary along the applicator. Furthermore, the model cannot be used to calculate t_{delay} . It may be questioned, whether more sophisticated models, such as the time-dependent high-resolution model used by Van der Koijk *et al.* (1998), can produce the values needed in the complex clinical situation in which tissue properties are generally unknown. In vivo measurements of ERR and t_{delay} in various perfused tissues would give a better insight in this matter.

A more practical solution would be to use special afterloading catheters dedicated to IHT with one or more thermocouple probes at the outside of the catheter. With these thermometers tissue temperatures can be measured more directly. Additionally, it may even be possible to use the thermocouple probes to measure tissue properties and their variations during treatment. This would be valuable because acquisition of input parameters for power absorption and thermal computer models is considered an important problem. The temperature decay during the power-off periods gives information about the thermal properties of the tissue near the catheter. Furthermore, two or more thermocouple probes together might serve as an electrical impedance probe.

Although RF-filters are not strictly required if temperatures are measured after switching off the electrodes, they are useful. The risk of measurement errors due to local selfheating of the cold-junction connectors, particularly with single electrode applicators, is eliminated. Additionally, the thermometry system does not have to recover from RF-disturbance, so that the first 2 s of the temperature decay (2 s is the minimum required RF recovery time if no filter is used) can be measured as well. Furthermore, by using filters temperature measurements can be performed during heating. This gives the possibility to detect unexpected quick temperature rises, e.g. due to sudden perfusion changes, if power is switched on.

5. Conclusions

In a muscle-equivalent agar phantom the electrode temperatures overestimate the temperature rise of the surrounding tissue roughly by a factor two. However, ERR is not homogeneous along the applicator and it can be expected that ERR will be higher in perfused tissues. If the electrode power is switched off periodically, the electrode temperature about 5 s after power-off represents the maximum agar temperature quite well. Power-off temperature measurements are useful to avoid overestimation of tissue temperatures during clinical IHT. Nevertheless, the values and the stability of t_{delay} in perfused tissues have to be investigated first. Integration of thermometry into the afterloading

catheters may be another solution to overcome the present radial temperature artefact.

References

- Bach Andersen J, Baun A, Harmark K, Heinzl L, Raskmark P and Overgaard J, 1984, A hyperthermia system using a new type of inductive applicator. *IEEE Transactions on Biomedical Engineering* **BME-31**: 21-27.
- Carnochan P, Dickinson RJ and Joiner MC, 1986, The practical use of thermocouples for temperature measurement in clinical hyperthermia. *International Journal of Hyperthermia* **2**: 1-19.
- Chakraborty DP and Brezovich IA, 1982, Error sources affecting thermocouple thermometry in RF electromagnetic fields. *Journal of Microwave Power* **17**: 17-28.
- Crezee J, Van der Koijk JF, Kaatee RSJP and Lagendijk JJW, 1997, Implications of using thermocouple thermometry in 27 MHz multi-electrode capacitively coupled interstitial hyperthermia. *Physics in Medicine and Biology* **42**: 637-650
- De Leeuw AAC, Crezee J and Lagendijk JJW, 1993, Temperature and SAR measurements in deep-body hyperthermia with thermocouple thermometry. *International Journal of Hyperthermia* **9**: 685-697.
- Deurloo IKK, Visser AG, Morawska-Kaczynska M, Van Geel CAJF, Van Rhoon GC and Levendag PC, 1991, Application of a capacitive coupling interstitial hyperthermia system at 27 MHz; study of different applicator configurations. *Physics in Medicine and Biology* **36**: 119-132.
- Ishida T and Kato H, 1980, Muscle equivalent agar phantom for 13.56 MHz RF-induced hyperthermia. *Shimane Journal of Medical Science* **4**: 134-140.
- Kaatee RSJP, Kampmeijer AG, Van Hooije CMC, Van Rhoon GC, Kanis AP, Levendag PC and Visser AG, 1995, A 27 MHz current source interstitial hyperthermia system for small animals. *International Journal of Hyperthermia* **11**: 785-796.
- Kaatee RSJP, Crezee J, Kanis AP, Lagendijk JJW, Levendag PC and Visser AG, 1997, Spatial temperature control with a 27 MHz current source interstitial hyperthermia system. *International Journal of Radiation Oncology, Biology, Physics* **37**: 189-197.
- Lagendijk JJW and De Leeuw AAC, 1993, Thermocouple errors using multi-sensor thermocouple probes with common constantan wire. *International Journal of Hyperthermia* **9**: 763-764.
- Lagendijk JJW, Visser AG, Kaatee RSJP, Crezee J, Van der Koijk JF, De Bree J, Kotte ANTJ, Kanis AP, Levendag PC and Battermann JJ, 1995, The 27 MHz current source multi-electrode interstitial hyperthermia method. *Activity, International Nucletron-Oldelft Radiotherapy* **6**: 83-90.
- Marchal C, Nadi M, Hoffstetter S, Bey P, Pernot M and Prieur G, 1989, Practical interstitial method of heating at 27.12 MHz. *International Journal of Hyperthermia* **4**: 451-466.
- Ryan TP, Samulski TV, Lyons BE, Lee E, Holdren D, Fessenden P and Strohbehn JW, 1989, Thermal conduction effects associated with temperature measurements in proximity to radiofrequency electrodes and microwave antennas. *International Journal of Radiation Oncology, Biology, Physics* **16**: 1557-1564.

electrodes in interstitial hyperthermia. *Physics in Medicine and Biology*, submitted.

BACH ANDERSON, J., BAUN, A., HARMARK, K., HEINZL, L., RASMARK, P., OVERGAARD, J., 1984, A hyperthermia system using a new type of inductive applicator. *IEEE Transactions on Biomedical Engineering*, vol BME-31(1), 21-27

Visser AG, Deurloo IKK, Levendag PC, Ruifrok ACC, Cornet B and Van Rhoon GC, 1989a, An interstitial hyperthermia system at 27 MHz. *International Journal of Hyperthermia* 5: 265-276.

Dickinson RJ, 1985, Thermal conduction errors of manganin-constantan thermocouple arrays. *Physics in Medicine and Biology* 30: 445-453.

Chapter 5

Implications of using thermocouple thermometry in 27 MHz capacitively coupled interstitial hyperthermia; interference between thermometry and heating system

This chapter was published as:

Crezee J, Van der Koijk JF, Kaatee RSJP and Lagendijk JJW, 1997, Implications of using thermocouple thermometry in 27 MHz multi-electrode capacitively coupled interstitial hyperthermia. *Physics in Medicine and Biology* 42: 637-650.

Abstract

The 27 MHz Multi Electrode Current Source (MECS) interstitial hyperthermia system uses segmented electrodes, 10-20 mm long, to steer the 3D power deposition. This power control at a scale of 1-2 cm requires detailed and accurate temperature feedback data, to this end seven point thermocouples are integrated into the probes.

The aim of this work was to evaluate the feasibility and reliability of integrated thermometry in the 27 MHz MECS system, with special attention for interference between electrode and thermometry and its effect on system performance. We investigated the impact of a seven sensor thermocouple probe (Outer Diameter 150 μm) on the apparent impedance and power output of a 20 mm dual electrode (O.D. 1.5 mm) in a polyethylene catheter in a muscle equivalent medium ($\sigma_t = 0.6 \text{ Sm}^{-1}$).

The cross coupling between electrode and thermocouple was found to be small (1-2 pF) and to cause no problems in the dual electrode mode, and only minimal problems in the single electrode mode. Power loss into the thermometry system can be prevented using simple filters. The temperature readings are reliable and representative of the actual tissue temperature around

the electrode. Selfheating effects, occurring in some catheter materials, are eliminated by sampling the temperature after a short power off interval.

We conclude that integrated thermocouple thermometry is compatible with 27 MHz capacitively coupled interstitial hyperthermia. The performance of the system is not affected and the temperatures measured are a reliable indication of the maximum tissue temperatures.

1. Introduction

The Multi Electrode Current Source (MECS) interstitial hyperthermia system developed at the Departments of Radiotherapy and Biomedical Engineering of the University Hospital Utrecht and the Department of Clinical Physics of the Daniel Den Hoed Cancer Center in Rotterdam (Lagendijk 1990, et al. 1995, Kaatee et al. 1995) is based on the capacitively coupled 27 MHz rf heating technique for brachytherapy implant catheters (Visser et al. 1989, Marchal et al. 1989, Deurloo et al. 1991). The three dimensional power steering of the MECS system is an important feature, as power control on a centimetre scale or better greatly improves temperature uniformity (Crezee and Lagendijk 1992). Few techniques comply with this requirement: scanned focused ultrasound (SFUS) (Lagendijk et al. 1994) and interstitial heating techniques with three dimensional power control, like the ultrasound applicators developed by Diederich (1996) and the MECS system where each probe consists of multiple independently controllable electrodes to provide longitudinal temperature control along the catheter (van der Koijk et al. 1996, Kaatee et al. 1997). A disadvantage of SFUS techniques is the need for extensive invasive thermometry to provide feedback data for power control.

1.1. Thermometry

Three dimensional temperature control requires feedback of detailed thermometry data for power control, with a resolution matching the degrees of freedom available to power deposition (Hand 1993). Non-invasive thermometry techniques based on radiometry and ultrasound are promising but not yet sufficiently reliable, especially due to their sensitivity to blood flow changes (Hand 1993). Instead invasive thermometry is used, either integrated into the heating probes or in separate, non-heated catheters.

Thermometry in the electrode catheters is likely to give an impression of the maximum temperatures in the implant and to be suitable for power control of individual electrodes. The array of seven or fourteen point thermocouple strings in each catheter yields a detailed three dimensional temperature distribution without additional trauma to the patient. Disadvantages are that minimum tissue temperatures cannot be measured directly, and the proximity of the electrodes may cause temperature artifacts (Astrahan et al. 1988) and interfere with the operation of the electrodes.

Thermometry in separate non-heated catheters is likely to give an impression of the minimum tissue temperature, without selfheating effects. Disadvantage is the extra trauma inflicted on the patient, Emami et al. (1991) recommend minimum numbers of extra catheters ranging between two (for 3-8 heat sources) and six (for 33 or more heat sources). The 3D control provided by the segmented electrodes of the MECS system requires matching 3D thermometry, or equal numbers of heating and thermometry catheters. That is unacceptable: it would be more logical to improve temperature uniformity by using extra catheters for extra electrodes, not for thermometry.

The thermometry of the MECS system is therefore integrated into the electrode probes, each containing a seven point thermocouple string providing an average of two contacts per electrode. The system can handle 64 electrodes and 196 thermocouples. The objective of this paper is to evaluate the feasibility of integrated thermometry, and especially the effect of interference between thermometry and electrodes on the performance of the MECS system, and the reliability of integrated thermometry. Our thermometry system suppresses all electronic interference immediately after switching off the power, but during power on interference may induce currents in the thermocouple, heating the leads or the cold junction and causing temperature artifacts lasting the first seconds after power off (De Leeuw et al. 1993).

2. Theory

2.1. Principle of the MECS system

Shown in Figure 1 is a dual electrode, consisting of two electrodes with opposite phase in a single catheter. In this balanced dual electrode mode current flows from one electrode into the tissue around the electrode, then through the tissue to the other electrode, the plane between the electrodes perpendicular to the catheter is effectively at zero potential. The impedance of an electrode is the sum of the catheter and tissue impedance

$$Z_{el} = Z_{cath} + Z_t \approx \frac{1}{i2\pi f C_{cath}} + R_t \quad (1)$$

with $f = 27$ MHz and assuming $\text{Re } Z_{cath} \approx 0$ and $\text{Im } Z_t \approx 0$. The catheter with radius r_{cath} acts as a capacitor C_{cath} between the electrode and the tissue

$$C_{cath} = \frac{2\pi\epsilon_0\epsilon_{cath}l_{el}}{\ln(r_{cath}/r_{el})} \quad F \quad (2)$$

with $\epsilon_0 = 8.85 \times 10^{-12}$ Fm⁻¹ the free space permittivity, ϵ_{cath} the relative permittivity of the catheter, l_{el} the length and r_{el} the radius of the electrode (Visser et al. 1989). A 2 cm long electrode in a polyethylene (pe) catheter with $\epsilon_{cath} = 2$, $r_{el} = 0.8$ and $r_{cath} = 1.0$ mm, yields $C_{cath} \approx 10$ pF or $|Z_{cath}| \approx 600$

Ω . Re $Z_{\text{cath}} \approx 0$ because dielectric losses are negligible in pe ($\text{tg } \delta = 0.0004$), therefore all heat production is generated by the resistance in the tissue, which for a cylindrical geometry can be estimated to be

$$R_t = \frac{\ln(r_{\text{ground}}/r_{\text{cath}})}{2\pi\sigma_t l_{el}} \quad \Omega \quad (3)$$

with σ_t the conductivity of tissue and a cylindrical ground at r_{ground} . Equation 3 yields $R_t \approx 30 \Omega$ for the 2 cm long electrode in muscle with $\sigma_t = 0.6 \text{ Sm}^{-1}$ and assuming $r_{\text{ground}} \approx 10r_{\text{cath}}$. This agrees well with $R_t = 29.9 \Omega$ found in accurate 3-D numerical simulations in which the ground plane was correctly modelled between the electrodes (De Bree et al. 1996). The electrode acts like a current source since $R_t \ll |Z_{\text{cath}}|$ (Deurloo et al. 1991). The presence of an external ground plane allows imbalance between the plus and minus electrode, necessary for power control: Maximum power is about 1.5 W, lower levels are obtained by duty cycle modulation of the power.

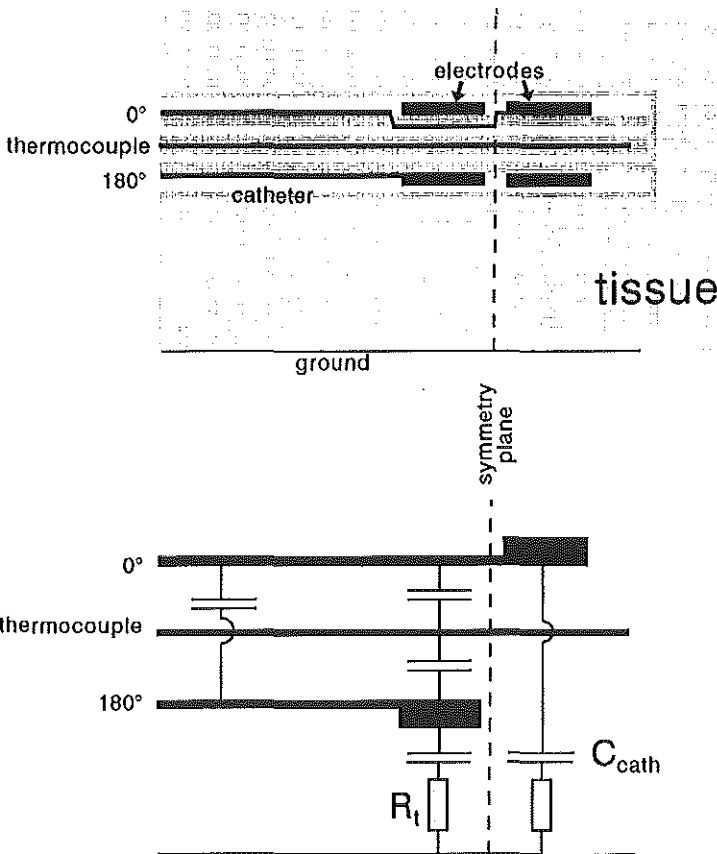


Figure 1. Schematic view of dual electrode

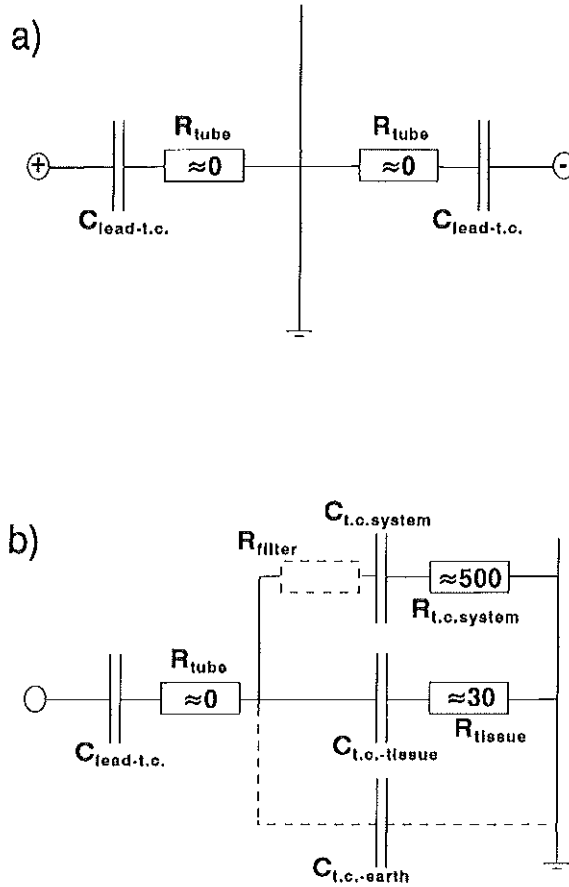


Figure 2. Route of secondary current through thermocouple to ground for dual electrode (2a) and single electrode (2b). Dotted: Two filtering methods discussed in section 2.3.

2.2. Interaction between electrode and thermocouple

A seven point thermocouple is located inside the dual electrode (Figure 1). The leads of each electrode (Outer Diameter $50 \mu\text{m}$) and the thermocouple (one manganin and seven constantan wires, total O.D. $150 \mu\text{m}$) run parallel for some distance. The resulting capacitive coupling is small but not negligible, about 1-2 pF (Appendix 1). Thus the leads of the thermocouple and other electrode provide alternative routes for the current, the apparent electrode admittance is

$$Y_{\text{app}} = Z_{\text{app}}^{-1} = Y_{\text{el}} + Y_{\text{tc}} + Y_{\text{ll}} \tag{4}$$

with Y_{tc} and Y_{ll} the admittance of the parallel routes into the thermocouple and the opposite lead, respectively. We are concerned with the impact of Y_{tc} on system performance, this depends on the configuration of the electrodes:

In the dual electrode mode a small capacitively coupled current flows from one lead and electrode to the thermocouple, and from the thermocouple to the lead and electrode of opposite phase. In this balanced situation the thermocouple is effectively at zero potential, there will be no current from the thermocouple to the thermometry system or the external ground plane (Figure 2a). Current directly from lead to thermocouple will cause no heat production provided low loss catheter materials are used. Indirect currents through the tissue are not favoured due to the comparatively high tissue-thermocouple impedance $|Z_{t-tc}|$ (Appendix 1).

Duty cycle power control implies during part of the cycle one electrode may be on while the other is off. In this unbalanced single electrode mode the thermocouple probe is not at zero potential and the current from the lead into the probe will flow to ground along different routes: The first across the catheter wall into the tissue to the external ground plane, causing tissue heating along the length of the thermocouple probe. The second and most important into the thermometry system, possibly causing cold junction heating and other temperature artifacts (Figure 2b). Measurement of the impedance of a 4 m seven sensor probe connected to the thermometry system yielded $\text{Re } Z_{\text{probe}} \approx 500 \Omega$, $\text{Im } Z_{\text{probe}} \approx 0$. Therefore in the single electrode mode

$$Z_{tc} = Z_{l-tc} + Z_{\text{probe}} \approx \frac{1}{i2\pi f C_{tc}} + R_{tc} \quad (5)$$

with $R_{tc} = \text{Re } Z_{tc} \approx \text{Re } Z_{\text{probe}}$, and C_{tc} the capacitive coupling between lead and thermocouple ($\approx 1\text{-}2 \text{ pF}$).

2.3. Simulation of apparent impedance and power loss in the single electrode mode

Analytical expressions for the effect of the presence of a thermocouple on the apparent impedance of the electrode Z_{app} and power loss in the single electrode mode are derived in Appendix 2. These were used to simulate the effect of insertion of a thermocouple into an electrode ($R_t = 40 \Omega$, $C_{\text{cath}} = 11.7 \text{ pF}$) by a gradual rise of C_{tc} from 0 to 3 pF, shown in Figure 3a. A range of possible thermocouple resistances R_{tc} between 10^{-1} and $10^6 \Omega$ is tested to get an impression of the critical range. For $R_{tc} < 10 \Omega$ the effect on Z_{app} is a reduction of $|\text{Im } Z_{\text{app}}|$, dissipation in the secondary circuit P_{tc} remains zero. For $R_{tc} > 10 \Omega$ the reduction of $|\text{Im } Z_{\text{app}}|$ is accompanied by an increase in $\text{Re } Z_{\text{app}}$ (20Ω for $R_{tc} = 1 \text{ k}\Omega$) and P_{tc} becomes significant (equals P_{el} for $R_{tc} = 1 \text{ k}\Omega$). When R_{tc} approaches $1 \text{ M}\Omega$ the impact of the secondary circuit becomes negligible. This behaviour is similar but more pronounced for an electrode with very low $R_t = 10 \Omega$ and $C_{\text{cath}} = 5.8 \text{ pF}$ (Figure 3b). The maximum increase in $\text{Re } Z_{\text{app}}$ is now 90Ω , combined with a P_{tc} ten times the primary dissipation P_{el} . The simulation in Figure 4 shows the R_{tc} dependence of P_{tc} for $C_{tc} = 1.5 \text{ pF}$, showing a peak at about $5 \text{ k}\Omega$ when $\text{Re } Z_{tc} \approx |\text{Im } Z_{tc}|$ (equation A2). The amplitude of the peak (equation A3) varies for different combinations of C_{cath} and R_t , it is

minimal when the capacitive coupling and tissue resistance in the primary circuit are maximal ($C_{cath} = 11.7 \text{ pF}$, $R_t = 40 \text{ }\Omega$).

The results in Figure 4 are based on the ratio between average power dissipation in the secondary and the primary circuit derived in Appendix 2 (equation A1):

$$\frac{P_{tc}}{P_{el}} \approx \frac{|Z_{el}|^2 R_{tc}}{|Z_{tc}|^2 R_t} \tag{6}$$

and suggest two methods for minimising P_{tc} . The first is a low pass filter in the thermocouple leads, achieving $|Z_{tc}| = \infty$, with the advantage that measurement of the temperature during power on is possible. Note that the filter does not block currents from the thermocouple via the tissue to the external ground, therefore the maximal achievable $|Z_{tc}| = |Z_{tc-t-ground}| < \infty$ (see Figure 2b).

A second method is to reduce R_{tc} to zero; then only the imaginary component of the apparent impedance $\text{Im } Z_{app}$ is affected by thermometry, with minimal heat loss due to the secondary current. A low resistance connection between the thermocouple leads and ground yields $R_{tc} \approx 0$ and blocks all other secondary routes. A capacitor $C_{tc-ground}$ is suitable as it does not affect the dc temperature signal of the thermocouple (Figure 2b).

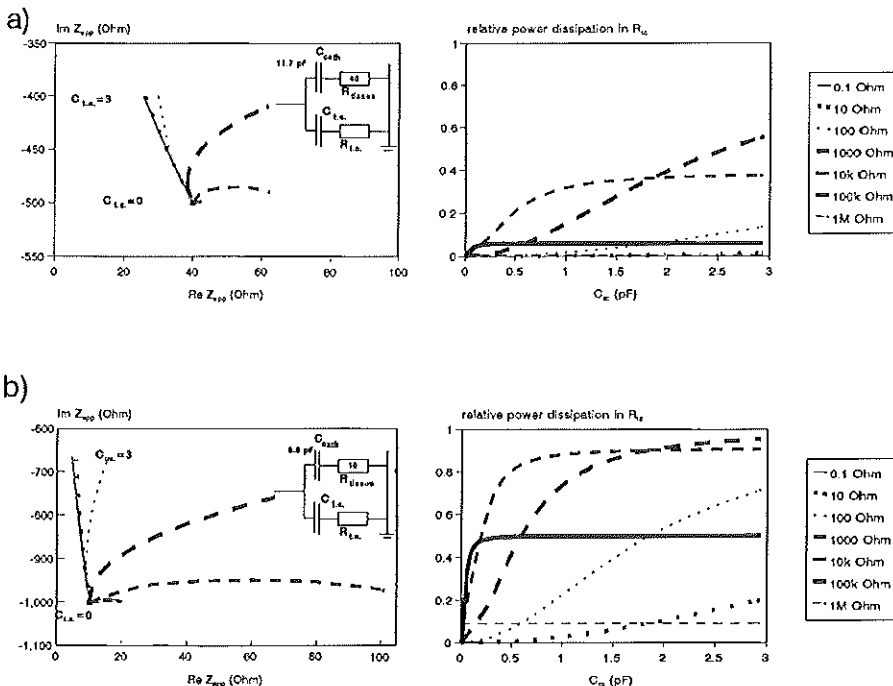


Figure 3. Apparent impedance Z_{app} and relative power loss $P_{tc}/(P_{tc} + P_t)$ simulated as a function of C_c for (a) $R_t = 40 \text{ }\Omega$, $\text{Im } Z_{cath} = -500 \text{ }\Omega$ and (b) $R_t = 10 \text{ }\Omega$, $\text{Im } Z_{cath} = -1000 \text{ }\Omega$.

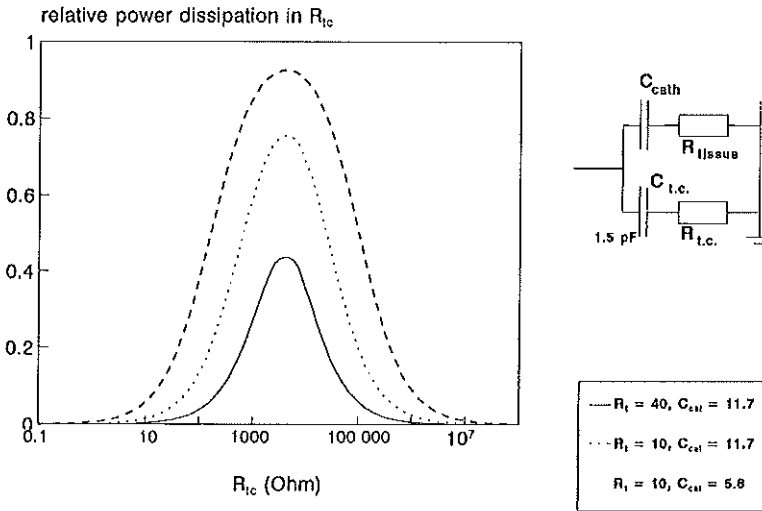


Figure 4. Relative power loss $P_{tc}/(P_{tc} + P_t)$ simulated as a function of R_{tc} for $C_{tc} = 1.5$ pF, $R_t = 10$ or 40 Ω and $\text{Im } Z_{cath} = -500$ or -1000 Ω .

3. Experiment

3.1. Materials and methods

A dual electrode consisting of two 20 mm long electrodes (copper foil, O.D. 1.5 mm) mounted on a 15 cm long pe tube (O.D. 1.2 mm) with a separation of 10 mm, connected with 50 μm thick leads, was inserted in a pe catheter (I.D. 1.6, O.D. 2.0 mm) in a muscle equivalent phantom: A 12x12x12 cm perspex container filled with a solution of 0.3% NaCl in Agar ($\sigma_t = 0.6 \text{ Sm}^{-1}$).

The apparent impedance Z_{app} was measured with respect to a flat copper electrode placed at the approximate location of the virtual ground plane in the balanced dual electrode mode (see Figure 1) using a vector impedance meter (HP 4193A). Unless otherwise stated the thermocouple probe was a seven sensor constantan-manganin probe contained in a 0.5 mm diameter teflon tube, with eight 50 μm leads and a length of 4 m (Ella CS). Resolution of the 196 channel thermometry system is 0.005 $^{\circ}\text{C}$ (De Leeuw et al. 1993). The capacitive short cut to ground was achieved using the capacitive coupling between the thermocouple leads and the thermocouple shielding, and connecting the latter to ground ($C_{tc\text{-ground}} \approx 200$ pF).

The effective electrode power P_{el} was obtained by measuring the temperature rise brought about by an implant of 2x2 dual electrodes (spacing 16 mm) in a well conducting tissue phantom containing $V = 700$ ml 0.45% NaCl solution yielding $R_t = 10$ Ω ; $P_{el} = \frac{1}{6} V \rho c d T/dt$. To facilitate measurement of the secondary dissipation P_{tc} the thermometry system and most of the 4 m thermocouple leads were replaced by an equivalent 500 Ω resistor placed in 70 ml of aquadest, P_{tc} was then determined by measuring the temperature rise

of the water. A capacitor provided the parallel short cut to ground.

3.2. Results

3.2.1. Interaction between lead and thermocouple

The presence of capacitive coupling between thermocouple and electrode is shown by monitoring the apparent impedance of the electrode Z_{app} while a 20 cm long, grounded thermocouple probe ($R_{tc} \approx 0$) is gradually inserted into the electrode, placed in a pe catheter in the muscle phantom (Figure 5). The result is the development of a second route to ground, parallel to the primary route from the electrode. As $\text{Re } Z_{tc} \approx 0$ the increase in the apparent capacity C_{app} directly reflects the increasing capacity in the parasitary route (equation A4): $C_{app} \approx C_{cath} + C_{tc}$ with $C_{cath} \approx 11$ pF and $C_{tc} \approx 1$ -1.5 pF, as predicted in Appendix 1.

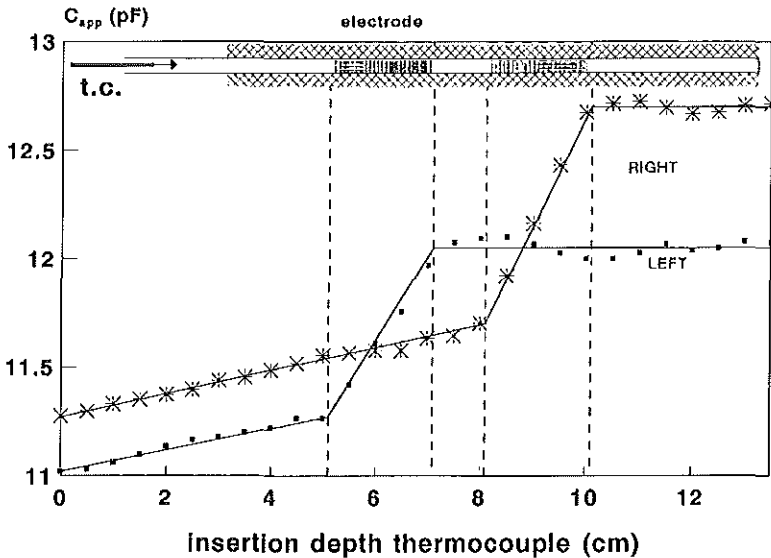


Figure 5. Apparent capacitive coupling C_{app} between electrode ($l_{el} = 20$, $r_{el} = 0.75$ mm) in pe catheter (I.D. 1.6, O.D. 2.0 mm) and tissue as a function of insertion depth of a seven sensor thermocouple probe with $R_{tc} \approx 0$.

The effect of a single sensor thermocouple probe on a poorly coupled single electrode ($C_{cath} \approx 6.5$ pF) in a muscle equivalent medium ($R_t \approx 30 \Omega$) is a reduction of $|\text{Im } Z_{app}|$ and an increase of $\text{Re } Z_{app}$ (Figure 6), similar to the curves in Figure 3 which were predicted to be associated with a significant dissipation in the thermometry system P_{tc} . A connection to ground $C_{tc-ground}$ reduces the effect on $\text{Re } Z_{app}$, a reduction predicted to eliminate the power loss P_{tc} . This predicted restoration of system performance was demonstrated by measurement of P_{el} and P_{tc} in a well conducting medium (Table 1): For a single

electrode the heat loss was 38% without $C_{tc-ground}$, with $C_{tc-ground}$ the loss was nil. The losses computed with equation 6 were 43% and 0%, respectively, with $R_{tc} = 500 \Omega$, $C_{tc} = 1.5 \text{ pF}$ and $C_{cath} = 11.7 \text{ pF}$. The tissue resistance $R_t = 10 \Omega$ was chosen very low to enhance the effect of the secondary circuit on system efficiency. Note that even under these unfavourable conditions losses are minimal for a dual electrode, as predicted in section 2.2.

Table 1. Relative power dissipation $P_{tc}/(P_{tc} + P_t)$ in thermometry circuit ($R_{tc} = 500 \Omega$, $C_{tc} = 1.5 \text{ pF}$) for a 20 mm electrode ($C_{cath} = 11.7 \text{ pF}$) in a tissue phantom ($R_t = 10 \Omega$): Measured and (computed) value.

electrode mode	without $C_{tc-ground}$	with $C_{tc-ground} = 0.01 \mu\text{F}$
dual	0.10 (0)	0 (0)
single	0.38 (0.43)	0 (0)

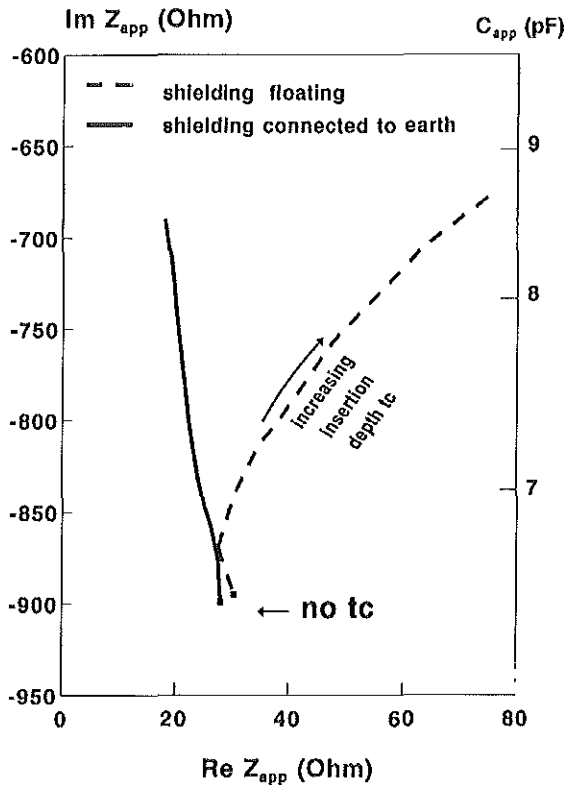


Figure 6. Apparent impedance Z_{app} of an electrode ($l_{el} = 20$, $r_{el} = 0.75 \text{ mm}$) in a pe catheter (I.D. 1.6, O.D. 2.0 mm) in muscle equivalent tissue as a function of insertion depth of a single sensor thermocouple probe, with and without short circuit to ground.

3.2.2. Reliability thermometry

A further test is whether the temperatures measured inside the probe reflect the actual tissue temperature, and without electronic artifacts. We found the temperature measured inside a 2 cm long electrode in a pe catheter is nearly equal to the temperature outside the catheter. The temperature decay after one minute of power on was determined both inside and outside the catheter, the difference is not significant (Figure 7). The absence of electronic artifacts was verified in a similar experiment by determining the temperature decay after one minute of power on, both with the integrated thermometry present and with a thermocouple introduced into the electrode *after* switching off the power. Again no significant difference was found (data not shown).

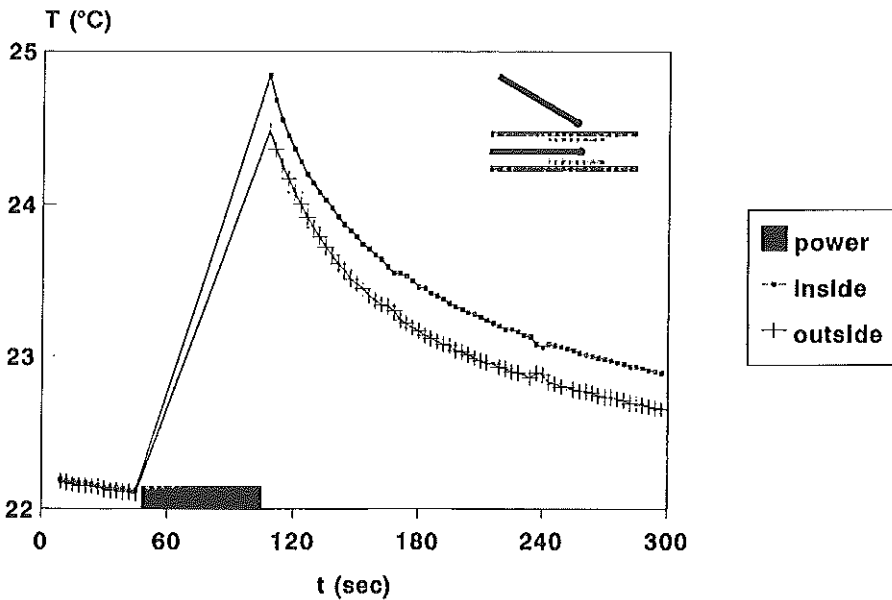


Figure 7. Comparison between the temperature decay measured inside and outside a two cm long electrode (O.D. 1.5 mm) in a pe catheter (I.D. 1.6, O.D. 2.0 mm) in muscle equivalent tissue after one minute of heating.

4. Discussion

Capacitive coupling between thermocouple and electrode can only cause problems for a dual electrode operating in the single electrode mode, but even that is unacceptable as it reduces our spatial power steering capacity. Equation A2 shows loss is maximal when the thermocouple resistance $R_{tc} \approx |\text{Im } Z_{tc}|$, the capacitive coupling between the lead and the thermocouple. For instance, for $C_{tc} = 1.5 \text{ pF}$ this is equivalent to $R_{tc} = 5 \text{ k}\Omega$. Fortunately R_{tc} is much lower in our system, $R_{tc} \approx 500 \Omega$, and the simulations in Figure 4 (backed by equation A3) also show power loss strongly depends on C_{cath} and

R_t ; losses are acceptable in normal tissue ($R_t > 30 \Omega$) with a normal capacitive coupling between electrode and tissue: $C_{\text{cath}} > 10 \text{ pF}$ as shown in Figure 5. To demonstrate the effect of filters on heat loss (Table 1) we used a special phantom with $R_t \approx 10 \Omega$, below the normal range: $30 < R_t < 180 \Omega$ for $10 < l_{\text{el}} < 20 \text{ mm}$ and $0.2 < \sigma_t < 0.6 \text{ Sm}^{-1}$ (fat-muscle). Furthermore, the combination of $R_t = 10 \Omega$ and $C_{\text{cath}} = 11.7 \text{ pF}$ is impossible, $R_t = 10 \Omega$ is equivalent to an electrode at least 6 cm long (depending on the medium), yielding $C_{\text{cath}} > 30 \text{ pF}$.

Thus no special measures are necessary for maintaining system efficiency, but low pass filters (currently developed at the Daniel den Hoed Cancer Center) have the advantage of allowing undisturbed measurement of the temperature during power on. The second type of filter is a capacitor between the thermocouple and ground, and suppresses secondary currents causing heating along the length of the thermocouple in the patient.

Reliable temperature feedback for each electrode is essential for achieving 3D power control: Temperature data acquired from within an electrode were found to give a reliable indication of the maximum tissue temperature. This is a significant advantage over techniques where power levels are controlled by thermometry in extra catheters yielding minimum rather than maximum tumour temperatures: That may lead to severe hot spots near the electrodes. The temperature inside reflects the temperature outside because no heat is generated in polyethylene, the temperature rise inside is achieved solely by conduction. Heat production does occur in high loss materials and causes a shift of the temperature maximum from the tissue to the interior of the probe; thermometry inside the probe overestimates the tissue temperature. A short power off interval allows the extra temperature rise in the very small volume of the probe to diffuse into the surrounding tissue, the registered temperature drops to the true tissue temperature. Another consequence of heat generation in the catheter wall is a reduction of the effective penetration depth of the system. In the worst case all power is dissipated in the probe, equivalent to the zero penetration depth or conductive heating.

Direct measurement of minimum tumour temperature is not possible using thermometry in the electrode catheters. We are currently investigating an indirect method for obtaining an impression of the minimum temperature in the implant without using extra thermometry catheters: After stationary temperatures have been reached we sequentially interrupt the power of each electrode for about one minute to allow the local temperature maximum around the electrode to diffuse away.

5. Conclusion

Thermocouple thermometry inside the catheters is compatible with 27 MHz capacitively coupled interstitial hyperthermia. The performance of the system is not affected and the temperatures measured are a reliable indication of the maximum tissue temperatures.

Appendix 1. capacitive coupling between electrode and thermocouple

The direct capacitive coupling C_{l-tc} between the leads of the electrode and the thermocouple is ($a \gg r_{lead,tc}$)

$$C_{l-tc} = \pi \epsilon_0 \epsilon_{cath} l / \ln(a / \sqrt{r_{tc} r_{lead}}) \quad [F]$$

with $\epsilon_{cath} = 2$ the relative permittivity of the polyethylene catheter wall, l the length of the parallel leads, $a = 0.6$ mm the distance between lead and thermocouple, $r_{lead} = 25 \mu\text{m}$ and $r_{tc} = 75 \mu\text{m}$ the radii of the thermocouple and the lead of the electrode, yielding a capacitive coupling of approximately 0.2 pF/cm. There is also an indirect route possible, from lead via tissue C_{l-t} to the thermocouple C_{t-tc} . However, parallel to C_{t-tc} is a tissue route to ground, and this route dominates since R_t is much smaller than $|Z_{t-tc}| > 1$ k Ω . Experimental results confirmed that the indirect coupling C_{l-t-tc} is negligible.

In addition we consider the direct capacitive coupling between the thermocouple and the electrode, with radius $r_{el} = 0.6$ mm

$$C_{el-tc} = \frac{2\pi\epsilon_0\epsilon_{cath}l_{el}}{\ln(r_{el}/r_{tc})} \quad F$$

yielding about 0.5 pF/cm. Overall the total secondary coupling $C_{tc} = C_{l-tc} + C_{el-tc}$ between lead/electrode and thermocouple ≈ 1 -2 pF, depending of the length of the lead and the electrode.

Appendix 2.

The impact of the presence of a thermocouple with capacitive coupling C_{tc} and resistance $\text{Re } Z_{tc}$ on the apparent impedance Z_{app} of an electrode with $\text{Re } Z_{el} = R_t$ and $\text{Im } Z_{el} = Z_{cath} = -i/2\pi f C_{cath}$:

$$Z_{app} = (Z_{el}^{-1} + Z_{tc}^{-1})^{-1} =$$

$$\frac{\text{Re } Z_{el}(\text{Im}^2 Z_{tc} + \text{Re}^2 Z_{tc}) + \text{Re } Z_{tc}(\text{Im}^2 Z_{el} + \text{Re}^2 Z_{el})}{(\text{Re } Z_{el} + \text{Re } Z_{tc})^2 + (\text{Im } Z_{el} + \text{Im } Z_{tc})^2} +$$

$$j \frac{(\text{Im } Z_{tc}(\text{Im}^2 Z_{el} + \text{Re}^2 Z_{el}) + \text{Im } Z_{el}(\text{Im}^2 Z_{tc} + \text{Re}^2 Z_{tc}))}{(\text{Re } Z_{el} + \text{Re } Z_{tc})^2 + (\text{Im } Z_{el} + \text{Im } Z_{tc})^2}$$

The corresponding time averaged power dissipation ratio is

$$\frac{P_{tc}}{P_{el}} = \frac{|Z_{el}|^2 \operatorname{Re} Z_{tc}}{|Z_{tc}|^2 \operatorname{Re} Z_{el}} \approx \frac{|Z_{el}|^2 R_{tc}}{|Z_{tc}|^2 R_t} \quad (\text{A1})$$

In Figure 4 this ratio is plotted as a function of $\operatorname{Re} Z_{tc}$ and reaches a maximum when

$$\frac{d}{d\operatorname{Re} Z_{tc}} \frac{P_{tc}}{P_{el}} = 0$$

which holds for

$$\operatorname{Re}^2 Z_{tc} = \operatorname{Im}^2 Z_{tc} \quad (\text{A2})$$

The maximal power ratio then becomes

$$\left. \frac{P_{tc}}{P_{el}} \right|_{\operatorname{Re} Z_{tc} = |\operatorname{Im} Z_{tc}|} = \frac{|Z_{el}|^2}{2\operatorname{Re} Z_{tc} \operatorname{Re} Z_{el}} \approx \frac{\operatorname{Im}^2 Z_{el}}{2R_{tc} R_t} \quad (\text{A3})$$

since $\operatorname{Re} Z_{el} \ll \operatorname{Im} Z_{el}$. Note the strong dependence on both C_{cath} and R_t . When $\operatorname{Re} Z_{tc} = 0$, for instance when the thermocouple is connected to ground with a large capacitor, Z_{app} simplifies to

$$Z_{\text{app}} = \frac{\operatorname{Re} Z_{el} \operatorname{Im}^2 Z_{tc} + j[\operatorname{Im} Z_{tc} (\operatorname{Im}^2 Z_{el} + \operatorname{Re}^2 Z_{el}) + \operatorname{Im} Z_{el} \operatorname{Im}^2 Z_{tc}]}{\operatorname{Re}^2 Z_{el} + (\operatorname{Im} Z_{el} + \operatorname{Im} Z_{tc})^2}$$

We divide numerator and denominator by $\operatorname{Im}^2 Z_{el}$ and get

$$\operatorname{Im} Z_{\text{app}} = \frac{\operatorname{Im} Z_{tc} \left(1 + \frac{\operatorname{Re}^2 Z_{el}}{\operatorname{Im}^2 Z_{el}}\right) + \frac{\operatorname{Im}^2 Z_{tc}}{\operatorname{Im} Z_{el}}}{\frac{\operatorname{Re}^2 Z_{el}}{\operatorname{Im}^2 Z_{el}} + \left(1 + \frac{\operatorname{Im} Z_{tc}}{\operatorname{Im} Z_{el}}\right)^2}$$

Then because the tissue resistance $R_t = \operatorname{Re} Z_{el} \ll \operatorname{Im} Z_{el}$, the impedance of the catheter wall,

$$\operatorname{Im} Z_{\text{app}} \approx \frac{\operatorname{Im} Z_{tc} \operatorname{Im} Z_{el}}{\operatorname{Im} Z_{tc} + \operatorname{Im} Z_{el}} \Rightarrow C_{\text{app}} \approx C_{\text{cath}} + C_{tc} \quad (\text{A4})$$

The change in C_{app} caused by insertion of a thermocouple into the probe is a direct measure for the secondary coupling between the lead and the thermocouple when $\text{Re } Z_{tc} = 0$.

References

- Astrahan MA, Luxton G, Sapozink MD and Petrovich Z, 1988, The accuracy of temperature measurements from within an interstitial microwave antenna. *International Journal of Hyperthermia* 4: 593-607.
- Crezee J, Mooibroek J, Bos CK and Lagendijk JJW, 1991, Interstitial heating: experiments in artificially perfused bovine tongues. *Physics in Medicine and Biology* 36: 823-833.
- Crezee J and Lagendijk JJW, 1992, Temperature uniformity during hyperthermia: the impact of large vessels. *Physics in Medicine and Biology* 37: 1321-1337.
- De Bree J, Van der Kolk JF and Lagendijk JJW, 1996, A 3D SAR model for current source interstitial hyperthermia. *IEEE Transactions on Biomedical Engineering* 43: 1038-1045.
- De Leeuw AAC, Crezee J and Lagendijk JJW, 1993, Temperature and SAR measurements in deep-body hyperthermia with thermocouple thermometry. *International Journal of Hyperthermia* 9: 685-697.
- Deurloo IKK, Visser AG, Morawska-Kaczynska M, Van Geel CAJF, Van Rhoon GC and Levendag PC, 1991, Application of a capacitive coupling interstitial hyperthermia system at 27 MHz; study of different applicator configurations. *Physics in Medicine and Biology* 36: 119-132.
- Diedrich CJ, 1996, Ultrasound applicators with integrated catheter-cooling for interstitial hyperthermia: theory and preliminary experiments. *International Journal of Hyperthermia* 12: 279-297.
- Emami B, Stauffer PR, Dewhirst MW, Prionas S, Ryan TP, Corry PM, Herman TS, Kapp DS, Myerson RJ, Samulski TV, Sapareto SA, Sapozink MD, Shrivastava PN and Waterman FM, 1991, RTOG quality assurance guidelines for interstitial hyperthermia. *International Journal of Radiation Oncology, Biology, Physics* 20: 1117-1124.
- Hand JW, 1993, Invasive thermometry practice for interstitial hyperthermia. In: *Interstitial and Intracavitary Thermoradiotherapy*. MH Seegenschmiedt and R Sauer (Berlin, Heidelberg: Springer-Verlag), pp 83-87.
- Kaatee RSJP, Kampmeijer AG, Van Hooije CMC, Van Rhoon GC, Kanis AP, Levendag PC and Visser AG, 1995, A 27 MHz current source interstitial hyperthermia system for small animals. *International Journal of Hyperthermia* 11: 785-796.
- Kaatee RSJP, Crezee J, Kanis AP, Lagendijk JJW, Levendag PC and Visser AG, 1997, Spatial temperature control with a 27 MHz current source interstitial hyperthermia system. *International Journal of Radiation Oncology, Biology, Physics* 37: 189-197.
- Lagendijk JJW, 1990, A microwave-like LCF interstitial hyperthermia system. *Strahlentherapie und Onkologie* 166: 521 (Abstract).
- Lagendijk JJW, Crezee J and Hand JW, 1994, Dose uniformity in scanned focused ultrasound

hyperthermia. *International Journal of Hyperthermia* 10: 775-784.

Legendijk JJW, Visser AG, Kaatee RSJP, Crezee J, Van der Koijk JF, De Bree J, Kotte ANTJ, Kanis AP, Levendag PC and Battermann JJ, 1995, The 27 MHz current source multi-electrode interstitial hyperthermia method. *Nucletron-Oldelft Activity Report* 6: 83-90.

Marchal C, Nadi M, Hoffstetter S, Bey P, Pernot M and Prieur G, 1989, Practical interstitial method of heating at 27.12 MHz. *International Journal of Hyperthermia* 4: 451-466.

Van der Koijk JF, Crezee J, Van Leeuwen GMJ, Battermann JJ and Legendijk JJW, 1996, Dose uniformity in MECS interstitial hyperthermia: the impact of longitudinal control in model anatomies. *Physics in Medicine and Biology* 41: 429-444.

Visser AG, Deurloo IKK, Levendag PC, Ruifrok ACC, Cornet B and Van Rhooen GC, 1989, An interstitial hyperthermia system at 27 MHz. *International Journal of Hyperthermia* 5: 265-276.
Astrahan MA, Luxton G, Sapozink MD, Petrovich Z, 1988, The accuracy of temperature measurements from within an interstitial microwave antenna. *International Journal of Hyperthermia* 4: 593-607.

Chapter 6

Spatial temperature control with a 27 MHz current source interstitial hyperthermia system

This chapter was published as:

Kaatee RSJP, Crezee J, Kanis AP, Lagendijk JJW, Levendag PC and Visser AG, 1997, Spatial temperature control with a 27 MHz current source interstitial hyperthermia system. *International Journal of Radiation Oncology, Biology, Physics* 37: 189-197.

Abstract

This paper gives an overview of the properties of a 27 MHz current source (CS) interstitial hyperthermia (IHT) system, affecting temperature uniformity.

Applicators can be inserted in standard flexible afterloading catheters. Maximum temperatures are measured with seven point constantan-manganin thermocouple probes inside each applicator. Temperature can be controlled automatically using a simple control algorithm. Three dimensional power absorption and thermal models for inhomogeneous tissues are available to optimize applicator geometry and phase configuration. Properties of the interstitial heating system have been verified both in phantom experiments and in *in vivo* treatments of rhabdomyosarcomas implanted in the flank of a rat.

An experiment with four electrodes in one catheter proves that longitudinal control of the specific absorption rate (SAR) is feasible. Local cooling applied by cold water circulation through a catheter perpendicular to the afterloading catheter could be compensated by independent control of electrode power. Furthermore, comparison of two different phase configurations using four dual electrode applicators shows that the SAR distribution can be manipulated significantly, utilizing the phase of the electrodes. Finally, the temperature can be controlled safely and model calculations are in fair agreement with the measurements.

Using the features of the 27 MHz CS-IHT system, spatial temperature control is possible at approximately 1.5 cm.

1. Introduction

The goal of hyperthermia is to achieve a certain elevated temperature over the whole tumor volume, without overheating surrounding normal tissue.

The actual value of the required minimum tumour temperature is still a point of discussion. Traditionally, clinicians aimed at temperatures equal to or higher than 42-43°C for relatively short treatment times of about 1 h, both in treatments with external heating (Kapp *et al.*, 1990) and with interstitial heating (Seegenschmiedt *et al.*, 1992).

More recently, the effectiveness of concurrent, long duration (45-72 h), mild (41°C) hyperthermia (HT), and radiotherapy (RT) has been investigated experimentally (Armour *et al.*, 1994a; Armour *et al.*, 1994b) and clinically (Garcia *et al.*, 1992; Marchosky *et al.*, 1992).

At present, the minimum tumour temperature realized in practice is often lower than was aimed for in the treatment protocol. Sometimes this is due to limitations in applicator power, but a more fundamental reason is that large vessels (Crezee *et al.*, 1992) and spatial variations in thermal and electrical tissue properties cause inhomogeneous heating, which cannot be compensated because of insufficient spatial control of power deposition. In this case, further increasing of applicator power would lead to excessive normal tissue temperatures or hot spots in the tumour, resulting in pain and/or unacceptable toxicity. Therefore, to avoid under dosed regions in the tumour, three dimensional control of the specific absorption rate (SAR), on the same scale as the tissue heterogeneity, is needed.

However, 3D SAR steering alone is not enough. Firstly, it must be known where the cold spots are. Modeling calculations could be used to predict the temperature distribution. However, as long as tissue properties and their time dependence cannot be determined exactly, and thus reliable calculation of the temperature distribution is not possible, measurements are indispensable.

In clinical hyperthermia treatment of recurrent breast cancer, it was found that the treatment series average of the maximum temperature measured at the coldest spot in the tumour is related inversely to the number of invasive tumour measurement points (Van der Zee *et al.*, 1992). Therefore, temperature measurements should be done preferably at the same spatial scale as the tumour heterogeneity. Depending on the reliability of modelling calculations, the number of measurement points might be reduced.

Experiments in artificially perfused bovine tongues (Crezee *et al.*, 1991) and modelling calculations of the temperature distribution in heterogeneous brain tissue with realistic vessel trees (Lagendijk *et al.*, 1994b) showed that power deposition and temperature measurement with a spatial resolution of about 1 cm in three directions are needed to obtain a homogeneous temperature distribution. One way to accomplish this is through interstitial hyperthermia, provided that independent longitudinal control per afterloading catheter is feasible. The high density of applicators and thermometers enables compensation for spatial variations in blood flow and tissue properties. In addition, overheating of normal tissue can be avoided. However, a drawback of most

IHT systems is that the exchange of energy between applicator and tissue is limited to a small area around the catheter (electromagnetic systems) or, even worse, to the catheter surface (hot source systems), which might result in an inhomogeneous temperature distribution if not enough applicators are used.

This paper describes the features of the 27 MHz current source (CS) interstitial hyperthermia (IHT) system, focusing on the possibilities to improve the homogeneity of the temperature distribution.

2. Methods and Materials

2.1. The 27 MHz current source hyperthermia system

The 27 MHz CS IHT system has been developed in a collaboration between the University Hospital Utrecht and the Dr. Daniel den Hoed Cancer Center Rotterdam (DDHCC) (Lagendijk *et al.*, 1994c). Three units can be distinguished, i.e., a heating system, a thermometry system, and a control unit.

The heating system, based on the 27 MHz current source heating method (Marchal *et al.*, 1989; Visser *et al.*, 1989; Deurloo *et al.*, 1991), has two coherent groups of 32 channels, which are 180° out of phase. To maintain the strict phase relation between the channels, duty cycle power steering is used (5 W per channel adjustable with steps of 0.25 W).

Multielectrode applicators can be inserted in standard brachytherapy afterloading catheters (inner diameter (ID): 1.5 mm, outer diameter (OD): 2.0 mm).

A schematic design of a dual-electrode applicator with two segments of conducting paint (Electrodag 1415, Acheson Industries) on a polythene catheter is shown in Figure 1. A thin (50 μm) copper feeder wire is connected to each segment.

Temperature measurements are performed with seven point constantan-manganin thermocouple probes (probe diameter: 0.5 mm, ELLA-CS Czech Republic). Fast data-acquisition (all 196 channels within 320 ms) is feasible with a high resolution (0.005°C) thermometry system (De Leeuw *et al.*, 1993).

The third unit, a UNIX workstation (Silicon Graphics Iris Indigo R3000), provides the connection between power supply, thermometry, and operator. The main features of the treatment software (C++) are pretreatment quality check of applicators and thermometry, automatic or manual temperature control per electrode, clear display, and automatic storage of treatment data and a user friendly graphical user interface.

The phantom experiments were performed in muscle-equivalent agar phantoms (1 l H₂O, 30 g agar, 3.2 g NaCl, 37 ml formaldehyde) (Ishida *et al.*, 1980), with low loss ($\text{tg}\delta = 0.005$), polyoxymethylene (POM) afterloading catheters (1.5 mm ID, 2.0 mm OD, supplied by Nucletron Corporation, The Netherlands).

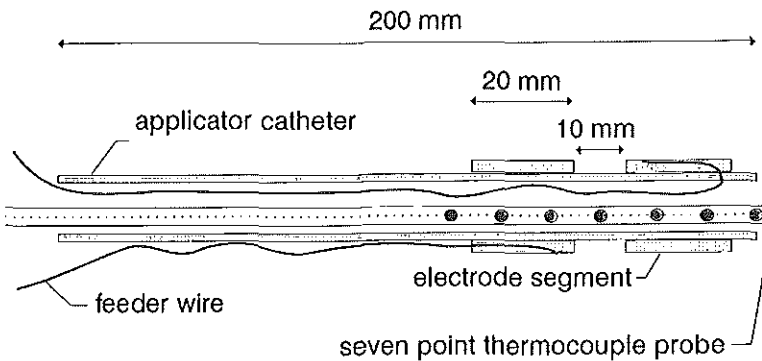


Figure 1. Schematic design of the dual electrode applicator.

2.2. Modelling calculations

The software, used for the calculations, has been developed by the hyperthermia group in Utrecht (De Bree *et al.*, 1994; Kotte *et al.*, 1994).

Using a quasi-static approximation of the Maxwell equations, the electric potential distribution and the power absorption distribution can be computed for a certain volume if the electrical properties (electrical conductivity (σ), relative permittivity (ϵ_r)) and the position of current and/or voltage sources are known (SAR model). Subsequently, the temperature distribution can be calculated at any time (thermal model) from the SAR distribution, the density (ρ), and the thermal properties (specific heat capacity (c_p), thermal conductivity (k), perfusion). Both models are three dimensional, at a resolution of 1 mm and for heterogeneous tissues. The tissue properties used for the computations are shown in Table 1.

Table 1. Tissue properties used for the modelling calculations

tissue	ρ [kg m ⁻³]	σ [$\Omega^{-1}\text{m}^{-1}$]	ϵ_r []	c_p [J kg ⁻¹ K ⁻¹]	k [W m ⁻¹ K ⁻¹]
agar	1000	0.6	80	3590	0.6
muscle	1020	0.6	113	3500	0.6
fat	900	0.43	20	2300	0.2

3. Results: System features affecting temperature uniformity

3.1. Current source applicators

The impedance associated with the capacitive coupling between the electrodes

and the surrounding tissue, through the wall of the afterloading catheter, is high compared to the tissue resistance. A typical impedance for a 20 mm electrode (OD = 1.5 mm) inside a polyoxymethylene (POM) catheter (OD = 2 mm) in muscular tissue is about 50Ω - $600j\Omega$. Therefore, the electrodes behave like current sources (Visser *et al.*, 1989) with a uniform current density along the afterloading catheter, which is relatively independent on applicator geometry. Even electrodes with opposite phase can be inserted in the same catheter (Deurloo *et al.*, 1991; Lagendijk, 1991). Furthermore, because coupling between the feeder wire and the tissue appears to be negligible, the heated region is limited to the physical size of the electrodes and thus can be chosen freely by choosing length and position of the electrodes. The effectively absorbed power per electrode, which has been obtained from calorimetric measurements, is typically in the range 1-1.5 W.

A disadvantage of electromagnetic hyperthermia systems in general is that energy absorption is strongly dependent on the permittivity and the electrical conductivity of the tissue. If a current source electrode is surrounded by different tissue types, inhomogeneous heating may occur. This is clearly demonstrated in Figure 2. One of the electrodes of a dual electrode applicator is placed partly in fat and partly in muscle. This results in a hotspot on the fat side and stresses the importance of both treatment planning and longitudinal temperature control.

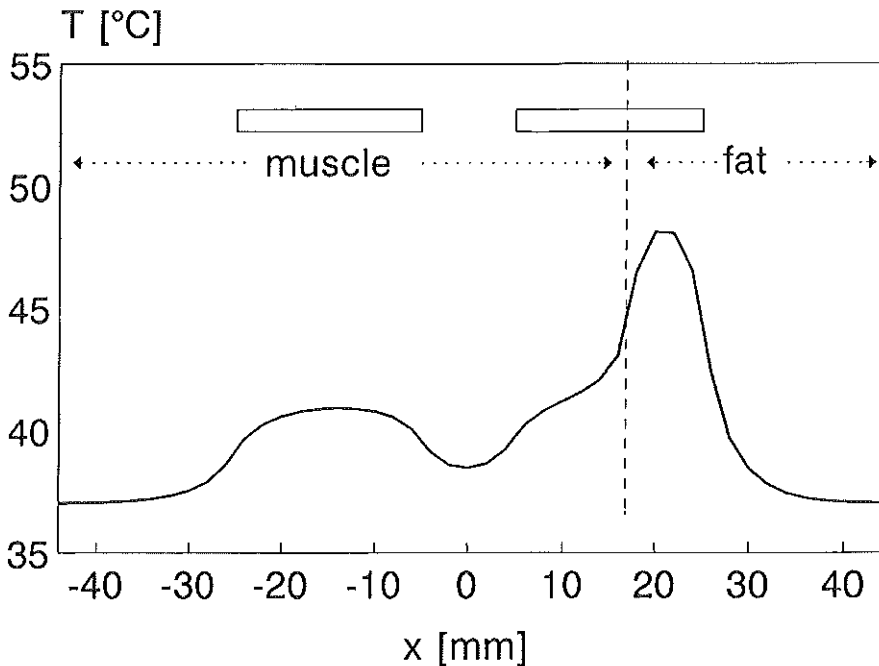


Figure 2. The calculated temperature distribution, after 5 min of heating, along a dual electrode applicator, with one of the electrodes partly in fat and partly in muscle (properties in Table 1). A hot spot occurs in the fatty tissue.

3.2. Longitudinal SAR control

Because blood vessel structure and heterogeneity of the tissue properties are three dimensional, 3D SAR control is needed as well. This can be obtained with segmented applicators, but requires a relatively large number of heating channels. With the current source IHT system the power of 64 electrodes can be controlled independently. Figure 3 demonstrates the ability of the system of longitudinal SAR control with four electrodes of 20 mm and a longitudinal spacing of 10 mm (Figure 3a). The experimental setup involved two dual electrode applicators inserted in a POM afterloading catheter from opposite sites. Temperatures were measured with a seven point thermocouple probe in each applicator. In Figure 3b two power configurations are compared. Firstly, with equal power per electrode and secondly, with decreasing power from a duty cycle of 100% for the left electrode to 25% for the right electrode. The temperature change distribution along the catheter, after 1 min of heating, was calculated (solid lines) and measured (circles and triangles). It can be seen that the temperature rise is fairly proportional to the electrode power.

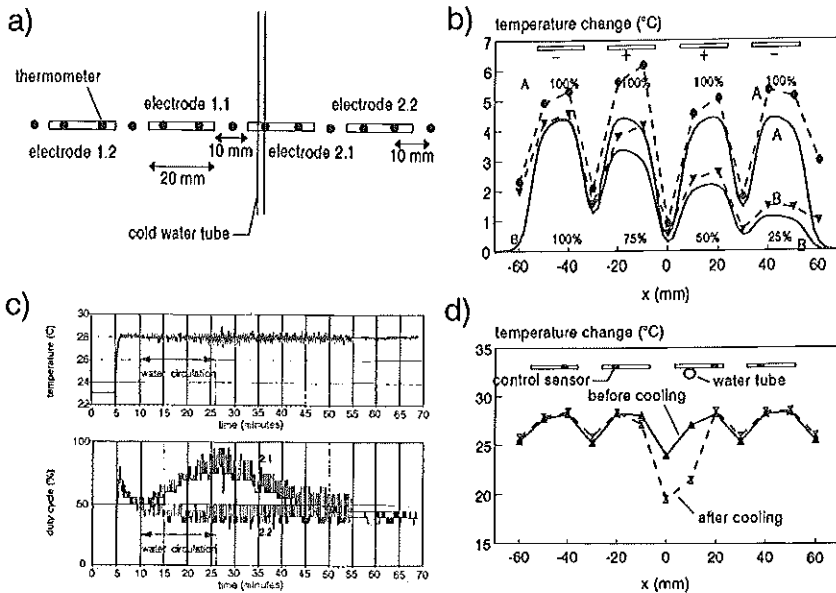


Figure 3. Longitudinal SAR control. (a) Schematic design of the experimental set-up. (b) The temperature change distribution, after 1 min of heating, calculated (solid lines) and measured in the applicators (symbols) for two different electrode power configurations (A: duty cycles of 100% for all electrodes and B: duty cycles of 100%, 75%, 50%, and 25%). Local cooling, through circulation of water with a temperature of 2°C was applied in (c) and (d). Control temperature and electrode power as a function of time are shown in (c). All control temperatures were easily maintained at the target temperature (28°C). To keep the figure clear, only the curves of the electrodes 2.1 and 2.2 are shown. The temperature distribution along the electrodes before and just after the water circulation are shown in (d). Although the control temperatures were kept at the target value, a cold spot arises near the cooling catheter.

An example of compensating local cooling utilizing longitudinal SAR control is shown in Figure 3 (a-b). To realize cooling at one position along the afterloading catheter, cold (2°C) water was circulated through an extra afterloading catheter perpendicular to the applicators. In each electrode one control thermometer was chosen. The target temperature for these sensors was set at 28°C. When the target temperature was reached, at $t=10$ min, water circulation was started. All control temperatures were maintained at the target value until the water circulation was stopped at $t=26$ min (Figure 3c). During the period of water circulation, only the control sensor closest to the cold water tube has been cooled, which can be seen in the power-time diagram, in the lower panel of Figure 3c. To keep this figure clear, the temperature and power curves of the electrodes 1.1 and 1.2, which were almost identical to those of electrode 2.2, have been excluded. This confirms that independent temperature control per electrode is possible. Figure 3d shows the temperature distribution measured along the electrodes, before and just after the water circulation. Although the control sensors have been kept at the target temperature, the temperature in the centre has dropped, due to the applied cooling. This demonstrates the importance of temperature measurements outside the electrodes to detect these cold spots. Because thermometry is seldom sufficiently extensive, temperature measurements should be combined with reliable temperature computations. Furthermore, sufficient electrode power and electrode lengths which match the tissue inhomogeneity are essential for good longitudinal control.

3.3. Phase configuration SAR control

The SAR distribution does not only depend on electrode geometry and power amplitude, but also on the power phase. The effect of the phase configuration on the temperature distribution is clearly shown in Figure 4. Four dual electrode applicators are inserted in four parallel catheters, implanted in a square (15 x 15 mm²) geometry (Figure 4a). The temperature distribution along the central axis, parallel to the applicators, was calculated (solid lines) and measured (circles and triangles) after 1 min of heating for two different phase configurations (Figure 4b). If all tip electrodes have the same phase (Situation A), then maximum energy absorption is found in the centre of the implant. This is due to constructive interference of the electric fields of the applicators. The maximum turns into a minimum if the electrode connections are inverted for two of the applicators (Situation B).

4.4. Automatic temperature control

For a large number of electrodes, manual power steering is not convenient and it could even be dangerous. Automatic temperature control is to be preferred.

The 27 MHz CS-IHT-system uses a straightforward control algorithm to

calculate the power duty cycle as a function of the temperature measured inside the electrode. In case more than one temperature sensor per electrode is used, the sensor with the highest temperature is chosen to be the control sensor. First, the target temperature (T_{target}) and the control cycle time (t_{cycle}) are chosen. The latter must be sufficiently short to be alert to sudden changes in perfusion and to minimize temperature fluctuations if the optimal power is between two adjustable levels. Cycle times in the range of 30-60 s appear to be safe if low loss afterloading catheters, e.g., POM ($\text{tg}\delta=0.005$) are used. However, 15 s are needed for absorbing material such as nylon ($\text{tg}\delta=0.04$).

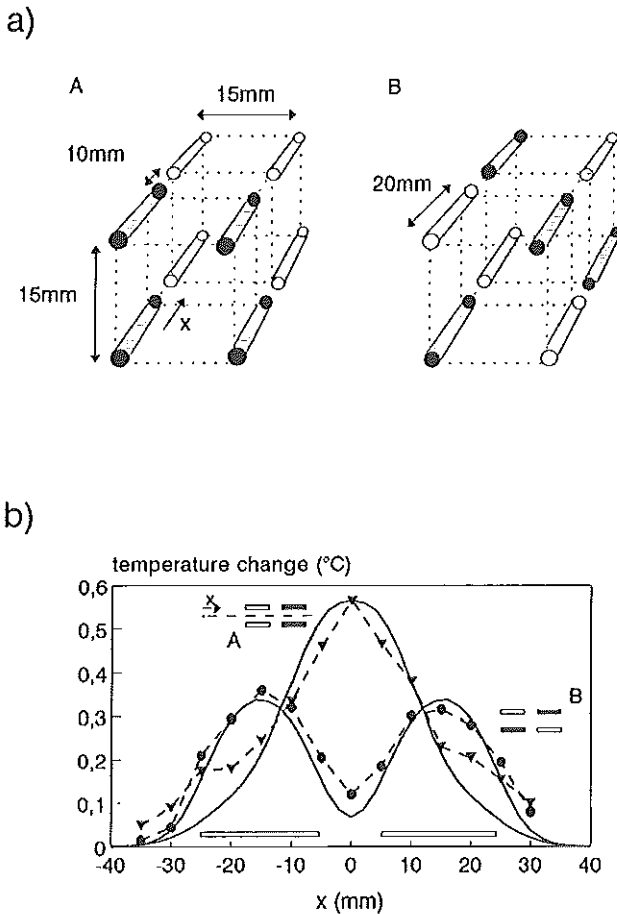


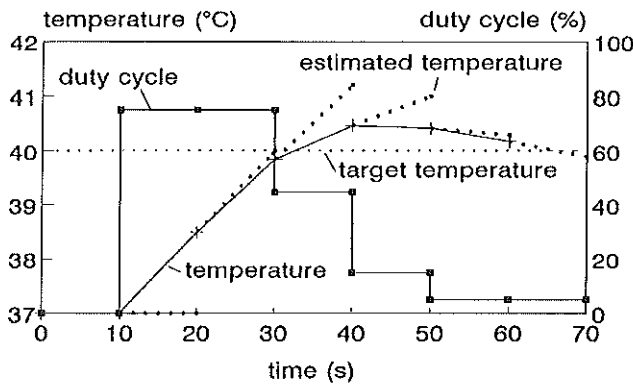
Figure 4. Phase configuration SAR control. a) Four dual electrode applicators have been inserted in four parallel POM catheters in an agar phantom. The dark and the light electrodes are 180° out of phase. Two phase configurations have been compared (A and B). b) The temperature change distribution, after 1 min of heating, was calculated (solid lines) and measured (symbols) along the central axis parallel with the applicators. For configuration A the maximum temperature rise was found in the centre, due to constructive interference of the E-fields. The temperature distribution for configuration B has a minimum in the centre.

The temperature is measured during every t_{cycle} , and the temperature expected for the next measurement ($T_{\text{estimated}}$) is linearly extrapolated from the previous temperature (T_{previous}) and the present temperature (T_{present}). Then the duty cycle change is taken to be proportional with the difference between T_{target} and $T_{\text{estimated}}$:

$$\Delta dc = \alpha(T_{\text{target}} - T_{\text{estimated}}) \tag{1}$$

with α the control factor. The control method is visualized in Figure 5a.

a)



b)

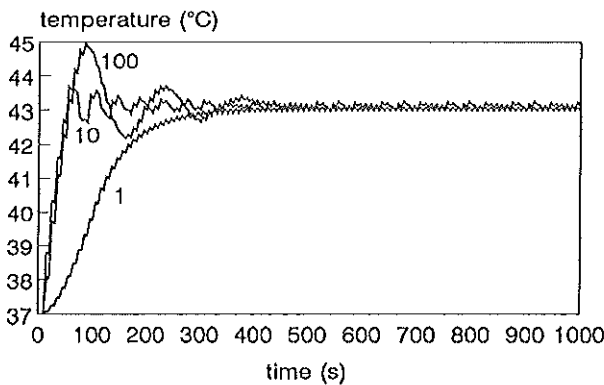


Fig. 5. The automatic control algorithm. (a) Visualization of the algorithm. At $t=0$ the target temperature was set at 40°C and the control factor was taken 25 (see text). (b) Temperature-time diagram for three different control factors ($\alpha=1, 10$ or $100, T_{\text{target}} = 43^{\circ}\text{C}$).

The first requirement for automatic temperature control is obviously that it must be safe. The following considerations are relevant in this respect. First, maximum energy absorption will be close to the electrodes. Therefore, with temperature sensors inside all electrodes, the maximum tumour temperatures are always detected. Furthermore, continuous readout of the thermocouple voltages, during a control cycle, is possible using RF filtering. Power will be turned off independently of the control algorithm if the measured temperature is higher than a chosen maximum, or if it is unrealistically low, e.g., due to a defect RF filter or a shifted sensor or applicator.

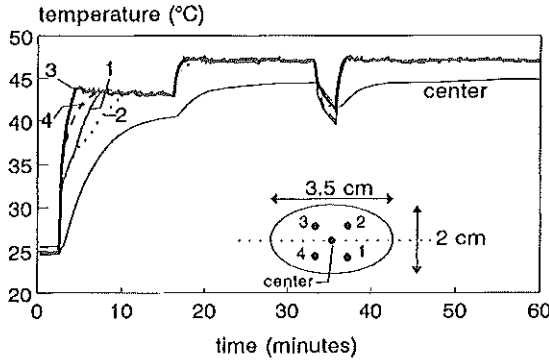
Besides being safe, the algorithm must work properly, which means that once T_{target} has been set, it must be reached quickly and maintained stable. Before the treatment starts, a power pulse is given for each electrode to check the functionality and the set-up definition of applicators and thermometry. T_{target} is reached more rapidly if the control factor α is increased, but a temperature overshoot might occur (Figure 5b). In clinical practice, α is in the range of 5-10 and can be kept the same for all applicators during the whole treatment.

In Figure 6 an example is given of an automatically controlled ($\alpha=6$, $t_{\text{cycle}}=10\text{s}$) IHT treatment of a rhabdomyosarcoma in the flank of a female WagRij rat. Four POM afterloading catheters were implanted with 10 mm spacing. Two single electrode applicators (2 cm long) with equal phase and two with opposite phase were inserted. The temperature was measured in the electrodes and, via an extra thermometry catheter, in the tumour centre. First, the target temperature for the electrodes was set at 43°C which is about 18°C above the low (due to anaesthesia) starting temperature of 25°C. The differences in heating up rate are due to spatial variations in blood flow and/or tissue properties, because power-temperature characteristics in an agar phantom were the same for all applicators. After about 16 min, the target temperature was increased to 47°C to improve the central temperature. Halfway the treatment power was turned off for 150 s. The slow decrease in the centre demonstrates that the temperature is more or less homogeneous between the electrodes. The relatively rapid temperature fall in the electrodes just after power was turned off shows that only a small region around the electrodes has a high (47°C) temperature. The core temperature, which was measured in the rectum, was stable during the treatment.

4. Discussion

The SAR and thermal models used to calculate the SAR distributions and the temperature distributions have been found to be useful tools for the optimization and evaluation of the treatment. The calculations predict the positions of hot and cold spots accurately. In general, quantitative prediction of clinical temperature distributions is difficult, for two reasons. Firstly, the models need further refinement. Applicator description and modelling of perfusion are the main challenges in this respect.

a)



b)

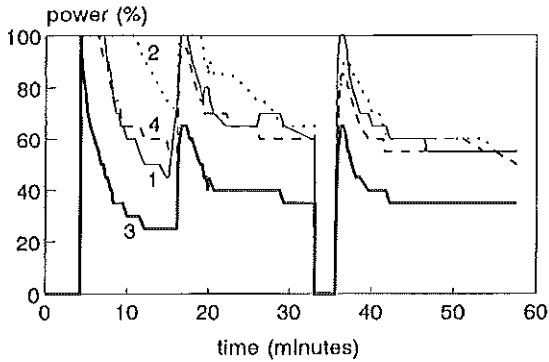


Fig. 6. Automatic temperature control during a treatment of a rhabdomyosarcoma growing in the flank of a female WagRij rat. The tumour was implanted with a 10 mm square implant in which four 20 mm long single electrode applicators were inserted. The temperature was measured in each applicator (control sensors) and in the centre of the tumour. First, the target temperature of the automatic temperature control was set at 43°C. Later, at $t=16$ min, it was increased to 47°C. Halfway through the treatment power was turned off for 150 s. The temperature-time (a) and power-time (b) diagrams are shown. The control factor during the treatment was 7.

Secondly, accurate input parameters, i.e., tissue properties and blood flow, cannot always be obtained with the current imaging techniques (CT, MRI, MRA). Therefore, extensive invasive temperature measurements remain necessary. However, the qualitative temperature distributions calculated with the 3D models, which are available for the 27 MHz current source IHT system, are very useful for optimization of the treatment quality. After implantation of the afterloading catheters, pretreatment computations can be used to find the optimal applicator geometry, e.g., electrode position relative to tissue transitions (Figure 2), and to maximize the advantages of phase configuration

SAR control. Extra thermometry can be placed at locations where cold spots are expected. Furthermore, the modelling calculations can serve as a measure for the treatment quality. In combination with the measured temperatures, a good estimation of the thermal dose is possible, which is essential for the evaluation of clinical trials.

The current source behaviour of the applicators may have advantages over other interstitial heating techniques for some applications.

Compared to local current field (LCF) radiofrequency (RF) heating, the current source heating method is more suitable for irregular implants, i.e., implants with varying separations between neighbouring catheters or with curved catheters. In case of LCF-RF IHT, nonparallel implanted galvanically coupled applicators (voltage sources) can lead to severe hot spots (Strohbehn *et al.*, 1986).

Furthermore, the current injection is homogeneous along the electrodes and independent from length and position of the electrodes. This is an advantage over microwave antennas, where the temperature distribution strongly depends on insertion depth and a cold tip is often seen (Ryan, 1991). The latter is an important drawback, if an increased implantation depth beyond the distant tumour edge is not possible. In addition, using the current source system, better normal tissue sparing is achieved in case of deep-seated tumours, because there is no heating along the feed line. It is important to realize that a homogeneous temperature distribution along the electrodes is achieved only if the tissue around the electrodes is homogeneous (see Figure 2). Therefore, short electrodes should be used and electrode placement over tissue boundaries should be avoided.

Direct energy absorption in tissue at a distance from the afterloading catheter, is a pro compared to heating via thermal conduction alone, because a higher heat penetration depth can be expected, resulting in a more homogeneous temperature distribution, for a certain applicator density.

Effective heating depths, defined as the radial distance from the applicator at which the temperature rise is 50% of the maximum temperature rise, have been calculated for single cylindrical hot source, RF-LCF, and ultrasound applicators with an outside diameter of 2 mm (Diedrich *et al.*, 1993). The one dimensional steady state solution of the bioheat transfer equation in a medium with perfusion of $2.0 \text{ kg m}^{-3} \text{ s}^{-1}$ was calculated, using a finite difference technique. The effective heating radius of a RF-LCF electrode (7.3 mm) was significantly higher than with thermal conduction only (2.7 mm). As in RF-LCF heating, the power absorption around a CS applicator is proportional to $1/r^2$, which gives a heating radius of 7.3 mm. It should be mentioned that dielectric losses in some afterloading catheter materials such as nylon, could decrease this value. The highest effective heating depths were achieved with ultrasound applicators (10 mm at 9 MHz, 11.5 mm at 5 MHz, and 15.4 mm at 1 MHz). An estimation of the effective heating depth of a single microwave antenna operating at 915 MHz can be obtained from the *in vivo* measurements in muscle tissue (Sato *et al.*, 1988). The heating depth, measured at the position of the antenna gap, was about 11 mm for a dipole antenna and about

9 mm for a helical coil antenna. Both antennas had a 3.5 cm long tip and were inserted to a depth of 7 cm.

With arrays of coherent electromagnetic sources it might be possible to improve the power absorption at depth, through constructive interference of the absorption distributions of individual applicators. The experiment reported in section 3.3 demonstrated that manipulation of the specific absorption rate at depth is possible.

The degree of spatial temperature control strongly depends on the electrode density. In brachytherapy, the distance chosen between afterloading catheters is usually in the range of 1-1.5 cm. The minimum electrode length needed for sufficient coupling between electrode and tissue is about 1.5 cm. At present, dual electrode applicators are used, but applicators with three electrodes are being tested. So, if an afterloading catheter is accessible from both sides, maximum longitudinal control, i.e., on a 1.5 cm scale, can be obtained over a length of 7.5 cm, including the longitudinal spacing (0.5 cm) between the electrodes. The maximum tumour volume which can be treated is dependent on the available number of heating channels.

With the 64 channels of the clinical heating system, maximum spatial control can be achieved within one heating session, in a volume of $4.5 \times 4.5 \times 7.5 \text{ cm}^3$.

To handle this relatively large number of applicators, safe automatic temperature control is a necessity in interstitial hyperthermia.

The only external hyperthermia method which has the ability of even sub-centimetre spatial SAR control, is scanned focused ultrasound (SFUS) (Hunt, 1990). In theory, very homogeneous thermal dose distributions are possible (Legendijk *et al.*, 1994a). Disadvantages are high absorption in bone and reflection at tissue-air interfaces. As mentioned above, thermometry catheters will be needed for SAR control but can be thinner than standard afterloading catheters. In contrast with most IHT techniques, hot spots are not always detected, which could make SFUS treatments less safe.

Inadequate heating technology and thermal dosimetry are considered a probable cause of failure of trials comparing thermoradiotherapy with radiotherapy alone (Moros *et al.*, 1994).

To improve this situation, three dimensional temperature control is essential.

The 27 MHz current source IHT system has several features, enabling it to attain a fairly homogeneous temperature distribution. Further development of treatment planning techniques is needed to exploit the possibilities of improved spatial temperature control.

Acknowledgements

The authors wish to thank Ms. Inge Dijkstra for her work on polishing the manuscript. This study is supported by the Dutch Cancer Society (Grant DDHK 91-13) and by Nucletron Corporation Veenendaal.

References

- Armour EP, Wang Z, Corry PM, Chen PY and Martinez A, 1994a, Hyperthermic enhancement of high dose-rate irradiation in 9L gliosarcoma cells. *International Journal of Radiation Oncology, Biology, Physics* **28**: 171-177.
- Armour EP, Wang Z, Corry PM and Martinez A, 1994b, Thermotolerance and radiation sensitizing effects of long duration mild temperature hyperthermia. *International Journal of Hyperthermia* **10**: 315-324.
- Crezee J, Mooibroek J, Bos CK and Lagendijk JJW, 1991, Interstitial heating: experiments in artificially perfused bovine tongues. *Physics in Medicine and Biology* **36**: 823-833.
- Crezee J and Lagendijk JJW, 1992, Temperature uniformity during hyperthermia: the impact of large vessels. *Physics in Medicine and Biology* **37**: 1321-1337.
- De Bree J, Van der Koijk JF and Lagendijk JJW, 1994, A fast calculation method of SAR for interstitial hyperthermia. *Programme and Abstract book ESRB/ESHO* (abstract 44).
- De Leeuw AAC, Crezee J and Lagendijk JJW, 1993, Temperature and SAR measurements in deep-body hyperthermia with thermocouple thermometry. *International Journal of Hyperthermia* **5**: 685-697.
- Deurloo IKK, Visser AG, Morawska-Kaczynska M, Van Geel CAJF, Van Rhoon GC and Levendag PC, 1991, Application of a capacitive coupling interstitial hyperthermia system at 27 MHz; study of different applicator configurations. *Physics in Medicine and Biology* **36**: 119-132.
- Diedrich CJ and Hynynen KH, 1993, Ultrasound technology for interstitial hyperthermia. In: *Interstitial and Intracavitary Thermo-radiotherapy*. MH Seegenschmiedt and R Sauer, eds. (Berlin, Heidelberg, New York: Springer-Verlag), pp 55-61.
- Garcia MD, Nussbaum GH, Fathman AE, Drzymala RE, Bleyer MW, DeFord JA, Welsh DM and Halverson KJ, 1992, Concurrent Iridium-192 brachytherapy and long-duration, conductive interstitial hyperthermia for the treatment of recurrent carcinoma of the prostate: a feasibility study. *Endocurietherapy/Hyperthermia Oncology* **8**: 151-158.
- Hunt JW, 1990, Principals of ultrasound used for generating localized hyperthermia. In: *An Introduction to the Practical Aspects of Clinical Hyperthermia*. SB Field and JW Hand, eds. (London: Taylor & Francis), pp 371-422.
- Ishida T and Kato H, 1980, Muscle equivalent agar phantom for 13.56 MHz RF-induced hyperthermia. *Shimane Journal of Medical Science* **4**: 134-140.
- Kapp DS and Meyer JL, 1990, Clinical hyperthermic practice: non-invasive heating. In: *An Introduction to the Practical Aspects of Clinical Hyperthermia*. SB Field and JW Hand, eds. (London: Taylor & Francis), pp 143-171.
- Kotte ANTJ, De Bree J, Crezee J, Van der Koijk JF, Van Leeuwen GMJ and Lagendijk JJW, 1994, A thermal model featuring a semi-analytical discrete vessel description. *Abstract book ESRB/ESHO* (abstract 154).
- Lagendijk JJW, 1991, A 3-D SAR model for voltage and current source LCF interstitial hyperthermia systems. *Strahlentherapie und Onkologie* **167**: 329.
- Lagendijk JJW, Crezee J and Hand JW, 1994a, Dose uniformity in scanned ultrasound hyperthermia. *International Journal of Hyperthermia* **6**: 775-784.

Legendijk JJW, Van der Koijk JF, Visser AG, Kaatee RSJP, Crezee J, De Bree J, Kotte ANTJ, Kanis AP, Levendag PC and Battermann JJ, 1994b, Dose uniformity with the 27 MHz multi-electrode current source interstitial hyperthermia method. In: *Brachytherapy Review. Proceedings German Brachytherapy Conference, Freiburg, November 1994. Freiburg Oncology Series, Monograph No. 1*. G Bruggmoser and RF Mould, eds. (Freiburg: Albert-Ludwigs-University Freiburg FRG), pp 38-44.

Legendijk JJW, Visser AG, Kaatee RSJP, Crezee J, Van der Koijk JF, De Bree J, Kotte ANTJ, Kanis AP, Levendag PC and Battermann JJ, 1994c, The 27 MHz current source multi-electrode interstitial hyperthermia method. *Activity, International Nucletron-Oldelft Radiotherapy* 6: 83-90.

Marchal C, Nadi M, Hoffstetter S, Bey P, Pernot M and Prieur G, 1989, Practical interstitial method of heating at 27.12 MHz. *International Journal of Hyperthermia* 4: 451-466.

Marchosky JA, Welsh DM, Horn BA and Van Amburg AL, 1992, Experience with long-duration interstitial hyperthermia and systemic BCNU in the treatment of recurrent malignant brain tumours. In: *Hyperthermic Oncology 1992. Proceedings of the 6th International Congress on Hyperthermic Oncology (IHO). Tucson, Arizona, April 27-May 1, 1992. Volume 1 (Summary Papers)*. EW Gerner, ed. (Tucson: Arizona Board of Regents), pp 387.

Moros E, Scott CA, Emami B, Perez CA, Asbell S, Swift P, Grigsby PW, Montesano A, Rubin P, Curran W, Del Rowe J, Arastu H and Fu KK, 1994, Adequacy of treatment analysis of an interstitial thermo-radiotherapy study (RTOG 84-19). In: Abstract book 42nd Meeting of the Radiation Research Society and the 14th Meeting of the North American Hyperthermia Society. pp P01-13.

Ryan TP, 1991, Comparison of six microwave antennas for hyperthermia treatment of cancer: SAR results for single antennas and arrays. *International Journal of Radiation Oncology, Biology, Physics* 21: 403-413.

Satoh T, Stauffer PR and Fike JR, 1988, Thermal distribution studies of helical coil microwave antennas for interstitial hyperthermia. *International Journal of Radiation Oncology, Biology, Physics* 15: 1209-1218.

Seegenschmiedt MH and Sauer R, 1992, The current role of interstitial thermo-radiotherapy. *Strahlentherapie und Onkologie* 168: 119-140.

Strohbehn JW and Mechling JA, 1986, Interstitial techniques for clinical hyperthermia. In: *Physical Techniques for Clinical Hyperthermia*. JW Hand and JR James, eds. (Somerset, England: Research Studies Press), pp 210-287.

Van der Zee J, Van Rhoon GC, Verloop-van 't Hof EM, Van der Ploeg SK, Rietveld PJM and Van den Berg AP, 1992, The importance of adequate heating techniques for therapeutic outcome. In: *Hyperthermic Oncology 1992. Proceedings of the 6th International Congress on Hyperthermic Oncology (IHO). Tucson, Arizona, April 27-May 1, 1992. Volume 2*. EW Gerner and TC Cetas, eds. (Tucson: Arizona Board of Regents), pp 349-352.

Visser AG, Deurloo IKK, Levendag PC, Ruifrok ACC, Cornet B and Van Rhoon GC, 1989, An interstitial hyperthermia system at 27 MHz. *International Journal of Hyperthermia* 5: 265-276.

.....

Chapter 7

Clinical thermometry using a 27 MHz multi electrode current source interstitial hyperthermia system in brain tumours

This chapter was submitted as:

Kaatee RSJP, Nowak PCJM, Van de Zee J, De Bree J, Kanis AP, Crezee J, Levendag , Levendag PC and Visser AG, 1999, Clinical thermometry, using the 27 MHz multi electrode current source interstitial hyperthermia system in brain tumours; methods of thermometry use in interstitial hyperthermia. *Radiotherapy and Oncology*.

Abstract

In interstitial hyperthermia temperature measurements are mainly performed inside heating applicators and therefore, give the maximum temperatures in a rather heterogeneous temperature distribution. The problem of how to estimate lesion temperatures using the multi-electrode current-source (MECS) interstitial hyperthermia (IHT) system in the brain is studied, for two implants at either extreme of the volume range encountered in clinical practice.

A small (diameter:1 cm) and a large (diameter:4 cm) target volume were heated with 2 and 18 electrodes (length:1 cm), respectively. Temperatures were measured with thermocouple probes in the electrodes and in an extra afterloading catheter at the edge of the target volume. The edge temperature was used to set the target temperature for the electrodes which were controlled automatically. Each control cycle was divided in a power-on and a power-off period. From the temperature decay during the latter period information was obtained about the temperature between the electrodes. The significance of these data was examined through model calculations.

The desired minimum temperature of 40°C at the edge of the target

volume could be reached and maintained easily. Although the hot spots near the electrodes were high (about 50°C), they were also very local. The temperature decay method shows that most of the tissue temperatures in the target volumes were in the range of 40°C to 44°C.

In conclusion, it is feasible to heat the brain adequately using the MECS-IHT system. Furthermore the electrode temperatures read during heating are not suitable to assess the temperature distribution. For this purpose, extra sensors outside the electrodes and/or application of the decay-method are required.

1. Introduction

With respect to the use of thermometry for optimization and evaluation of the treatment quality, interstitial hyperthermia (IHT) differs from external heating techniques, due to its characteristic temperature distributions with hot spots around the electrodes (Levendag *et al*, 1993).

In fact, applicator temperatures are only useful to control the maximum tissue temperature. However, sensors inside the applicator often overestimate the tissue temperature, due to self-heating of the applicator and/or thermometer. Measurements in thermometry catheters, i.e. without a working applicator, give in general reliable tissue temperatures if sufficient precautions are taken. These sensors, if placed in the centre between the applicators and at the edge of the target volume, give information about the local minima in the temperature distribution. Knowledge about the minimum temperature in the target volume is important for good treatment control. Therefore, quality assurance demands for number and place of the sensors, as were defined in the RTOG QA-guidelines for IHT by Emami *et al* (1991) should be followed. In case of inhomogeneous perfusion and/or the presence of large blood vessels even more thermometers should be used. However, in practice the number of catheters which can be implanted is limited by patient tolerance. Furthermore the homogeneity of the temperature distribution strongly depends on the electrode density. Therefore a compromise has to be made between heating catheters and thermometry catheters which often leads to a shortage of information about the minimum temperatures.

In some situations minimum temperature control is possible using the applicator temperatures only. DeFord *et al.*(1991) was able to estimate the minimum temperatures between conductive interstitial applicators in brain tissue, as a function of the ratio between the applicator power and the temperature rise in the applicator. Another way to judge the temperature distribution during the treatment using applicator temperatures, is to study the temperature decay after turning off the power. This should give information about the lower tissue temperatures at some distance of the applicator. In addition these power-off intervals reduce self-heating artifacts, if present. However, Newman *et al.* (1990) have demonstrated that calculation of thermal tissue properties, using clinical thermal washout data requires correct modelling of the heating geometry, the actual thermal boundary conditions,

and the initial temperature distribution. Using the applicator-temperature decay to estimate the temperatures elsewhere will be even more difficult.

Evaluation of the treatment in terms of the commonly used treatment quality parameters, as were summarized by Erb and Seegenschmiedt (1995), using the available measured temperatures without extra information, is even more difficult than to control the minimum temperature. Because of the relatively high temperature gradients (typically 1°C/mm) associated with interstitial heating, the sensor density, needed to calculate the delivered thermal dose with parameters such as T_{90} and T_{mean} , should be much higher than for external heating techniques, probably too high to be feasible.

Model calculations could be a solution to this problem. Tissue properties can be varied until the calculated temperature distribution corresponds well with the temperature data obtained during the treatment. Subsequently, thermal dose parameters can be computed.

The use of thermometry in applicator catheters and thermometry catheters in the clinical situation will be discussed for the 27 MHz multi-electrode current-source (MECS) IHT system. This system has been developed in a collaboration between the university hospital Utrecht and the Daniel den Hoed Cancer Centre Rotterdam. Promising features of MECS-IHT regarding 3D spatial temperature control have already been confirmed in model calculations (Kaatee *et al.*, 1997, Lagendijk *et al.*, 1994, Van de Koijk *et al.*, 1996), in muscle-equivalent phantom measurements (Deurloo *et al.*, 1991, Kaatee *et al.*, 1997, Visser *et al.*, 1989) and in vivo, in rhabdomyosarcomas growing in the flank of a rat (Kaatee *et al.*, 1995). Clinical application of the MECS-IHT system involves treatments of high grade (grade III/IV) gliomas. The experience in the Daniel den Hoed Cancer Centre with IHT of high grade gliomas, until August 1997, is based on the treatments of 7 patients. In this paper methods of thermometry use are investigated for two of these treatments, i.e. the treatment of a small (diameter: 1 cm, 2 electrodes) and of a large (diameter: 4 cm, 18 electrodes) target volume.

2. Materials and Methods

2.1. The 27 MHz multi-electrode current-source interstitial hyperthermia system

The 27 MHz current source hyperthermia system can be split into three sections, i.e. a 27 MHz heating unit, a thermometry system, and a workstation for treatment planning and treatment control. The power system has 64 coherent channels, divided into two groups with a phase difference of 180°. Duty cycle power steering (from 0 to 100% of a cycle time of 200 ms, in steps of 5%) is used to maintain the strict phase relation between the channels. The electromagnetic energy is deposited in the tissue by multi-

electrode applicators, inserted in plastic afterloading catheters.

Temperature measurements are performed with 7-points constantan-manganin thermocouple probes (ELLA-CS, Czech Republic). Fast data-acquisition (all 196 channels read within 320 ms) is feasible using a high resolution (0.005°C) thermometry system (De Leeuw *et al.*, 1993)

A UNIX-workstation provides the connection between thermometry, power supply and operator. Some features of the treatment control software are: automatic or manual temperature control per electrode, clear display and automatic storage of treatment data and a user-friendly graphical user interface.

Furthermore the work station is used for treatment planning. Three-dimensional models are available for calculation of the distributions of power absorption and temperature, for heterogeneous tissues.

A more extensive description of the MECS-system has been given by Lagendijk *et al.* (1994).

2.2. Placement of afterloading catheters, applicators and thermometers

In general target dimensions in the brain are in the range of 10 to 50 mm. Typically 1 to 10 afterloading catheters are implanted parallel at distances of about 5-10 mm. The catheters have blunt tips to minimize damage to the blood vessels and are made of a special type of nylon which has a low dielectric loss ($\tan\delta \approx 0.002$) The latter is necessary to avoid large absorption of electromagnetic energy in the catheter wall.

In figure 1 a top view of the small and the large implant, discussed in this paper, are shown. The catheters denoted by closed circles are used for thermometry only. In the other catheters dual-electrode applicators are inserted with 10 mm long electrodes at a longitudinal distance of 5 mm, with a 7-point thermocouple probe (7.5 or 10 mm distance between the measure points) inside (Kaatee *et al.*, 1997b). Two concentric circles denote that the afterloading catheter is inserted through a hollow titanium screw which is used for fixation of the implant template to the skull. Thermocouple-probe and applicators are fixed to the catheters using luer-lock adapters (Cook). All tip-electrodes are connected with the same phase. The phase of the other electrodes are shifted 180°. Inside each applicator, the temperature is measured with 7-point manganin-constantan thermocouple probes. In most applicators the distance between the points is 7.5 mm and in the others 10 mm. In the thermometry catheter the temperature was measured at 14 points with a 5 mm resolution.

The electrodes were placed mostly inside the target volume to avoid hot spots in the surrounding normal tissue. Only in case of the small target volume the electrodes exceeded the target volume boundary by 5 mm at each side, to be able to deliver sufficient energy to compensate for heat flow due to blood flow and thermal conduction (Kaatee *et al.* 1997b).

2.3. Treatment schedule and goal

After surgery the patients received 33 fractions of 1.8 Gy external radiotherapy (ERT) followed by a combination of IHT and pulsed dose rate (PDR) interstitial radiotherapy (IRT). The latter consisted of 4 fractions per day (8:00, 11:00, 14:00 and 17:00 hours) of 2 Gy per fraction and an overall dose of 24 Gy. On the first whole day of the brachytherapy treatment three IHT-sessions of about two hours were administered between the PDR-fractions. The treatment goal was to achieve a minimum temperature of 40 °C in the treatment volume as long as possible.

2.4. Treatment control

In each electrode one temperature sensor was selected as control sensor. The temperature measured with this sensor is used to control the power of the corresponding electrode. A control cycle consists of a power-on period and a power-off period to measure temperatures. The power-off period is divided into a "recovery period", to allow the electronic disturbance of the data-acquisition equipment to disappear, and the actual "measurement period", during which temperatures are measured with a frequency of 1 measurement per second. Except from the recovery period which must be at least 1 s, the length of the various periods can be chosen freely. The choice of the control cycle parameters is somewhat arbitrary. In general, longer power-off time gives more temperature-decay information but requires a longer power-on period to maintain the effective power at a certain level which makes the automatic control procedure less alert. In case of the large implant the power-on, recovery and measurement times were 10, 2 and 3 s respectively. For the small implant these times were 55, 2 and 8 s. To heat a smaller target volume, a higher absorption density is required (Kaatee *et al.*, 1997b). Therefore, the ratio between power-on and power-off time is higher for the small than for the large implant.

During the power-off period the temperature decreases. The temperature which is controlled by the automatic temperature control algorithm is the last measured temperature during a measurement interval. If the power-off time is chosen correctly then the controlled temperature corresponds with the maximum tissue temperature just outside the afterloading catheter wall. Unfortunately, the required power-off time is not only related with the type of applicator and afterloading catheter but depends also on the tissue properties and on the geometry of the implant. Therefore short term (0-15 s) decay of the applicator temperatures, after all electrodes were switched off simultaneously, was studied to determine the waiting time after which the electrode temperatures can be interpreted as maximum tissue temperatures.

In practice, the actual value of the maximum tissue temperature was considered of less importance than the obtained minimum temperature in the target volume

The temperature measured with the sensor in the thermometry catheters close to the edge of the target volume was taken as a first estimation of the minimum temperature. The electrode target temperature was kept equal in all electrodes, and was adjusted until an edge temperature of 40°C was reached. In case of the large implant, occasionally the electrodes in one of the afterloading catheters were turned off for 1-2 minutes, to obtain information about local minimum tissue temperatures in a certain region of the target volume.

2.5. Model calculations

Model calculations were performed after the treatment of the large implant to determine the meaning of the applicator temperatures, 1-2 minutes after the power is switched off in relation with local minimum tissue temperatures.

The models used for the computation of the power absorption density and the resulting temperature distribution, have been described by De Bree *et al.* (1996)

and Kotte *et al.* (1996), respectively.

The patient tissue geometry was obtained using CT-data and was divided into voxels with a resolution of 1 mm in three dimensions. Each voxel was classified as either brain tissue or air or bone depending on its Hounsfield value. No distinction could be made between grey and white matter. The tissue properties used for the calculation are given in table 1. The air was kept at a fixed temperature of 25 °C. Heat transfer from skin to the air was taken into account using a heat transfer coefficient of 8.1 W m⁻²K⁻¹.

Because discrete vessel data were not available, blood flow was incorporated in the model using the heat sink theory (Pennes, 1948). Blood flow rates (w_b) of 0.5 and 50 (initial value) ml/100g tissue/min were chosen for bone and brain tissue respectively. The latter was varied to match the computational results with the clinical measurements. The specific heat capacity coefficient of blood (c_b) was set at 3825 Jkg⁻¹ K⁻¹. Each metal electrode and the afterloading catheter in which it is inserted are modelled together as a current source electrode. Because a voxel size of 1 mm is too large for accurate numerical modelling of the interaction between electrodes and the surrounding tissue, this was implemented analytically (De Bree *et al.* 1996, Van der Koijk *et al.* 1997b). This was possible because the electrodes are described as a geometrical objects, independent of the tissue grid resolution.

The goal of the simulations was to reproduce the clinical temperature decay measurements for 1-2 minutes, by varying the blood flow rate of the brain tissue. In an iterative procedure, the electrode powers, i.e. the current injections, were modified and the resulting power absorption and temperature distributions were calculated, until all steady state electrode temperatures reached a certain target temperature. Subsequently, the electrodes in one catheter were turned off and the power absorption was calculated for this new

situation. Next, the temperature decrease was calculated and compared with the clinical decay measurements. The whole simulation was repeated, while the brain blood flow rate was varied, until a good agreement between computation and measurement was found.

Table 1. Tissue properties used for the model calculations ¹

Medium	σ [$\Omega^{-1} \text{ m}^{-1}$]	ϵ_r []	ρ [kgm^{-3}]	c [$\text{Jkg}^{-1} \text{ K}^{-1}$]	k [$\text{Wm}^{-1} \text{ K}^{-1}$]
air	0	1	1.3	0.001	0.004
brain	0.39	150	1000	3600	0.53
bone	0.04	9	1600	1400	0.65

¹ data obtained from the COMAC BME task group report of the European Society for Hyperthermic Oncology (1992): Treatment planning and modelling in hyperthermia

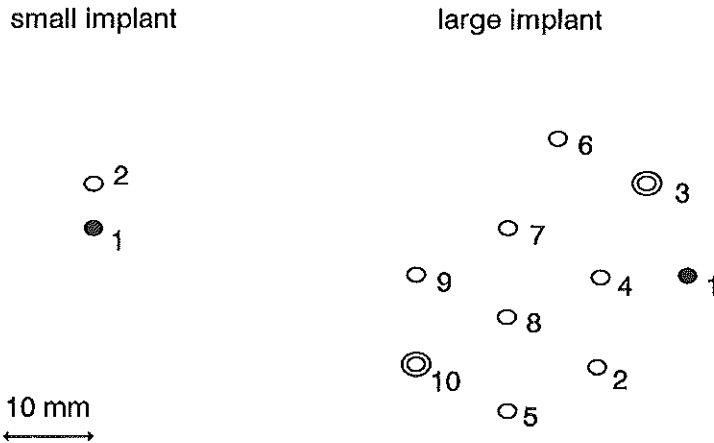


Figure 1. Top view of two brain implants. a) small implant with 2 catheters. b) large implant with 10 catheters. The closed circles denote catheters used for thermometry only and the double circles represent catheters inserted through a hollow titanium screw.

3. Results

Figure 2 displays the electrode temperatures as a function of the time after the power of all electrodes was switched off (t_{Poff}). For the large implant (section b) the steepest and the most gradual decay are shown, which were found in the skull-side-electrode in catheter 3 and in the tip-electrode in catheter 8 respectively. In addition, the edge temperatures measured in the thermometry catheters are shown. In general, a faster temperature decrease was found in the electrodes which were closest to the skull and in those at the edge of the

implant. Because the automatic control algorithm uses the last measured temperature of each control cycle, the maximum electrode temperatures, i.e. at $t_{\text{poff}} = 0$ s, obtained through extrapolation of the curves, vary per electrode and are higher in the skull-side and edge-side electrodes. In case of the small implant, the temperature measured in the electrodes at $t_{\text{poff}} = 9.5$ s, had to be 44°C to reach the wanted 40°C at the edge of the target volume. For the large implant a target temperature of 45°C , in this case measured at $t_{\text{poff}} = 4.5$ s, was needed. The electrode temperatures at $t_{\text{poff}} = 0$ in the small implant were several degrees higher than in the large implant. Furthermore, it can be seen that the electrode temperatures decrease steeply during the first 10 seconds while the temperatures measured in the thermometry catheter do not change at all during a short time of power-off.

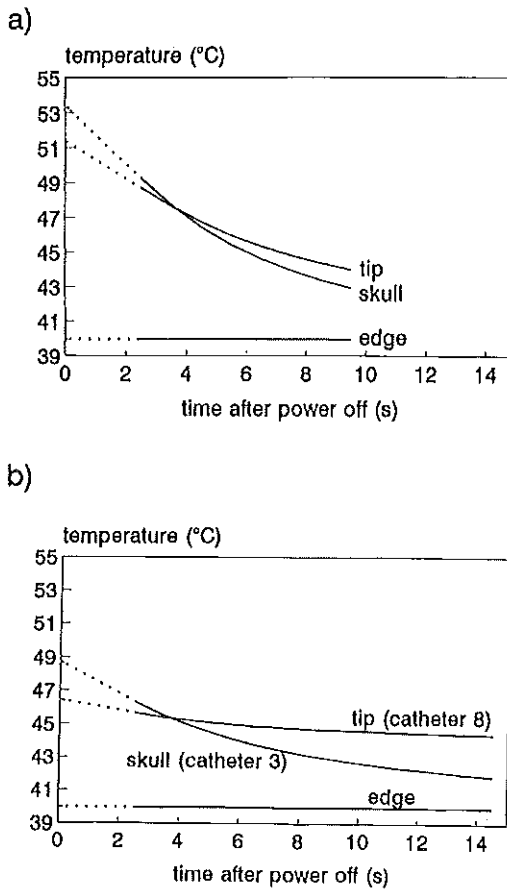


Figure 2. The electrode temperatures as a function of the time after switching off all electrodes. a) The temperatures in the electrodes of the small implant and the edge temperature measured in the thermometry catheter. b) The temperatures in two electrodes of the large implant, i.e. the tip-electrode in catheter 8 and the skull-side electrode in catheter 3 and the edge temperature measured in the thermometry catheter. The curves are extrapolated to $t_{\text{poff}} = 0$ s.

In figure 3 the temperature distributions along the catheters are shown. For the small implant, the distributions, 2.5 s and 9.5 s after switching off both electrodes, is displayed (fig.3a) and for the large implant t_{poff} was 14.5 s (fig. 3b). Figure 3a shows that the temperature inhomogeneity along the applicator which is still present at $t_{\text{poff}} = 2.5$ s almost has disappeared at $t_{\text{poff}} = 9.5$ s. The temperature distribution along the thermometry catheter does not change at all during the first 9.5 s. The vertical stripes in figure 3 correspond with the positions where each catheter crosses the edges of the target volume. Looking at the temperatures at these positions it is clear that at $t_{\text{poff}} = 14.5$ s most parts of the large target volume have been at a temperature between 40 and 45 °C. There are only two exceptions which are found in the catheters 3 and 10 near the skull. These are the catheters inserted via the metal screws used for fixation of the implantation template. These screws provide a relatively high thermal conduction along the catheter causing an underestimation of the temperatures near the screws at $t_{\text{poff}} = 14.5$ s.

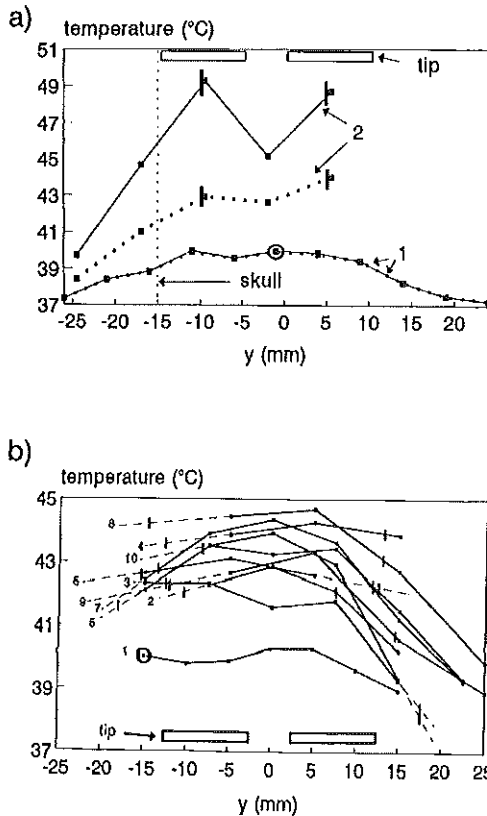


Figure 3. The temperature distributions along the catheters. a) The small implant, $t_{\text{poff}} = 2.5$ s (solid lines) and $t_{\text{poff}} = 9.5$ s (dotted lines). b) The large implant, $t_{\text{poff}} = 14.5$ s. The encircled points give the temperatures measured in the thermometry catheter at the edge of the target volume, the vertical marks indicate the edges of the target volume for each catheter. Furthermore the numbers correspond with the catheter numbers in figure 1.

During the large-implant treatment occasionally an applicator, i.e. consisting of two electrodes, was turned off for a longer period of time to obtain more information about the temperature of a larger area around one of the applicators. In figure 4 the temperature decrease during multiple control cycles is shown for two situations. In section a) the applicator in the central catheter 8 was turned of and in section b) this was done for the applicator in catheter 9 which is located at the edge opposite to the edge of the thermometry catheter 1. To keep the figures clear only the temperatures measured in the electrodes close to the skull in the catheters 8 and 9 and at the edge in the thermometry catheter are given and only the last measured temperature per control cycle is shown. The electrode temperatures at $t_{\text{Poff}} = 0$ are different in both sections, because the target temperature for the electrodes were not the same i.e, 45°C and 44°C in the figures 4a and 4b respectively. Figure 4 demonstrates that the central region of the target volume has been at least 44°C. Furthermore it can be seen that the temperature in catheter 9 remains fairly stable after about 60 s and still above 41°C.

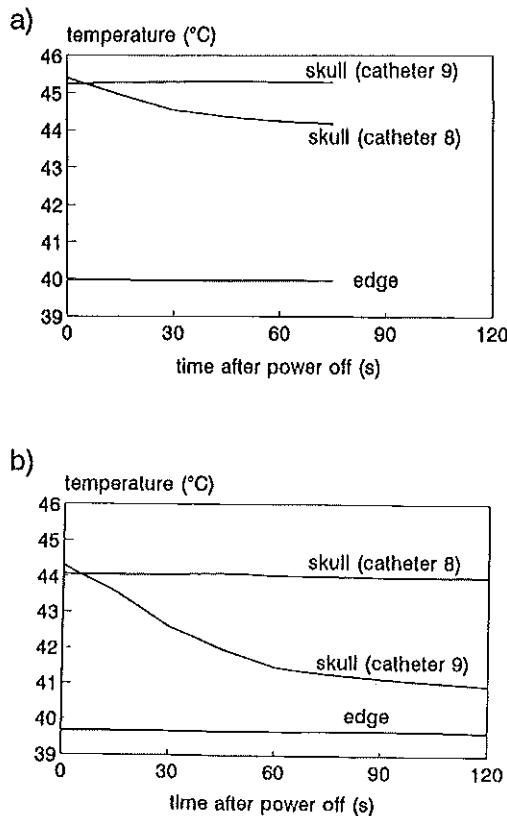


Figure 4. Temperature decrease in the electrodes close to the skull in the catheters 8 and 9 and at the edge in the thermometry catheter 1, after one applicator was turned off for 1-2 minutes. a) the applicator in catheter 8 was turned off b) The applicator in catheter 9 was turned off.

The measurements presented in figure 4 could be reproduced through model calculations using a blood flow 23.5 ml/100g tissue/min. This is illustrated in figure 5b which corresponds with the results in figure 4b. Figure 5a shows the steady state temperature distribution in a plane through the skull-side electrodes, perpendicular to the afterloading catheters. The electrode target temperature was 44°C. Local cold spots between the catheters are not below 40°C. Furthermore, it can be seen that at all edges of the target volume, i.e. convex hull around and at 5 mm distance of the electrodes, the temperature has been above 40°C.

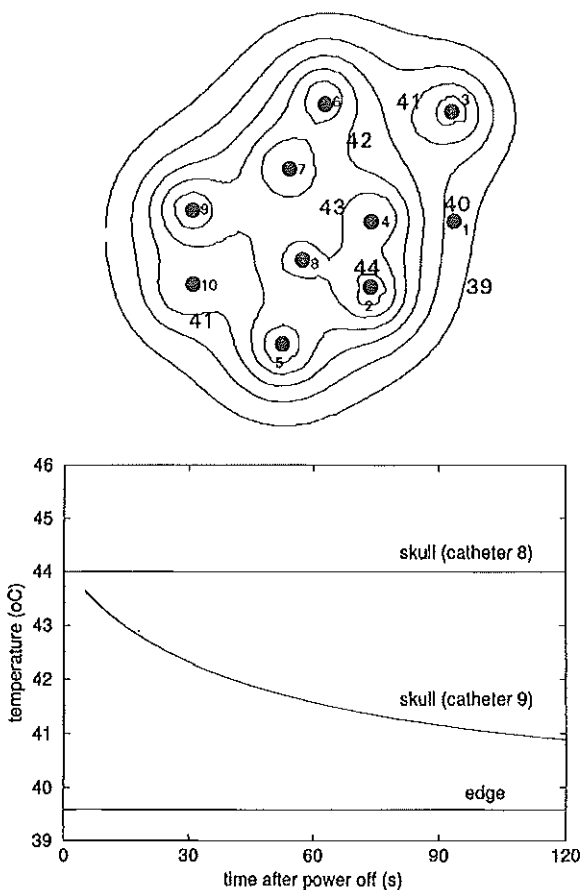


Figure 5. a) calculated steady-state temperature distribution in a plane across the skull-side electrodes perpendicular to the afterloading catheters. b) Calculated temperature decay in the skull-side electrode in afterloading catheter 9, after the electrodes in this catheter were switched off.

4. Discussion

It is clear that temperature measurements in interstitial hyperthermia require a critical interpretation. This is mainly due to the characteristic temperature distribution with hot spots around the applicators. Therefore, knowledge about temperatures inside applicators during heating is not sufficient to decide whether the treatment quality is good. Applicator temperatures are a poor measure for minimum temperature in the target volume (T_{\min}), and in case of the MECS-system the maximum tissue temperature just outside the afterloading catheters (T_{\max}) is overestimated, due to energy absorption in the applicator and in the afterloading catheter (Van der Koijk *et al.* 1997a). Regarding treatment safety, it is an advantage that the tissue temperature is never higher than the temperature in the electrodes ($T_{\text{electrode}}$). By measuring the temperature after switching off power, no RF filtering of the thermocouple signals is needed and a better estimation of the maximum tissue temperature can be achieved. The interval between power-off and measurement must be at least 1-2 seconds to allow the electromagnetic disturbance of the thermometry system to disappear, and just long enough to let the $T_{\text{electrode}}$ decrease to the value of T_{\max} at the moment power was switched off. The interval depends on the applicator type and on the afterloading catheter properties and dimensions. A rough estimate can be obtained using the diffusion time of heat conduction obtained from the one-dimensional differential heat equation:

$$\tau = \frac{\rho c r^2}{4k} \quad (1)$$

For a distance between thermometer and tissue: $r = 10^{-3}$ m and for a medium in between with a density: $\rho = 1500$ kg m⁻³, an effective heat conductivity: $k = 0.25$ W m⁻¹ °C⁻¹ and a specific heat coefficient: $c = 1500$ J Kg⁻¹ °C⁻¹, this diffusion time is about 2 s. Furthermore the presence of air layers between thermometer and tissue, power absorption in the afterloading catheter and thermal conduction along the applicator will affect τ .

If the required power-off interval is measured in an agar muscle-equivalent phantom, using the applicator and afterloading catheter which are also used for IHT in the brain, it takes 5-6 s before $T_{\text{electrode}}$ is equal to T_{\max} at the moment the power was switched off (data not shown).

However, in clinical practice the actual waiting time needed also depends on the temperature gradient in the tissue near the electrode and thus on factors like the presence of neighbouring electrodes, the electrode spacing and the thermal properties of the tissue. Because of these remaining uncertainties and regarding the steep gradients in figure 2 (typically 1 °C/s) electrode temperatures measured 5 s after power-off are only a rough estimate of T_{\max} .

It could be questioned if the knowledge of the actual hot spot temperatures is really important for the quality of the treatment. The main goal of

hyperthermia is to reach a certain minimum temperature elevation in the whole target volume. Therefore, a practical approach for treatment control is to choose a somewhat arbitrary power-off time and adjust the last measured electrode temperatures until the wanted T_{\min} is reached, without looking at the actual electrode temperatures. However, this requires information about the minimum tissue temperature. Measurement of temperatures in extra thermometry catheters can provide this information but due to patient tolerance and the risks associated with implanting additional catheters such measurements are generally very limited. Under certain restrictions it might be sufficient to measure only the temperature at, or just outside the edge of the tumour, at one position, and use this value to set the temperature for all electrodes. This is only allowed if the measured edge temperature can be assumed to be the minimum temperature in the target volume. Therefore the tissue must be reasonably homogeneous regarding the perfusion and electrical properties and the electrodes must lay within the target volume. Furthermore, the distance between the edge sensor and the nearest electrode must be at least half of the largest distance between neighbouring electrodes to ensure that the local minima between the applicators are not lower than the measured edge temperature. Even if these conditions are met it is recommended to stop periodically the heating in one of the afterloading catheters to investigate the local minimum tissue temperature in other parts of the target volume. The power-off time required to obtain reliable information about T_{\min} depends on the spacing between the catheters and the blood perfusion. At present, estimation of the required waiting time by model calculations during the treatment is too time-consuming. A practical method to estimate T_{\min} is to wait until the measured temperature decay curves (figure 4) are largely levelled off. This method appears to be reliable in a homogeneous medium as is demonstrated in figure 5. It is obvious that for the small implant T_{\min} can not be determined this way. In this case either an extra thermometry catheter or sufficient data of previous treatments from which electrode temperature decay information could be derived are needed.

Model calculation results, which use the electrode temperatures as input data, should be examined with care. Accurate modelling of self-heating of the applicators and the afterloading catheters is difficult. The power absorption inside the electrodes was omitted completely in the presented model calculations and therefore the calculated temperature inside the electrodes was underestimated. For the estimation of the average blood perfusion rate, the temperatures in the central electrode-voxel and its direct neighbour voxels were averaged. The target for this mean electrode temperature was set at the same value as the clinical electrode target temperature 4.5 s after power-off. Despite the uncertainties about the temperatures close to the electrodes, the calculated and measured long term (60-120 s) temperature decays can be brought in close agreement with each other by varying only the blood perfusion rate in the thermal model (see figures 4b and 5b).

Although the computations give a good idea about the temperature of electrode spacing related cold spots, colder regions induced by larger vessels

remain invisible. The effects of discrete vasculature on the temperature distribution can be studied with the present thermal models (Kotte *et al*, 1996) but it is not easy to obtain the required vessel data, e.g. by phase contrast magnetic resonance angiography. More information about spatial variations of blood flow can be obtained if the long term decay method is used to estimate blood perfusion rates per electrode region. Although modelling calculation has its limitations it gives additional information which can improve both treatment control and treatment evaluation methods.

Regarding the performance of the MECS-IHT system, it can be said that it is feasible to reach a minimum temperature of 40°C in both small and large target volumes. In the centre of the large implant the temperature was about 44°C (figure 4) except of small local hot spots near the electrodes of less than 50°C (figure 2b). To reach the desired minimum temperature of 40°C in the small implant the electrode temperatures had to be several degrees higher (figure 2a). In figure 3a was shown that at $t_{\text{Poff}} = 9.5$ s the applicator temperature was decreased to about 43°C while the temperature at 5mm distance had not changed at all. According to equation 1 and table 1, a time of 9.5 s corresponds with a radial diffusion of about 2 mm. This demonstrates that the high temperatures are limited to a small area near the electrodes.

Acknowledgements

This study was supported by the Dutch Cancer Society and by Nucletron Corporation Veenendaal. Furthermore, the authors want to thank I.K.K. Kolkman-Deurloo for supplying the catheter coordinates needed for the model calculations.

References

- COMAC BME task group report of the European Society for Hyperthermic Oncology (1992): Treatment planning and modelling in hyperthermia
- Crezee J and Lagendijk JJW, 1990, Measurements of temperature profiles around large artificial vessels in perfused tissue. *Physics in Medicine and Biology* 35: 905-923.
- De Bree J, Van der Koijk JF and Lagendijk JJW, 1996, A 3D SAR model for current source interstitial hyperthermia. *IEEE Transactions on Biomedical Engineering* 43: 1038-1045.
- De Leeuw AAC, Crezee J and Lagendijk JJW, 1993, Temperature and SAR measurements in deep-body hyperthermia with thermocouple thermometry. *International Journal of Hyperthermia* 9: 685-697.
- DeFord JA, Babbs CF, Patel UH, Bleyer MW, Marchosky JA and Moran CJ, 1991, Effective estimation and computer control of minimum tumour temperature during conductive interstitial hyperthermia. *International Journal of Hyperthermia* 7: 441-453.
- Deurloo IKK, Visser AG, Morawska-Kaczynska M, Van Geel CAJF, Van Rhooen GC and Levendag PC, 1991, Application of a capacitive coupling interstitial hyperthermia system at 27 MHz; study of different applicator configurations. *Physics in Medicine and Biology* 36: 119-132.

Emami B, Stauffer PR, Dewhirst MW, Prionas S, Ryan TP, Corry PM, Herman TS, Kapp DS, Myerson RJ, Samulski TV, Sapareto SA, Sapozink MD, Shrivastava PN and Waterman FM, 1991, RTOG quality assurance guidelines for interstitial hyperthermia. *International Journal of Radiation Oncology, Biology, Physics* 20: 1117-1124.

Erb J and Seegenschmiedt MH, 1995, Appendix: Tabulation of parameters for hyperthermic data evaluation. In: *Thermoradiotherapy and Thermochemotherapy, Volume 2*. MH Seegenschmiedt, P Fessenden and CC Vernon (Berlin, Heidelberg: Springer-Verlag), pp 395-403.

Kaatee RSJP, Kampmeijer AG, Van Hooije CMC, Van Rhoon GC, Kanis AP, Levendag PC and Visser AG, 1995, A 27 MHz current source interstitial hyperthermia system for small animals. *International Journal of Hyperthermia* 11: 785-796.

Kaatee RSJP, Crezee J, Kanis AP, Lagendijk JJW, Levendag PC and Visser AG, 1997a, Spatial temperature control with a 27 MHz current source interstitial hyperthermia system. *International Journal of Radiation Oncology, Biology, Physics* 37: 189-197.

Kaatee RSJP, Crezee J, Kanis AP, Lagendijk JJW, Levendag PC and Visser AG, 1997b, Design of applicators for a 27 MHz multi-electrode current source interstitial hyperthermia system: impedance matching and effective power. *Physics in Medicine and Biology* 42: 1087-1108.

Kotte ANTJ, De Bree J, Van der Koijk JF and Lagendijk JJW, 1996, Thermal model for hyperthermia treatment planning incorporating geometrical vessel description. In: *Quantitative Imaging in Oncology*. K Faulker, B Carey, A Crellin and RM Harrison (London: British Institute of Radiology), pp 87-89.

Lagendijk JJW, Van der Koijk JF, Visser AG, Kaatee RSJP, Crezee J, De Bree J, Kotte ANTJ, Kanis AP, Levendag PC and Battermann JJ, 1994, Dose uniformity with the 27 MHz multi-electrode current source interstitial hyperthermia method. In: *Brachytherapy Review. Proceedings German Brachytherapy Conference, Freiburg, November 1994. Freiburg Oncology Series, Monograph No. 1*. G Bruggmoser and RF Mould (Freiburg: Albert-Ludwigs-University Freiburg FRG), pp 38-44.

Lagendijk JJW, Visser AG, Kaatee RSJP, Crezee J, Van der Koijk JF, De Bree J, Kotte ANTJ, Kanis AP, Levendag PC and Battermann JJ, 1995, The 27 MHz current source multi-electrode interstitial hyperthermia method. *Nucletron-Oldelft Activity Report* 6: 83-90.

Levendag PC, Kaatee RSJP, Visser AG, Kolkman-Deurloo IKK, Van Rhoon GC, Meeuwis CA, Van Geel CAJF and Van Hooije CMC, 1993, Interstitial radiation and/or interstitial hyperthermia for advanced and/or recurrent cancers in the head and neck: a pilot study. In: *Interstitial and Intracavitary Thermoradiotherapy*. MH Seegenschmiedt and R Sauer (Berlin, Heidelberg: Springer-Verlag), pp 233-239.

Marchal C, Nadi M, Hoffstetter S, Bey P, Pernot M and Prieur G, 1989, Practical interstitial method of heating at 27.12 MHz. *International Journal of Hyperthermia* 4: 451-466.

Newman WH, Lele PP and Bowman HF, 1990, Limitations and significance of thermal washout data obtained during microwave and ultrasound hyperthermia. *International Journal of Hyperthermia* 6: 771-784.

Pennes HH, 1948, Analysis of tissue and arterial blood temperatures in the resting human forearm. *Journal of Applied Physiology* 1: 93-122.

Van der Koijk JF, Crezee J, Van Leeuwen GMJ, Battermann JJ and Lagendijk JJW, 1996, Dose uniformity in MECS interstitial hyperthermia: the impact of longitudinal control in model anatomies. *Physics in Medicine and Biology* 41: 429-444.

Van der Koijk JF, Crezee J and Lagendijk JJW, 1997a, Thermal properties of capacitively coupled electrodes in interstitial hyperthermia. *Physics in Medicine and Biology*, Submitted.

Van der Koijk JF, De Bree J, Crezee J and Lagendijk JJW, 1997b, Numerical analysis of capacitively coupled electrodes for interstitial hyperthermia. *International Journal of Hyperthermia*, submitted.

Visser AG, Deurloo IKK, Levendag PC, Ruifrok ACC, Cornet B and Van Rhoon GC, 1989, An interstitial hyperthermia system at 27 MHz. *International Journal of Hyperthermia* 5: 265-276.

Summary and general discussion

1. Introduction

Hyperthermia is a cancer therapy, which is normally applied in combination with other treatment modalities such as radiotherapy or chemotherapy. The aim of hyperthermia is to increase tumour temperatures to 40-45°C. The rationale for hyperthermia is that it improves the effectiveness of the combined therapy, without increasing the toxicity. A number of randomised trials have demonstrated the effectiveness of hyperthermia, especially in combination with radiotherapy.

A heating technique which has been developed to be combined with interstitial radiotherapy (IRT) is interstitial hyperthermia (IHT). In IHT, the heating applicators are placed inside the target volume. The development of the 27 MHz current-source interstitial heating method started in the middle eighties. In a collaboration between the University Hospital Utrecht and the Daniel den Hoed Cancer Center in Rotterdam, the multi-electrode current-source (MECS) IHT system has been developed. Basically, this system consists of three units. Firstly, the actual heating system, including a 27 MHz electromagnetic power unit and multi-electrode applicators. Secondly, a 196-channel thermometry system with 7-point manganin-constantan thermocouple thermometers. Thirdly, a computer plus treatment control software which provides the connection between the first two units and the operator. The applicators, consisting of one or more electrodes, can be inserted in the same plastic catheters which are implanted in the target volume, for afterloading IRT. Because the impedance of the catheter wall compared with the tissue impedance is relatively high, the electrodes behave like current sources. The power unit has 2 groups of 32 channels with opposite phase. The power can be controlled separately for each channel. Current flows from the electrodes with one phase, to the electrodes with a phase shift of 180° and is dissipated

in the tissue. The actual temperature rise is measured with thermocouple probes inside applicators or inside extra non-heating catheters. The main advantage of interstitial treatment is that locally a high dose can be delivered while the surrounding normal tissue is spared. For adequate heating of the target volume a sufficiently high power absorption density in the tissue and good spatial temperature control are the major requirements.

In this study, which was supported by the Dutch Cancer Society, the performance of the MECS-IHT system was examined, focusing on the efficiency of the power deposition in tissue and on the homogeneity of the temperature distribution. Furthermore the system was introduced in the clinic and a current-source IHT system for small animals has been developed.

2. An interstitial hyperthermia system for small animals

To study the effectiveness of interstitial hyperthermia in combination with interstitial radiotherapy in tumours growing in the flank of a rat, a 4 channel version of a current-source IHT-system has been developed. The heating system consists of four single-electrode applicators each with independent impedance tuning and connected to four 27 MHz generators. Current flows from the electrodes to an external ground plane underneath the rat. Temperatures are measured with single-point thermocouple probes inside each electrode and with an extra 7-point thermocouple thermometer perpendicular to the electrodes. RF-filters, constructed with ferrite toroids, enable continuous temperature measurement, which is not disturbed by the 27 MHz electromagnetic field.

This system has been used to treat various solid tumours with volumes in the range 1500-2000 mm³. Temperatures up to 46 °C at the edges of the tumour, which can be seen as the minimum temperatures are easily reached within 4-10 minutes. The clear display of the temperatures and the limited number of electrodes make it feasible to control the minimum temperature within $\pm 0.5^{\circ}\text{C}$ during a treatment period up to 2 hours, by manual power steering.

3. Efficiency of the power deposition in the tissue

An important requirement for reaching a certain temperature elevation is that the power, actually delivered to the tissue, is sufficiently high. To check this for the MECS system, firstly, the required power absorption density for different situations was approximated through model calculations and secondly, the efficiency of the energy transport from generator to tissue was investigated.

Using a simple spherical tumour model, an estimation of the power absorption density, needed to reach a certain minimum temperature, can be calculated as a function of the tumour size, the electrode density and the effective heat

conductivity coefficient (k_{eff}) of the tissue. Electrodes with a length of 2 cm, inserted in afterloading catheters, with a spacing of 1.5 cm, are representative for clinical practice. In this situation, the effective power per electrode (P_{eff}), needed to reach a temperature of 43°C at the edge of a well perfused tumour ($k_{\text{eff}} = 3 \text{ Wm}^{-1} \text{ }^\circ\text{C}^{-1}$) with a diameter of 4 cm is about 0.5 W. Because the generator power is 5 W per heating channel, the efficiency of the energy transport in this situation must be at least 10%, if each electrode is connected to one heating channel.

The heating efficiency is mainly determined by the method used to match the electrode impedance with the impedance of the generator. This impedance matching is necessary to minimise power reflection. In the MECS-IHT system the impedance of the applicator placed in the tissue is transformed to 800 Ω by adjusting the length of the transmission line between applicator and generator. For fine tuning, a small inductance or capacitor can be added to the applicator. The maximum efficiency, utilising this matching procedure, is in the range 35-45%, depending on the exact applicator impedance. The remaining generator power is absorbed in the transmission line. In practice, the effective power is reduced further due to applicator losses. Depending on applicator design and electrical properties of the tissue the applicator efficiency is 60-70%. This gives an overall efficiency of 20-30%. Measurements in saline phantoms with properly-matched 2cm-electrodes show that the effective power per electrode is typically 1 W, corresponding with an efficiency of 20%, which is in agreement with the model predictions. For most practical situations this is sufficient.

4. System features affecting the temperature homogeneity

An important advantage of IHT is the possibility of three dimensional spatial control of the power deposition on a cm-scale, due to the high density of applicators and thermometers inside the target volume. This enables sparing of normal tissue and compensation for spatial variation in tissue cooling, caused by the heterogeneity of blood perfusion and the thermal properties of the tissue. On the other hand, the power absorption distribution on a mm-scale is heterogeneous: Most of the energy is absorbed near the applicators and this fact may result in large differences between maximum and minimum temperatures in the target volume. Therefore, in case of IHT, treatment planning and treatment control are even more important than they are for external heating methods.

First of all, the quality of the temperature distribution depends on the geometry of the afterloading catheters. If the distance between the catheters increases, the temperature heterogeneity also rapidly increases. For the current source heating method a spacing of maximally 15 mm appears to be acceptable. In general, this maximum is considered sufficiently large, especially because catheter distances exceeding 15 mm, are also in interstitial radiotherapy in many cases regarded as inadequate.

An advantage of the capacitive coupling between the electrodes and the tissue is that the electrodes act as current sources. Because the catheter wall impedance is high compared to the tissue impedance, the current injection is homogeneous along the electrode independently of the electrode length and the electrode placement relatively to the other electrodes. This makes the current source heating method suitable for irregular implants, i.e. nonparallel and/or curved catheters. Furthermore, length and position of the heated area along a afterloading catheter can be chosen freely. However, it should be noticed that homogeneous heating along an electrode is only possible if the properties of the surrounding tissue are homogeneous too.

Short electrodes should be used for an optimal spatial control of the power deposition and to avoid electrode placement over tissue boundaries. Furthermore, because the variations in blood perfusion are three-dimensional, longitudinal power control, i.e. using several electrodes in one catheter, is required. At the moment dual-electrode applicators, with 10 mm long electrodes separated by 5 mm, are frequently used in clinical practice. A high electrode density implies a large number of electrodes of which the power has to be controlled independently. Manual control, is inconvenient and could even be dangerous. Therefore a simple but adequate control algorithm has been developed to control the temperatures measured inside the electrodes automatically.

The power absorption distribution depends not only on the magnitude of the electrode powers but on the power phase configuration as well. The absorption pattern in the tissue can be changed considerably, if the phase of some of the electrodes is altered. To exploit the features of the MECS-IHT maximally in order to improve the homogeneity of the temperature distribution, treatment planning is essential. For this purpose, software is available to calculate the power absorption and the resulting temperature distribution for a certain electrode configuration, if the electrical and thermal tissue properties are known.

5. Thermometry

An IHT temperature distribution depends on the position, power and phase of the electrodes and the thermal properties of the tissue. In general, the temperatures measured inside the electrodes are considered to be maximum tissue temperatures while the minimum temperatures are expected to be located in between the afterloading catheters and at the edge of the implanted volume. Information about the latter can be obtained either through implanting extra catheters for thermometry only or from decay characteristics of the applicator temperatures after switching off the power.

Regarding the accuracy of thermocouple thermometry in MECS-IHT, there are two main reasons for measurements errors (i.e. the difference between the temperature reading and the tissue temperature at the position of interest): 1) the presence of the 27 MHz electromagnetic field and 2) the fact that the

thermometers are not in direct contact with the tissue.

The high capacitive coupling between thermocouple probes and heating applicator (1-5 pF) induces 27 MHz current in the thermocouple leads, resulting in disturbance of the thermocouple-voltage reading and causing measurement errors due to self heating of the thermometer. Undisturbed measurement is possible with specially designed 7-channel RF-filters or by interrupting the RF-power for at least 2 s.

Furthermore, the thermal resistance between a thermocouple probe and the tissue, caused by layers of plastic and air in between, can induce measurement errors if there is a temperature gradient along the afterloading catheter. In IHT, high temperature gradients of 1-2 °C/mm are not exceptional. Measurement errors made with manganin-constantan thermocouple probes in standard afterloading catheters are comparable with those induced by a 0.5 mm shift of the probe. This is considered to be acceptable, especially because the uncertainty about the exact sensor position relative to the target volume is generally larger (≥ 1 mm).

The differences between the temperatures measured inside an applicator (T_{in}) and the tissue temperature just outside the afterloading catheter (T_{out}) are considerably larger, due to energy dissipation in the applicator and the catheter wall. Using clinical dual-electrode applicators in standard brachytherapy catheters, ΔT_{in} is typically twice as high as ΔT_{out} . A one-dimensional cylindrical model was used to compute this artefact as a function of the dielectric properties of the afterloading catheter material, the power fraction absorbed in the applicator and the thermal properties of the surrounding tissue. The model gives a good qualitative understanding of the measurement error, regarding applicator temperatures. However, extension of the model to three dimensions is required, for an accurate calculation of the artefact in clinical situations. A method to estimate the maximum tissue temperature is to study the temperature decay inside the applicator, after switching off the power. In an agar muscle equivalent phantom, about 5 s after the power is switched off, T_{in} in the electrodes represents the maximum tissue temperature just before the power was switched off.

6. Clinical thermometry, during MECS-IHT in brain tumours

In the Daniel den Hoed Cancer Center 7 patients with high grade (III/IV) gliomas have been treated with IHT as adjuvant to pulsed-dose-rate interstitial radiotherapy (PDR). Three heat fractions of about 2 hours were given between the four PDR-fractions on the first full day of irradiation. The target volumes (diameter:1-4 cm) were heated with 1 up to 9 dual-electrode applicators (electrode length: 1 cm) inserted in low-loss nylon afterloading catheters. The distance between the catheters was about 1 cm. The power was interrupted to measure temperatures. 7-point manganin-constantan thermocouple probes were inserted inside each applicator and, if present, in an extra afterloading catheter. The temperatures measured inside the electrodes were controlled

automatically at a certain target value. This electrode target temperature was increased until the required minimum tissue temperature of 40 °C was reached. Two methods were used to estimate the minimum tissue temperature. Firstly through direct measurement with a sensor in an thermometry catheter close to the edge of the target volume. Secondly, by switching off the electrodes of one of the applicators. About 1 minute after switching off the power the temperatures measured inside the applicator give an impression of the local minimum temperature of the surrounding tissue. The heating efficiency of the applicators was sufficient to reach the required minimum temperature of 40 °C . The homogeneity of the temperature distributions in the tissue was acceptable. The temperature of most of the target volume was in the range 40-43 °C. Hot spots with temperatures up to 46 °C were found in a small area around the electrodes.

7. Future developments and discussion

Using the MECS-IHT system, with distances between afterloading catheters of about 1 cm, brain tissue can be heated sufficiently, i.e. the required minimum temperature of 40°C can be reached. However, there are situations thinkable, in which adequate heating becomes more difficult, such as a higher target value for the minimum temperature, a decreased power absorption density or a larger heat transport in the tissue. For example, the power absorption density decreases if the afterloading catheters are implanted with larger spacing. Distances of 1.5 cm or even more are not exceptional for implants in the base of the tongue. Another factor which may lead to a shortage of power deposition in some parts of the target volume is heat induced pain. This problem can not be solved through a higher generator power or a larger heating efficiency. The only way to prevent pain is to keep the maximum tissue temperature sufficiently low. For example, in the tongue region, temperatures up to 45°C appear to be tolerable. This means that for higher minimum temperatures, the temperature distribution has to be more homogeneous. With respect to this requirement the MECS-IHT system is quite competitive with other IHT-systems. The energy deposition directly in the tissue at some distance of the afterloading catheter is an advantage over so called hot source systems (ferromagnetic seeds, hot water, electrical resistive applicators). Furthermore the heated region along the afterloading catheter is less dependant on factors as applicator size, insertion depth and catheter geometry and therefore can be chosen more freely than in case of IHT using microwave applicators or galvanically coupled RF-electrodes. Nevertheless the homogeneity obtained with the MECS-system can be improved further. This can be achieved by increasing the electrode density either through smaller distances between the afterloading catheters or by decreasing the length of the electrodes. At present dual-electrode applicators with 0.5 cm long electrodes and applicators with four electrodes are being tested. Furthermore, the power absorption and thus the temperature

distribution becomes less heterogeneous if less absorbing afterloading catheter materials, such as teflon or polythene are used and/or if the electrodes are connected in a such a way that, as much as possible, the power phase of neighbouring electrodes is different. The latter improves the homogeneity of the current density distribution. In addition it might be considered to increase the catheter diameter (power absorption is proportional to $1/r^2$) or to cool the applicators with water or air in order to reduce the hot spots near the electrodes. Most methods to improve the homogeneity have the disadvantage of decreasing the effective power absorption density. Increasing the number of afterloading catheters is the only way to improve both the magnitude and the spatial distribution of the power absorption density, but it is often considered less desirable, regarding patient tolerance.

The effective power per electrode can be enlarged by increasing either the input power or the heating efficiency. The first option can be achieved through connecting each electrode to more than one heating channel. It is obvious that this reduces the number of electrodes that can be used and thus reduces the maximum target volume that can be treated and/or the homogeneity of the temperature distribution. Furthermore, modification of applicator and fine-tuning elements can improve the heating efficiency but this gain is expected to be marginal. A more significant improvement of the heating efficiency may be achieved if a different impedance match technique is used. For example if the applicator impedance is transformed to 200 instead of 800 ohm the efficiency would increase with about a factor 2. However, it should be added that an impedance transformation to 200 ohm will be more sensitive for variations in the impedance of the applicator and the tissue. Furthermore the inductance, added to the applicator for fine tuning, will be larger and therefore more energy absorbing.

Although in some situations a power deficiency may occur using the present MECS-system, there are no fundamental limitations on the number of heating channels and the input power per channel. Therefore, from a technical point of view, there are no restrictions on the target volume and the power density in the tissue.

The research described in this thesis focused on the quality of the temperature distribution. Future studies may concentrate more on dose-effect relations. Generally, hyperthermia is more effective if it is given simultaneously with radiotherapy. In this respect, it would be interesting to integrate the MECS-applicators and the afterloading catheters, leaving a lumen for the radioactive sources. In addition the measurements of the maximum tissue temperatures can be improved if thermocouple probes are placed at the outer wall of these MECS-catheters.

At this moment, the quality of MECS-IHT can be improved furthermore through a number of technical and procedural changes. On the other hand, these modifications are in many situations not strictly required for adequate heating. Therefore, it can only be justified to put more efforts in further development, if there are sufficient clinical indications for IHT and will be in the future.

In general, IHT is considered a treatment option in the first place if IRT is part

of the standard treatment and secondly, if the effect of the standard treatment is expected to be insufficient (e.g. less than 60-70% local control of disease). Implantation of catheters only for IHT or addition of IHT to reduce the IRT dose in order to minimize radiation side-effects are possible treatment modalities but these options are not yet widely accepted as long as IHT is an experimental treatment. The only way to determine whether or not IHT in combination with radiotherapy is effective, is through a randomized trial. Therefore the third requirement for IHT should be that it can be evaluated in a randomized study. The main problem in this respect is that the incidence of cases obeying the first two requirements is often too low to obtain a meaningful answer in a reasonable time. Depending on the actual benefit of IHT, the number of patients needed for a statistically significant result varies from several tens to several hundreds. In the Daniel den Hoed Cancer Center, the incidence of possible indications such as high grade (III/IV) gliomas, (0% local control) and large (T3/T4) tumours in the base of the tongue (about 30% local control) are 0-5 and 5-10 patients per year respectively. However, this is not a unique problem in oncology and is generally approached, through a multi-centre study.

At present, the good results of recent randomized hyperthermia trials and the good heating performance of the MECS-IHT system in brain applications should encourage new randomized IHT-trials and further improvement of the MECS-IHT treatments.

Samenvatting en discussie

1. Inleiding

Hyperthermie is één van de behandelingsmethodes van kanker. Hierbij wordt gestreefd naar een verhoging van de temperatuur in de tumor tot 40-45°C. In het algemeen wordt hyperthermie toegepast in combinatie met één of meer andere therapieën zoals radiotherapie of chemotherapie. Hyperthermie op zich is weinig effectief maar het kan het resultaat van een therapie waar het mee gecombineerd wordt verbeteren zonder toename van de bijwerkingen. Voor een aantal situaties, zoals hyperthermie gecombineerd met radiotherapie bij baarmoederhalskanker, is de effectiviteit van de combinatietherapie aangetoond in studies waarbij d.m.v. loting werd bepaald (randomisatie) of een patiënt radiotherapie met of zonder hyperthermie kreeg.

Interstitiële (van binnen uit) hyperthermie (IHT) is een verwarmingsmethode die speciaal is ontwikkeld voor de combinatie met interstitiële radiotherapie (IRT). Eén van de interstitiële verwarmingstechnieken is de 27 MHz stroom-bron methode. De ontwikkeling hiervan startte in het midden van de jaren 80. In een samenwerking tussen het Academisch Ziekenhuis Utrecht en de Daniel den Hoed Kliniek in Rotterdam werd het zgn. MECS-IHT systeem ontwikkeld. MECS staat voor "multi-elektrode current-source". Het systeem bestaat grofweg uit drie onderdelen. Ten eerste, het eigenlijke verwarmingssysteem, dat 27 MHz vermogen produceert en via elektrodes op de plaats van bestemming brengt. Ten tweede een 196-kanaals thermometriesysteem en tenslotte nog een computer plus besturingsprogrammatuur die de verbinding vormt tussen de eerste twee onderdelen en de persoon die het MECS-systeem bedient. De elektrodes worden in, in het doelgebied geïmplanteerde kunststof slangetjes (katheters) geschoven, die ook gebruikt kunnen worden om IRT-stralingsbronnen te positioneren. Een IHT-applicator kan bestaan uit één of meerdere elektrodes. Het verwarmingssysteem heeft twee groepen van elk 32 kanalen waarvan de fase tegengesteld is. De 27 MHz-stroom tussen de "plus"-

en "min"-elektrodes wordt, ten gevolge van de weerstand die het ondervindt in het weefsel omgezet in warmte. Omdat de impedantie van een katheterwand relatief groot is vergeleken met de weerstand van het weefsel eromheen, gedragen de elektrodes zich als stroombronnen. De weefseltemperatuur wordt gemeten met behulp van thermokoppel-thermometers in de applicatoren en in niet voor verwarming gebruikte katheters.

Het voordeel van een interstitiële behandeling is dat er in een bepaald doelgebied een hoge dosis kan worden afgegeven terwijl het omringende gezonde weefsel zoveel mogelijk gespaard blijft. De belangrijkste vereisten voor adequate verwarming zijn dat de vermogensafgifte aan het weefsel ten eerste, voldoende is om warmteafvoer, bijvoorbeeld via het bloed, te compenseren en ten tweede, dat deze met een voldoende hoge ruimtelijke resolutie te regelen is, zodat een min of meer homogene temperatuurverdeling bereikt kan worden.

Het hier beschreven onderzoek werd mogelijk gemaakt door de financiële steun van de Nederlandse Kanker Bestrijding (Koningin Wilhelmina Fonds)

De mogelijkheden en beperkingen van het MECS-IHT systeem zijn onderzocht, waarbij de nadruk is gelegd op de effectiviteit van de vermogensafgifte aan het weefsel en op de homogeniteit van de temperatuurverdeling. Verder is het systeem geïntroduceerd in de kliniek en is er een compacte versie ontwikkeld voor IHT bij kleine proefdieren.

2. Een interstitiële hyperthermiesysteem voor kleine dieren

Om het effect van interstitiële hyperthermie gecombineerd met interstitiële radiotherapie op een tumor in de flank van een rat te bestuderen, is een 4-kanaals "current-source" IHT-systeem ontwikkeld. Dit systeem uit 4 verwarmingsmodules bestaande uit een 27 MHz generator, een elektrode en een elektrisch netwerk, dat dient om de impedantie van de elektrode plus rat aan te passen aan die van de generator en zo vermogensreflectie te minimaliseren. De 27 MHz stroom loopt tussen de elektrodes en een uitwendige aardeplaat onder de rat. De temperatuur wordt in iedere elektrode gemeten met een enkelpunts-thermokoppelthermometer en in een 7-punts-thermometer loodrecht op de elektrodes. Dankzij RF-filters, gebaseerd op toroiden om een ferrietkern, is het mogelijk om temperaturen te meten tijdens het verwarmen, zonder verstoring door het 27 MHz elektromagnetische veld. Dit IHT-systeem is gebruikt voor de behandeling van diverse tumoren met volumes van 1500 tot 2000 mm³. De gewenste minimumtemperaturen (44-46°C), gemeten aan de rand van zo'n tumor, werden bereikt binnen 4-10 minuten. Dankzij een duidelijke presentatie van de temperatuurgegevens en het geringe aantal applicatoren is het mogelijk de minimumtemperatuur gedurende ten minste 2 uur binnen $\pm 0.5^\circ\text{C}$ rond de streefwaarde te houden, d.m.v. handmatige regeling van de elektrodevermogens.

3. Effectieve vermogensafgifte aan het weefsel

Een belangrijke voorwaarde voor het bereiken van een bepaalde temperatuurverhoging is dat er voldoende vermogen in het weefsel terecht komt. Om na te gaan of het MECS-systeem aan deze voorwaarde voldoet is eerst een schatting gemaakt van hoeveel vermogen voldoende is. Ten tweede is er gekeken naar de efficiëntie van het energietransport tussen generator en weefsel.

Met behulp van eenvoudig bolvormig tumor model is een schatting gemaakt van het vermogen dat nodig is om een bepaalde minimum temperatuur te bereiken, als een functie van de tumorafmeting, de elektrodedichtheid en de effectieve warmtegeleidingscoëfficiënt (k_{eff}) van het weefsel. Een representatief voorbeeld voor de klinische praktijk is een implantaat met 2 cm lange elektrodes in katheters die 1.5 cm uit elkaar liggen. Om in dit geval een minimum temperatuur te kunnen bereiken aan de rand van een goed doorbloedde ($k_{\text{eff}} = 3 \text{ Wm}^{-1} \text{ }^\circ\text{C}$) tumor met een diameter van 4 cm is een effectief vermogen per elektrode (P_{eff}) nodig van ongeveer 0.5 W. Omdat het generator vermogen per verwarmingskanaal 5 W is, moet, uitgaande van één elektrode per kanaal, de efficiëntie van het energietransport dus minimaal 10% bedragen.

De efficiëntie van het verwarmingssysteem is in hoofdzaak afhankelijk van de methode die wordt gebruikt om de impedantie van een elektrode in het weefsel aan te passen aan die van de generator. Deze impedantieaanpassing is nodig om vermogensreflectie te minimaliseren. In het geval van het MECS-IHT systeem worden de elektrode-impedanties getransformeerd naar ongeveer 800 Ohm door de lengte van de kabel tussen elektrode en generator goed te kiezen. Voor een nauwkeuriger transformatie kan verder nog een kleine spoel of condensator worden toegevoegd aan de elektrode. De maximale efficiëntie die theoretisch op deze manier gehaald kan worden is, afhankelijk van de elektrode impedantie, zo'n 35 tot 45%. Het overige vermogen wordt in de kabel geabsorbeerd. In de praktijk zal het effectieve vermogen echter nog lager zijn door verliezen in de applicator. Afhankelijk van applicator ontwerp en de elektrische eigenschappen van het weefsel eromheen kan berekend worden dat de applicator-efficiëntie tussen de 60 en 70% zal liggen. Dit betekent dus dat de totale efficiëntie van het energietransport 20-30 % bedraagt. Metingen met 2 cm lange elektrodes in een zoutoplossing met spier-equivalente elektrische eigenschappen laten zien dat het effectieve vermogen per elektrode ongeveer 1 W is en de efficiëntie dus ongeveer 20%. Dit komt goed overeen met de berekende verwachte waarde en is voor de meeste praktisch situaties voldoende.

4. MECS-IHT eigenschappen en temperatuurhomogeniteit

Een voordeel van IHT is dat, dankzij het grote aantal applicatoren en thermometers, de vermogensafgifte aan het weefsel geregeld kan worden op een cm-schaal. Dit geeft de mogelijkheid om het gezonde weefsel te sparen en om lokale variaties in warmteafvoer, ten gevolge van de heterogeniteit van doorbloeding en/of thermische eigenschappen van het weefsel, te compenseren.

Daartegenover staat echter dat de energieabsorptie op een mm-schaal in het geval van IHT vrij inhomogeen is. De meeste energie wordt in de eerste millimeters weefsel rond de applicatoren geabsorbeerd, wat kan leiden tot grote verschillen tussen minimum en maximum temperaturen. Daarom zijn een goede temperatuurregeling en behandelingsvoorbereiding voor IHT nog belangrijker dan voor uitwendige verwarmingsmethodes.

De kwaliteit van de temperatuurverdeling hangt ten eerste af van de geometrie van de geïmplanteerde katheters. De temperatuurinhomogeniteit zal snel toenemen als de afstand tussen de katheters groter wordt. Voor de "current source" IHT-methode zijn katheterafstanden tot 15 mm nog acceptabel. Met deze beperking valt in het algemeen goed te leven, omdat ook in het geval van interstitiële radiotherapie afstanden groter dan 15 mm meestal als niet adequaat beschouwd worden.

Een voordeel van de capacatieve koppeling tussen de elektrodes en het weefsel is dat de elektrodes zich gedragen stroombronnen waarvan de stroomdichtheid langs een elektrode min of meer constant is, onafhankelijk van de posities en oriëntaties van de elektrodes ten opzichte van elkaar. Dit wordt veroorzaakt doordat de impedantie van de wand van de katheters relatief groot is vergeleken met de weerstand van het weefsel eromheen en constant is per eenheid van lengte. Dit maakt de "current source" verwarmingsmethode geschikt voor onregelmatige implantaten, dat wil zeggen met niet-parallelle en/of gekromde katheters. Een ander voordeel is dat de lengte en de positie van het verwarmde gebied vrij te kiezen zijn. Er moet echter wel opgemerkt worden dat homogene *verwarming* langs een elektrode alleen mogelijk is als het omringende weefsel langs die elektrode homogeen is.

Voor een goede driedimensionale regeling van de vermogensafgifte aan het weefsel moet, naast een voldoende kleine afstand tussen de katheters, de lengte van de elektrodes beperkt zijn. Dit brengt vaak met zich mee dat er meer dan één elektrode per katheter gebruikt moet worden. Momenteel worden in klinische toepassingen vaak applicatoren met 2 elektrodes van ieder 10 mm lang met een tussenruimte van 5 mm gebruikt. In praktijk betekent dit dat er meestal een groot aantal elektrodes gebruikt worden waarvan het vermogen voor ieder afzonderlijk geregeld moet worden. Handmatige regeling kan in dit geval moeilijk en misschien zelfs gevaarlijk zijn. Daarom is er voor het MECS-systeem een eenvoudige algoritme ontwikkeld waarmee de vermogens automatisch geregeld kunnen worden op basis van in de elektrodes gemeten temperaturen.

De verdeling van de vermogensabsorptie in het weefsel hangt niet alleen af

van de *hoogte* van de elektrodevermogens maar ook van de fase ervan. Een absorptie patroon kan aanzienlijk veranderen als de fase van een aantal van de elektrodes gewijzigd wordt.

Om de eigenschappen van het MECS-IHT systeem goed te kunnen benutten voor het bereiken van een zo homogeen mogelijke temperatuurverdeling is een goede voorbereiding van groot belang. Voor dit doel zijn er computerprogramma's beschikbaar waarmee de vermogensabsorptieverdeling en de resulterende temperatuurverdeling berekend kunnen worden voor een bepaalde elektrode configuratie, mits de elektrische en thermische weefseleigenschappen bekend zijn.

5. Thermometrie

De bereikte temperatuurverdeling hangt af van enerzijds de energieabsorptie, met andere woorden, van de verdeling van elektrodes, hoogte en fase van hun vermogens en elektrische eigenschappen van het weefsel, en anderzijds van de warmteafvoer, ofwel de thermische eigenschappen van het weefsel. De temperaturen gemeten in de elektrodes kunnen in het algemeen gezien worden als maximum weefseltemperaturen terwijl de posities van de temperatuurminima verwacht worden tussen de elektrodes in en aan de rand van het doelgebied. De minimum temperaturen kunnen rechtstreeks gemeten worden door extra katheters te implanteren voor thermometrie of kunnen geschat worden door de temperatuurafval in de applicatoren te bestuderen nadat er één of meer zijn uitgezet.

Wat de nauwkeurigheid van thermokoppel-thermometrie in combinatie met MECS-IHT betreft, zijn er twee hoofdoorzaken voor meetfouten (met een meetfout wordt hier bedoeld dat de afgelezen temperatuur afwijkt van de te meten weefseltemperatuur). Ten eerste, de aanwezigheid van een 27 MHz elektromagnetisch veld en ten tweede, het feit dat de thermometers niet direct contact maken met het weefsel.

De goede capacatieve koppeling tussen thermokoppel-thermometers in een applicator en de elektrodes (1-5 pF) kan een 27 MHz stroom in de thermokoppeldraden veroorzaken die resulteert in een verstoring van de uitlezing van de thermokoppelspanning en het opwarmen van de thermometer. Een ongestoorde meting is mogelijk dankzij speciaal hiervoor ontwikkelde 7-kanaals RF-filters of door het RF-vermogen minstens 2 s te onderbreken.

Meetfouten kunnen ook veroorzaakt worden door de thermische weerstand tussen thermokoppel en weefsel, ten gevolge van de tussenliggende kunststof en luchtlagen, in combinatie met een temperatuurgradiënt langs de katheter. Tijdens IHT zijn hoge temperatuurgradiënten van 1-2°C/mm mogelijk. De meetfout die met manganine-constantaan thermokoppels in een standaard katheter gemaakt wordt is vergelijkbaar met de fout die gemaakt wordt als de thermometer 0.5 mm wordt verschoven. Gezien het feit dat de positioneringsonzekerheid van een thermometer in het doelgebied in het algemeen groter is (≥ 1 mm) zijn deze fouten in de temperatuurmeting acceptabel.

Echter, de verschillen tussen de temperaturen gemeten in een applicator en de te meten weefseltemperaturen net buiten de katheter kunnen aanzienlijk groter zijn. Deze verschillen worden veroorzaakt door energieabsorptie in de applicator en de katheterwand.

In het geval van de applicatoren en katheters die klinisch gebruikt worden is de temperatuurstijging in een applicator ongeveer twee keer zo hoog als die in het weefsel net buiten de katheter. Met behulp van een eendimensionaal cilindrisch model is deze meetfout onderzocht als functie van de diëlectrische eigenschappen van het kathetermateriaal, van de relatieve vermogensabsorptie in de applicator en van de thermische eigenschappen van het omringende weefsel. Met behulp van het model kan slechts een kwalitatieve beschrijving van deze meetfout gegeven worden. Voor een nauwkeurige berekening van de fout in klinische situaties is een uitbreiding van het model naar drie dimensies vereist. Een methode om de maximum weefseltemperatuur te schatten is door de temperatuurafval in een applicator te bestuderen nadat het vermogen is uitgezet. In een spier-equivalent agarfantoom is de temperatuur in de applicator na ongeveer 5 s nadat het vermogen is uitgezet, gelijk aan de maximum weefseltemperatuur net voordat de applicator werd uitgezet.

6. Thermometrie tijdens MECS-IHT bij hersentumoren

In de Daniel den Hoed kliniek zijn 7 patiënten met hooggradige (III/IV) glioma's behandeld met IHT in combinatie met pulsed-dose-rate interstitiële radiotherapie (PDR-IRT). Op de eerste hele bestralingsdag, met 4 IRT-fracties met een interval van drie uur, werden drie warmtefracties van ieder 2 uur gegeven tussen de bestralingen in. De doelvolumes (diameter:1-4 cm) werden verwarmd met 1 tot 9 applicatoren met ieder twee 1 cm lange elektrodes. De applicatoren werden in nylon katheters geschoven die met een onderlinge afstand van ongeveer 1 cm in het doelgebied werden geïmplant. De temperatuur werd gemeten met 7-punts thermokoppel-thermometers in de applicatoren en soms in niet voor verwarming gebruikte katheters. Voor temperatuurmeting werd het vermogen periodiek onderbroken. De temperatuur in de elektrodes werden door middel van een automatische regeling op een ingestelde waarde gehouden. Deze streef temperatuur werd handmatig langzaam verhoogd totdat de gewenste minimum temperatuur van 40°C in het doelgebied was bereikt. Er werden twee methodes gebruikt om deze minimum temperaturen te schatten. Ofwel, door het meten van de temperatuur aan de rand van het doelvolumen in een niet voor verwarming gebruikte katheter. Ofwel door te meten in één van de applicatoren die tijdelijk werd uitgeschakeld. Na ongeveer 1 minuut geeft de applicator temperatuur een goede schatting van de lokale minimum temperatuur. De bereikte temperatuurverdelingen waren vrij homogeen. De temperatuur in het grootste deel van het doelvolumen lag tussen 40 en 43 °C. Lokaal rondom de elektrodes werden temperaturen tot 46°C gevonden.

7. Toekomstige ontwikkelingen en discussie

Met het MECS-IHT systeem en een afstand van 1 cm tussen de katheters kunnen hersentumoren verwarmd worden tot de gewenste minimumtemperatuur van 40°C. Er zijn echter situaties te bedenken waarbij voldoende verwarming een stuk moeilijker wordt. Bijvoorbeeld als er een hogere minimumtemperatuur nodig is, als de vermogensafgifte aan het weefsel minder effectief is of als de warmteafvoer groter is dan in het geval van de hersenbehandeling. De vermogensafgifte per eenheid van volume neemt onder andere af naarmate de elektrodes verder uit elkaar liggen. Voor implantaten in de tongbasis zijn afstanden tussen de katheters van meer dan 1.5 cm niet uitzonderlijk. Het in te stellen vermogen wordt soms beperkt door warmte-gerelateerde pijn, met als mogelijk gevolg een tekort aan vermogen in andere delen van het doelvolume. Dit probleem kan niet opgelost worden met behulp van een generator die meer vermogen levert of door een efficiëntere warmteafgifte van de applicatoren. Om pijn te voorkomen moet de maximum weefseltemperatuur laag blijven. In de tong bijvoorbeeld is 45°C in het algemeen nog te verdragen maar neemt de kans op pijn snel toe als het weefsel warmer wordt. Het is dus van belang om te streven naar een zo homogeen mogelijke temperatuurverdeling, zeker naarmate de gewenste minimumtemperatuur toeneemt. Wat dit betreft kan het MECS-IHT systeem goed concurreren met andere IHT-systemen. De rechtstreekse vermogensafgifte aan het weefsel op enige afstand van de katheters is een voordeel ten opzichte van verwarming via warmtegeleiding alleen zoals in het geval van de zogenaamde *hot source* IHT-systemen (ferromagnetische zaadjes, warm-water-applicatoren, weerstandsapplicatoren). Verder is, vergeleken met IHT-systemen die gebaseerd zijn op microgolf antennes of galvanisch gekoppelde RF-elektrodes, het verwarmde gebied langs een applicator minder afhankelijk van factoren als applicatorafmeting, insteekdiepte en kathetergeometrie.

De homogeniteit van de verwarming met het MECS-systeem kan echter nog verder verbeterd worden. Ten eerste, door de elektrodedichtheid te vergroten, door de afstand tussen de katheters te verkleinen en/of door het aantal elektrodes per eenheid van lengte katheter te verhogen. Ten tweede, zal de vermogensabsorptieverdeling en dus de temperatuurverdeling minder heterogeen worden als er kathetermaterialen gebruikt worden met een lage diëlektrische absorptie zoals teflon of polyethyleen. Ten derde, kan de homogeniteit van de stroomdichtheidsverdeling nog verbeterd worden als de elektrodes zo worden aangesloten dat de vermogensfases van buur-elektrodes zoveel mogelijk tegengesteld zijn. Ten slotte, kan overwogen worden om katheters met een grotere diameter te gebruiken (de vermogensabsorptie neemt namelijk af met $1/r^2$) en/of om de applicatoren met water of lucht te koelen. Hierdoor zouden de hoge temperaturen net rond de elektrodes gedrukt kunnen worden.

Methodes om de homogeniteit van de temperatuurverdeling te verbeteren hebben vaak als nadeel dat de effectieve vermogensafgifte aan het weefsel afneemt. Vergroten van de elektrodedichtheid is de enige manier om zowel de

ruimtelijke verdeling als de grootte van de vermogensabsorptie te verbeteren. Dit houdt in dat er meer katheters geïmplantéerd moeten worden, maar er is een limiet aan het aantal katheters dat een patiënt kan verdragen.

Het effectieve vermogen per elektrode kan vergroot worden door óf het aangeboden vermogen óf de verwarmingsefficiëntie te vergroten. De eerste optie kan met het huidige MECS-systeem gerealiseerd worden door een elektrode aan meer dan één kanaal van het verwarmingssysteem aan te sluiten. Het is duidelijk dat er dan minder elektrodes gebruikt kunnen worden en dus het maximaal te behandelen doelvolume en/of de homogeniteit van de temperatuurverdeling kleiner zullen zijn. De efficiëntie van de applicatoren kan mogelijk nog iets verbeterd worden door aanpassingen van het applicator-ontwerp, maar de winst hiervan zal marginaal zijn. Een meer substantiële efficiëntiewinst kan verkregen worden door een andere methode te kiezen om de applicatorimpedantie aan de generatorimpedantie aan te passen. Als de applicatorimpedantie bijvoorbeeld wordt getransformeerd naar 200 in plaats van naar 800 Ohm, dan zou de verwarming ongeveer twee keer zo efficiënt worden. Hierbij moet wel opgemerkt worden dat bij transformatie naar 200 Ohm, de efficiëntie meer zal variëren bij eventuele variaties van de applicatorimpedantie en dat de voor impedantieaanpassing benodigde inductie groter is en daardoor meer energie zal absorberen.

Met het huidige MECS-systeem zijn er situaties denkbaar waarin er onvoldoende vermogen beschikbaar is. Er zijn echter geen fundamentele beperkingen aan het aantal verwarmingskanalen of aan het vermogen per kanaal, dus uit technisch oogpunt zijn er geen beperkingen voor het maximaal verwarmbare volume of de te bereiken temperatuur.

Het onderzoek beschreven in dit proefschrift heeft vooral betrekking op de kwaliteit van de temperatuurverdeling. Eventuele toekomstige studies zullen meer gericht zijn op dosis-effect relaties. Hyperthermie is in het algemeen meer effectief indien het gelijktijdig met radiotherapie wordt toegepast. Voor deze toepassing zou het interessant zijn om de katheters te integreren met holle MECS-IHT applicatoren waarin ruimte is voor de radioactieve IRT-bronnen. Daarbij zou het meten van de maximum weefseltemperaturen verbeterd kunnen worden door de thermokoppel-thermometers te bevestigen aan de buitenkant van deze MECS-IHT-katheters.

In principe kan MECS-IHT nog verder verbeterd worden. In de meeste situaties is dit echter niet strikt noodzakelijk om adequaat te kunnen verwarmen. Daarom is het alleen te rechtvaardigen om meer mankracht en middelen in de verdere ontwikkeling van MECS-IHT te steken als er voldoende klinische toepassingsmogelijkheden voor IHT zijn. In het algemeen is IHT een behandeloptie mits 1) IRT deel uitmaakt van de bestaande standaardbehandeling en 2) als het verwachte resultaat van die standaardbehandeling onbevredigend is (bijvoorbeeld een lokale controle van de ziekte van minder dan 60 à 70%). Implantatie van katheters alleen voor IHT of het toevoegen van IHT met als doel de IRT-dosis verlagen zonder verlies van effect maar met minder stralingsbijwerkingen, zijn ook mogelijkheden. Deze opties zijn echter voorlopig nog niet algemeen geaccepteerd zolang IHT nog een experimentele behande

ling is. De enige manier om aan te tonen dat IHT in combinatie met radiotherapie wel of niet effectief is, is door middel van een gerandomiseerd onderzoek. Daarom zou de derde eis voor het toepassen van IHT moeten zijn dat de resultaten evalueerbaar zijn binnen een gerandomiseerde studie. Het belangrijkste probleem hierbij is dat het aantal patiënten per jaar dat aan de eerste twee voorwaarden voor IHT voldoet meestal te laag is om binnen een redelijke tijd een zinvol antwoord te krijgen op de effectiviteitsvraag. Afhankelijk van de uiteindelijke winst ten gevolge van IHT varieert het benodigde aantal patiënten voor een statistisch significant resultaat van enige tientallen tot een paar honderd. In de Daniel den Hoed Kliniek is de frequentie waarmee mogelijke IHT-indicaties zoals hooggradige (III/IV) glioma's (0% lokale controle) en grote (T3/T4) tumoren in de tongbasis (ongeveer 30% lokale controle) voorkomen, ongeveer 0-5 respectievelijk 5-10 patiënten per jaar. Het probleem van lage aantallen, voor een studie in aanmerking komende, patiënten is echter niet uniek in de oncologie en wordt vaak opgelost door de studie met meerdere behandelcentra samen uit te voeren.

Op dit moment, geven de goede resultaten van recente gerandomiseerde hyperthermie studies en de goede verwarmingsresultaten van het MECS-IHT systeem bij hersentumoren aanleiding om nieuwe gerandomiseerde IHT-studies te starten en MECS-IHT behandelingen verder te verbeteren.

Bibliography

Kaatee RSJP, Kampmeijer AG, Van Hooije CMC, Van Rhoon GC, Kanis AP, Levendag PC and Visser AG, 1995, A 27 MHz current source interstitial hyperthermia system for small animals. *International Journal of Hyperthermia* 11: 785-796.

Kaatee RSJP, Crezee J, Kanis AP, Lagendijk JJW, Levendag PC and Visser AG, 1997, Spatial temperature control with a 27 MHz current source interstitial hyperthermia system. *International Journal of Radiation Oncology, Biology, Physics* 37: 189-197.

Kaatee RSJP, Crezee J, Kanis AP, Lagendijk JJW, Levendag PC and Visser AG, 1997, Design of applicators for a 27 MHz multi-electrode current source interstitial hyperthermia system: impedance matching and effective power. *Physics in Medicine and Biology* 42:1087-1108.

Kaatee RSJP, Crezee J and Visser AG, 1999, Temperature measurement errors with thermocouples inside 27 MHz multi-electrode current source interstitial hyperthermia applicators. *Physics in Medicine and Biology* 44:1499-1511.

Kaatee RSJP, Crezee J, Kanis AP, Lagendijk JJW, Levendag PC and Visser AG, 1999, Clinical thermometry with the 27 MHz current source interstitial hyperthermia system in brain tumours. *Radiotherapy and Oncology*. (submitted).

Kaatee, R.S.J.P.; Van Rhoon, G.C. 1999 An electric field measurement system, using a two-dimensional array of diodes. *International Journal of Hyperthermia* 15:441-454.

Van Geel CAJF, Visser AG, Van Hooije CMC, Van den Aardweg GJMJ,

Kolkman-Deurloo IKK, Kaatee RSJP and Levendag PC, 1994, Interstitial hyperthermia and interstitial radiotherapy of a rat rhabdomyosarcoma; effects of sequential treatment and consequences for clonogenic repopulation. *International Journal of Hyperthermia* 10:835-844.

Crezee J, Van der Koijk JF, Kaatee RSJP and Lagendijk JJW, 1997, Implications of using thermocouple thermometry in 27 MHz multi-electrode capacitively coupled interstitial hyperthermia. *Physics in Medicine and Biology* 42:637-650.

Crezee J, Kaatee RSJP, Van der Koijk JF and Lagendijk JJW, 1999, Spatial steering with quadruple electrodes in 27 MHz capacitively coupled interstitial hyperthermia. *International Journal of Hyperthermia* 15:145-156.

Visser AG, Van Hooije CMC, Van den Berg AP, Kaatee RSJP and Levendag PC, 1999, Equivalence of continuous and fractionated irradiation in a rat tumor model and conditions for optimum thermal enhancement. *International Journal of Radiation Oncology, Biology and Physics*. (submitted).

Levendag PC, Kaatee RSJP, Visser AG Kolkman-Deurloo IKK, Van Rhooon, GC Meeuwis CA, Van Geel CAJF and Van Hooije CMC, Interstitial radiation and/or interstitial hyperthermia for advanced and/or recurrent cancers in the head and neck: a pilot study. In: Seegenschmiedt MH, Sauer R, (eds), 1993, *Interstitial and Intracavitary Thermoradiotherapy*. Berlin, Heidelberg: Springer-Verlag: 233-239.

Visser AG, Kaatee RSJP and Levendag PC, Radiofrequency techniques for interstitial hyperthermia. In: Seegenschmiedt MH, Sauer R, (eds), 1993, *Interstitial and Intracavitary Thermoradiotherapy*. Berlin, Heidelberg: Springer-Verlag:35-41.

Visser AG and Kaatee RSJP, Technical quality assurance for interstitial hyperthermia. In: Seegenschmiedt MH, Sauer R, (eds), 1993, *Interstitial and Intracavitary Thermoradiotherapy*. Berlin, Heidelberg: Springer-Verlag:341-345.

Dankwoord

"Wat in het vat zit verzuurt niet!" Dat zal wel, maar een beetje blij dat het boekje nu gedrukt is ben ik toch wel. Het is mogelijk dat de zuurgraad toch enigszins verhoogd is, maar wie het waagt om na dit dankwoord nog verder te lezen zal ontdekken dat dit in de hyperthermie juist een pluspunt is. Alle medeplichtigen aan dat wat aan dit proefschrift voorafging, en dat zijn er heel wat, wil ik graag bedanken. Slechts een aantal hoofdschuldigen zal ik hieronder bij naam noemen.

Toen ik in 1991 bij de Daniel den Hoed Kliniek kwam solliciteren voelde ik me meteen op mijn gemak. Gerard van Rhoon deed wel zijn best om mij grondig aan de tand te voelen maar Inger-Karine (toen nog) Deurloo deed al zijn pogingen stranden. Ongeveer een week later zat ik in een luxe hotel mij te verdiepen in de basisbeginselen van de oncologie en ik kan u verzekeren dat valt niet mee na een jaartje dienstplicht. Eenmaal, in "huis" kwam ik terecht in de roze zone naast mijn lotgenoten van photodynamische therapie (PDT). Net als zij deed ik namelijk niets met ioniserende straling dus een plaatsje op de afdeling Klinische Fysica was iets te hoog gegrepen (twee verdiepingen om precies te zijn). Gezien het onderwerp van mijn onderzoek "interstitiële hyperthermie (IHT)" begreep ik dat ik eigenlijk bij de afdeling Hyperthermie moest zijn. Bijna goed. Ik bleek namelijk geen hyperthermist, maar zo'n "interstitiële" te zijn. Het ligt daarom voor de hand om allereerst mijn "soort" te bedanken.

Inger-Karine (tegenwoordig) Kolkman-Deurloo, collega Veni Vidi Fysicus en mijn eerste kamergenoot. Sinds die eerste dag tot op heden heb ik jouw oprechte belangstelling in mijn welbevinden, op het werk maar ook privé, zeer kunnen waarderen. Andries Visser, man van wine(gums)en klassieke muziek. Rap, je kunt het niet aanhoren maar je was het wel als ik je hulp nodig had. Iets moest niet, maar was wenselijk en dat maakte je voor mij een goede

begeleider. Bart Kanis, je hebt wat moeten afzien als je mij weer eens zag solderen. Co-auteur van elk artikel in dit proefschrift en in een glansrol als mijzelf tijdens mijn bruiloft. Wie kan er meer geschikt zijn als paranimf dan jij.

Verder heb ik goede herinneringen aan al die keren dat we rond de Kandinski van Hyperthermie de problemen van de wereld zaten op te lossen. Alle aanzittenden wil ik onder andere hiervoor bedanken. Cobi van der Zee, de moeder van de afdeling (en eigenlijk ook van de hyperthermie familie in heel Europa). Je wetenschappelijke carrière is ontzagwekkend maar ik heb nog meer respect voor hoe je met patiënten omgaat. Gerard van Rhoo, optimist tot op het bot. Meer dan eens heb je in mijn ogen doodlopende sporen weer verbonden met een uitgebreid net van mogelijkheden. Paul Rietveld, zonder jou was het vat nog wel even dicht gebleven. Na een paar weken van opmerkingen, telefoontjes en mailtjes, heb ik eieren voor mijn geld gekozen en de EUR gebeld om een promotiedatum af te spreken. Ook wil ik je bedanken voor je vele praktische houtje-touwtje-knip-en-plak oplossingen voor experimenteerprobleempjes. Pia Broekmeyer en Lia Verloop jullie hebben mij geleerd dat het behandelen van patiënten datgene is waardoor een hyperthermist zich onderscheid van een interstitiële. Ik hoop dat ik nu ook een klein beetje een hyperthermist geworden ben. Ad (paddestoel) van de Berg, jouw kennis van de hyperthermie literatuur was indrukwekkend. Susanne van de Ploeg, Saskia van de Merwe, Jacqueline Peer, Lucina de Graaf en Jorine Juffermans bedankt voor jullie opgewekte humeur. Joop Stakenborg, we missen jouw hoog-frequente begaafdheid. Inge Dijkstra en Paula Groot, bedankt voor jullie werk aan het uiterlijk van het boekje. Ali Ameziane, dankzij jouw kan ik ook nu nog iets vinden in het lab. Tot slot, Isabelle Conradus, Gerton Kampmeier, Arie Hobbel, Leila van der Voet en Paul Knops bedankt, omdat jullie als praktikant een belangrijke schakel waren tussen veel ideeën en de realisatie daarvan. Ieder van jullie kan zijn werk terugvinden in dit proefschrift.

Het door de Nederlandse Kankerbestrijding gefinancierde (waarvoor dank) onderzoeksproject bezat naast de in dit boekje beschreven technische tak, een minstens zo interessante radiobiologische component. Iedereen die bijdroeg aan het altijd boeiende wekelijkse projectoverleg wil ik hiervoor bedanken. Christel van Hooije, jij hebt me laten zien hoe je bestralingsexperimenten met ratten op een ethisch verantwoorde manier kunt uitvoeren. Bedankt ook voor jouw hulp bij de *in vivo* tests van apparatuur, die een essentiële tussenstap vormde op weg naar de klinische introductie van IHT.

Zodra het onderzoek praktisch begon te worden (lees: er patiënten behandeld konden gaan worden) nam het aantal mensen dat er bij betrokken was exponentieel toe. Dim Noteboom, Dick Sipkema, Conny de Pan en hun collega's van de afdeling brachytherapie, Elly Korevaar en de verpleging van AO en de radiotherapeuten waaronder Peter Levendag en Peter Nowak, allen bedankt voor het vertrouwen.

Verder wil ik nog bedanken de medewerkers van Medische Fotografie en Hans Vuik in het bijzonder voor je "vandaag brengen, gisteren klaar" principe en de vaklui uit de Instrumentmakerij waar we helaas het vakmanschap en de humor van Dick Van Sluis moeten missen.

Wat Klinische Fysica betreft is alles goedgekomen. Alle overgebleven IHT-ers (en ook de PDT-ers) van weleer huizen tegenwoordig twee verdiepingen hoger. Jullie allemaal bedankt voor de goede sfeer en de leuke SOPs en SOEPs die ik met jullie overleefd heb. Het feit dat er bij jullie de laatste tijd lustig op los gepromoveerd wordt heeft ongetwijfeld bijgedragen aan de afronding van mijn boekje.

Het mag duidelijk zijn dat er veel afdelingen in huis bij het onderzoek betrokken zijn geweest met als gunstig bijeffect vrijwel onbeperkt gebak eten.

In het Academisch Ziekenhuis Utrecht heb ik weliswaar minder gebak gegeten maar de samenwerking met Hans Crezee, Jan Lagendijk, John van de Koijk, Jacob de Bree, Hugo Kroeze en Cees Ligtfoot was aangenaam en heeft flink bijgedragen aan de inhoud van dit boekje.

Op dit moment staat het IHT-onderzoek al weer enige tijd op een laag pitje, het verwarmingssysteem wordt elders nuttig gebruikt, en nu is het proefschrift ook nog af.

Toch zal ik altijd een beetje een interstiële blijven.



Curriculum Vitae

Robert Kaatee werd op 14 oktober 1964 in Toronto geboren. In 1983 behaalde hij het V.W.O. diploma aan het Sint Vitus College te Bussum. Daarna studeerde hij Technische Natuurkunde aan de Universiteit Twente. Het afstudeeronderzoek had als titel "De afname van fluorescentie-depolarisatie ten gevolge van Förster resonance energy transfer, toegepast als principe voor een immuunsensor" en werd verricht in de vakgroep Biofysische Techniek. Het doctoraal diploma werd behaald in augustus 1989. Na het vervullen van de dienstplicht trad hij in dienst van de Daniel den Hoed Kliniek waar hij bij de afdelingen Klinische Fysica & Instrumentatie en Hyperthermie werkte aan een door de Nederlandse Kanker Bestrijding (NKB) gefinancierd project getiteld "Combination of high-dose-rate and low-dose-rate brachytherapy with interstitial hyperthermia: study of mechanism in an experimental model and physical development". Dit onderzoek heeft geresulteerd in dit proefschrift. Vanaf oktober 1995 tot februari 1997 werkte hij een NKB-project met als titel "Clinical verification and optimisation of the quality of large superficial tumours of the chest wall en vervolgens aan een Revolving Fund-project met als onderwerp "Hoge-precisie radiotherapie bij het cervix carcinoom". Sinds februari 1999 werkt hij wederom aan een door het NKB gefinancierd project: "Advanced applications of an Electronic Portal Imaging Device (EPID) for high precision radiotherapy" en is in opleiding tot klinisch fysicus in de radiotherapie.

Hij is gehuwd met Tjitske Westra en vader van Femke en Lotte.
